CRANFIELD UNIVERSITY

ONDREJ CHALOUPKA

MODELLING EVOLUTION OF ANISOTROPY IN METALS USING CRYSTAL PLASTICITY

SCHOOL OF ENGINEERING

MSc by Research

MSc BY RESEARCH

Academic Year: 2011 - 2013

Supervisor: Dr James Campbell

March 2013

CRANFIELD UNIVERSITY

SCHOOL OF ENGINEERING
MSc by Research

MSc BY RESEARCH

Academic Year 2011 - 2013

ONDREJ CHALOUPKA

MODELLING EVOLUTION OF ANISOTROPY IN METALS USING CRYSTAL PLASTICITY

Supervisor: Dr James Campbell
March 2013

ABSTRACT

Many metals used in modern engineering exhibit anisotropy. A common assumption when modelling anisotropic metals is that the level of anisotropy is fixed throughout the calculation. As it is well understood that processes such as cold rolling, forging or shock loading change the level of anisotropy, it is clear that this assumption is not accurate when dealing with large deformations.

The aim of this project was to develop a tool capable to predict large deformations of a single crystal or crystalline aggregate of a metal of interest and able to trace an evolution of anisotropy within the material.

The outcome of this project is a verified computational tool capable of predicting large deformations in metals. This computational tool is built on the Crystal Plasticity Finite Element Method (CPFEM). The CPFEM in this project is an implementation of an existing constitutive model, based on the crystal plasticity theory (the single crystal strength model), into the framework of the FEA software DYNA3D®.

Accuracy of the new tool was validated for a large deformation of a single crystal of an annealed OFHC copper at room temperature. The implementation was also tested for a large deformation of a polycrystalline aggregate comprised of 512 crystals of an annealed anisotropic OFHC copper in a uniaxial compression and tension test. Here sufficient agreement with the experimental data was not achieved and further investigation was proposed in order to find out the cause of the discrepancy. Moreover, the behaviour of anisotropic metals during a large deformation was modelled and it was demonstrated that this tool is able to trace the evolution of anisotropy.

The main benefit of having this computational tool lies in virtual material testing. This testing has the advantage over experiments in time and cost expenses. This tool and its future improvements, which were proposed, will allow studying evolution of anisotropy in FCC and BCC materials during dynamic finite deformations, which can lead to current material models improvement.

Keywords:

CPFEM, Dislocation slip, FCC system, Explicit FEA, Elastic plastic deformation

ACKNOWLEDGEMENTS

I would like to express my deep gratitude to Dr James Campbell, my research supervisor, for his patient guidance, enthusiastic encouragement and useful critiques of this research work.

I would also like to extend my thanks to Paula Rodriguez Gonzalez and my family for their support and encouragement throughout my study.

TABLE OF CONTENTS

LIST OF FIGURES

LIST OF TABLES

LIST OF ABBREVIATIONS

CU	Cranfield University
CS	Coordinate System
FE	Finite Element
FEM	Finite Element Method
FEA	Finite Element Analysis
CPFEM	Crystal Plasticity Finite Element Methods
BCC	Body Centred Cubic
FCC	Face Centred Cubic
RVE	Representative Volume Element
OFHC	Oxygen Free High Conductivity
HCP	Hexagonal Close Packed

NOTATION

Vectors are written as bold, italic capital symbols ($\boldsymbol{A}, \boldsymbol{B}$), if they are expressed in terms of reference configuration Ω_0 and as bold, italic faced lowercase symbols ($\boldsymbol{a}, \boldsymbol{b}$), when they are defined with respect to the current configuration Ω. Second order tensors are written as bold capital symbols ($\mathbf{A}, \mathbf{B}$), if they are expressed in terms of reference configuration Ω_0 and as bold faced lowercase symbols ($\mathbf{a}, \mathbf{b}$), when they are defined with respect to the current configuration Ω. Fourth order tensor are written as capital double struck letters ($\mathbb{A}, \mathbb{B}$) when stated in terms of reference configuration Ω_0 and as double struck lower case letters ($\mathbb{a}, \mathbb{b}$) when termed in current configuration Ω. The magnitude of tensors of any order is denoted by italic-faced lowercase letters and symbols (h, γ). Cartesian components of vectors, second order tensors and fourth order tensors are written as $a_i\,(A_i)$, $a_{ij}\,(A_{ij})$ and $a_{ijkl}\,(A_{ijkl})$ respectively. The dot product between two vectors is represent as $\boldsymbol{a} \cdot \boldsymbol{b} = \boldsymbol{a}\boldsymbol{b} = a_i b_i$, between a vector and a second order tensor $\boldsymbol{a} \cdot \mathbf{b} = \boldsymbol{a}\mathbf{b} = a_{ij} b_j$, between two second orders $\mathbf{a} \cdot \mathbf{b} = \mathbf{a}\mathbf{b} = a_{ij} b_{jk}$. The tensor product between two vectors is given as $\boldsymbol{a} \otimes \boldsymbol{b} = a_i b_j$ and double dot product between fourth order tensor and second order tensor defined as $\mathbb{a} : \mathbf{b} = a_{ijkl} b_{kl}$. The transpose and the inverse are denoted by superscript T and -1 respectively.

1 INTRODUCTION

Plasticity in metals describes permanent deformation, which occurs when the level of deformation reaches a certain point (yielding point). Plasticity is in particular fields of engineering desirable (e.g. industrial forging), but in cases where metallic structures are designed to withstand a certain load before yielding occurs, plasticity is unacceptable. Either way, an understanding of plasticity nature and the ability to predict metal behaviour during elastic-plastic deformation is crucial in the modern world, where engineering structures are inseparable part of our daily life.

Robert Hooke in the 17th century discovered that during the reversible part of deformation (elastic deformation) the relation between applied load and material elongation is linear and can be linked with a particular constant (Hooke's law). For the region of the plastic deformation the mechanical response is nonlinear. Hence, prediction of such behaviour is not a trivial task and during its modelling, certain simplifications and assumptions have to be made.

An assumption of metal isotropy in relatively small elastic-plastic deformation analyses is extensively used for its simplicity and accuracy. To predict yielding of an isotropic material subject to various combinations of stresses, the Von Mises criterion [1] is commonly used. But an assumption of material isotropy becomes less accurate when a metal undergoes a very large deformation. It is well known that processes such as cold rolling, forging or shock loading change the level of anisotropy due to microstructure distortion. R. Hill proposed in 1948 generalized form of the Von Mises criterion which accounts for anisotropic (more precisely orthotropic) plasticity but it was found out, that it cannot accurately represents some materials [2]. Lately, many improvements and suggestions of the Hill criterion have been proposed (see Introduction of reference [2]), but typically with the assumption that the level of anisotropy in a metal is fixed throughout the calculation. However, this supposition in some particular cases can cause insufficient accuracy in predicting material response to mechanical loading (e.g. springback effect after the sheet metal stamping process [3]) and does not allow us to fully predict physical phenomena of metal

deformation. Therefore, new approach of analysing anisotropic metals based on material microstructure is needed.

At the beginning of the 20th century a new method to obtain specimen of a single crystal of metal together with a new method of determining the crystallographic direction by using X-ray diffractometer were discovered and lead to the discovery that plastic deformation results from the sliding of certain crystallographic planes in certain directions. Lately Boas and Schmid in 1930 [4] observed that a single crystal during the plastic deformation rotates and the material anisotropy evolves. Another question arose when it was carried out that the energy needed to break bonds between atoms due to slip of crystallographic planes is much higher than the energy which was measured in experiments. That was lately explained by line imperfections in the crystal lattice called the dislocations. This theory of plastic deformation which is happening due to massive flow of dislocations within the material could be confirmed in the fifties thanks to the electronic microscope invention [4].

The physical nature of plastic deformation in metals can be describe in terms of continuum mechanics, which is a common approach used for solving engineering problems as working with material on the atomistic level is not in engineering scale applicable. In the 80s when computers became more available and more powerful, models of a single crystal or a crystalline aggregate described using continuum mechanics were implemented into computers as software, e.g. into FE solvers. This appeared as very successful approach and development of the continuum models and their implementation continues to this day. Their main advantage lies in the ability to describe the nature of metallic anisotropy and its evolution during finite deformation and in the possibility to deal with complex inner and outer boundary conditions due to FEM framework [5].

The Crystal Plasticity Finite Element Methods (CPFEM) developed during the last 25 years are now versatile tool that is able to predict mechanical deformations of anisotropic single crystals or crystalline aggregates by modelling mechanical structures at the level of individual grains [5]. They

employ constitutive models based on single crystal plasticity theory within the framework of the Finite Element Method (FEM) to run numerical analyses of mechanical deformations of single crystals or crystalline aggregates. Various CPFEM for different materials, scales and applications have been developed. For more information see Section 3.4.

The range of CPFEM applications is very extensive and it starts at micro-scale (e.g. bending of nanowire [6]) continues through meso-scale (e.g. analysis of coronary stent strut [7]) and ends at macro-scale (e.g. virtual material testing in automobile industry [8]).

An analysis of plasticity in metals can be a very complex task and usually it is needed to make simplifying assumptions. But when dealing with various materials and with some specific problems such as finite deformation, these assumptions can cause inaccuracy in the prediction of the material behaviour. However, better understanding of the nature of metal deformation, complex mathematical models and rapid growth of computational power, allow us to run still more accurate and sophisticated material numerical analysis.

1.1 Aims and Objectives

1.1.1 Motivation

Many metallic structures exhibit direction dependent (anisotropic) response to mechanical loading due to their microstructure. When modelling deformation of such metals, a common assumption is that the level of anisotropy doesn't change throughout calculation, which is not valid for large deformations.

Evolution of anisotropy has a significant impact on material properties. The Crashworthiness, Impact and Structural Mechanics group (CISM) at Cranfield University develops metallic material models and from on-going work, requirement to understand anisotropy evolution in metals during dynamic large deformations has arisen. The overall aim of the group's research in this field is to enhance understanding of anisotropy in metals towards improving material models, where these materials models will allow running more accurate simulations of engineering problems.

1.1.2 Project Aim

The aim of this project is to develop a computational tool that will be able to predict large deformations of a single crystal or crystalline aggregate of a metal of interest and will be able to trace an evolution of anisotropy within the material. This tool will be used in the future to study the anisotropic evolution in particular metals during dynamic finite deformations.

The metals of interest to the CISM group either have an FCC structures such as Copper (information about its material properties are broadly available [6; 9; 10] and that is convenient for model validation) and Aluminium, which is widely used in aerospace structure; or have a BCC structures, such as Tantalum.

1.1.3 Objectives

- Development of a computational tool (CPFEM), which will be an implementation of an existing constitutive model (the single crystal strength model) into the framework of the FEA software DYNA3D®.
- Validation and assessment of the tool and its ability to predict finite deformations and anisotropy evolution in a single crystal and polycrystalline aggregate of FCC metals.

1.2 Outline

Section 2 presents the crystal plasticity theory, which includes description of cubic crystals, microstructure of their aggregates, deformation mechanisms and a method of crystallographic projection. Section 3 introduces a basic concept of the continuum mechanics theory needed to understand the single crystal strength model, which is a mathematical description of the crystal plasticity theory. Section 4 explains how the single crystal strength model was implemented into the Finite Element (FE) framework as a material model and section 5 shows a validation procedure of this new CPFEM based on comparison of simulation analyses with experimental results. Section 6 demonstrates ability of the new method to capture an evolution of crystallographic orientation linked with an evolution of anisotropy in metals.

Section 7 provides a summary what has been done in this thesis. Section 8 makes conclusion of this work and proposes future projects.

2 CRYSTAL PLASTICITY

Crystal plasticity theory is based on the physical understanding of metals and their atomistic microstructure, where metals (crystalline aggregate) are composed of grains (single crystals), which are comprised with molecules and atoms. The following is sum of the current understanding of atomistic structure and its behaviour during deformation, where Dieter [1] and Macek [11] were used as the main sources of information.

2.1 Crystal Lattice and Dislocations

2.1.1 Crystal Lattice

In solid crystalline materials such as metals, atoms oscillate around their stable positions. These are arranged in a certain 3D pattern called a crystal lattice. The smallest repeating geometrical element (block of atoms) is called a unit cell and the crystal structure is obtained by their periodical repetition [11]. Depending on the form of the unit cell, 7 different crystallographic systems are defined, but this work accounts only for cubic crystallographic system (see Section 1.1.2), where the angles defining shape of unit cell are $\alpha = \beta = \gamma$ and the lengths characterizing the size are $a = b = c$, see Figure 1 [1]. Then according to the number and position of atoms within the cell, the face centred (FCC) cubic and the body centred cubic (BCC) structures are distinguished [1].

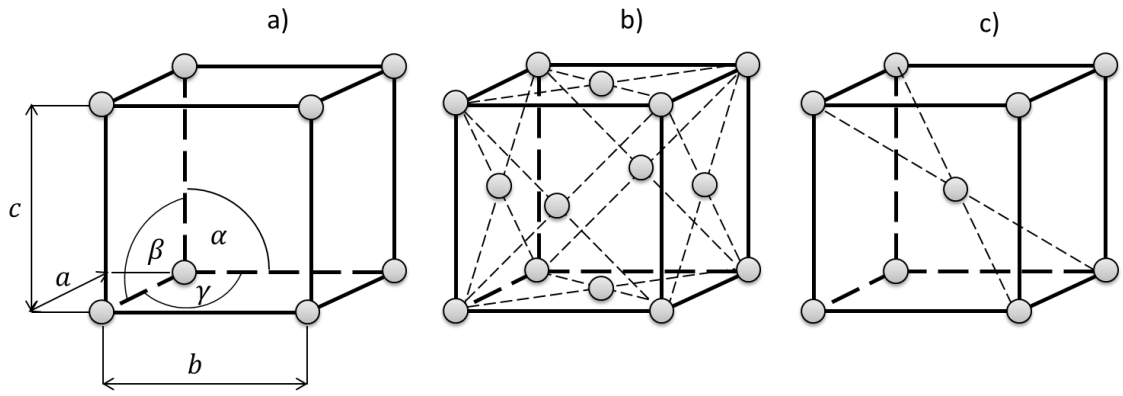

Figure 1 - Structure of crystallographic unit cells: a) Simple cubic, b) Face centred cubic (FCC) and c) Body centred cubic (BCC) [1]**.**

2.1.2 Miller Indices

To identify direction dependent properties in the crystal lattice, a unified description of crystallographic planes and directions was established. Imagine three dimensional Cartesian coordinate system with the axes x, y, z**,** and three vectors $\boldsymbol{a}, \boldsymbol{b}, \boldsymbol{c}$ which are determined by intersection of an arbitrary plane P and the axes x, y, z. Then the Miller indices for a plane $(h\ k\ l)$ are the reciprocation of the magnitudes of each vector $\boldsymbol{a}, \boldsymbol{b}, \boldsymbol{c}$ converted to smallest coprime integers [11]. If the intersection of P is with any negative coordinate axes, then it is represented in the Miller indices by an accent $\bar{}$ e.g. $(h\ \bar{k}\ l)$. If the Plane P is parallel to one of the axes $x,\ y,\ z$ then the particular Miller index is equal to zero e.g. $(h\ 0\ l)$. Miller index $[u\ v\ q]$ for a given direction $\boldsymbol{v}$ is obtained by converting coordinates of $\boldsymbol{v}$ to smallest coprime integers [11]. Examples are given in Figure 2.

The family of planes is noted as $\{\ h\ k\ l\ \}$, e.g. for family of planes {1 1 1} one gets set of planes: $(1\ 1\ 1), (\bar{1}\ 1\ 1), (1\ \bar{1}\ 1), (1\ 1\ \bar{1}), (\bar{1}\ \bar{1}\ \bar{1}), (\bar{1}\ \bar{1}\ 1), (\bar{1}\ 1\ \bar{1}), (1\ \bar{1}\ \bar{1})$.

Finally, the family of directions is noted as $< u\ v\ q >$, e.g. for family of directions $< 1\ 0\ 0 >$ one gets set of planes:$< 1\ 0\ 0 >, < 0\ 1\ 0 >, < 0\ 0\ 1 >, < \bar{1}\ 0\ 0 >, < 0\ \bar{1}\ 0 >, < 0\ 0\ \bar{1} >$.

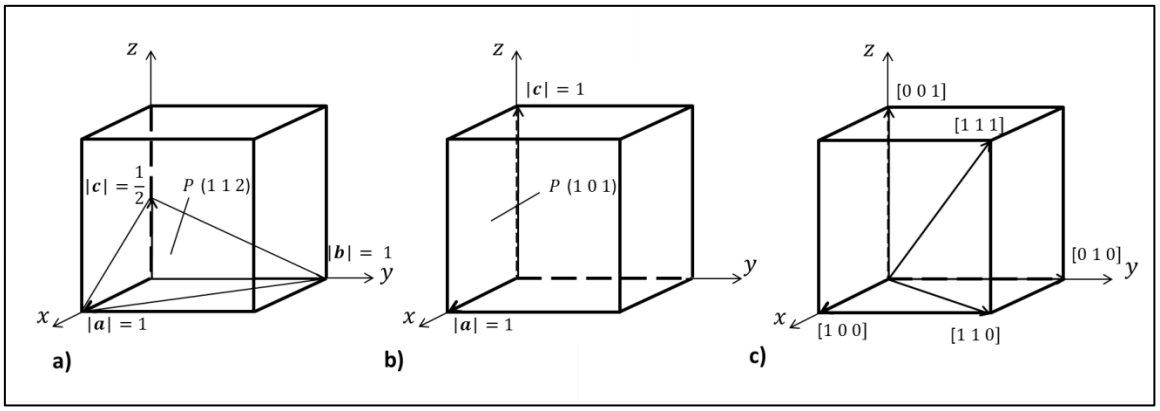

Figure 2 – a) An example of the Miller indices $(\mathbf{1\ 1\ 2})$ for a given plane P, b) An example of the Miller indices $(\mathbf{1\ 0\ 1})$ for a given plane P, c) Examples of the Miller indices $[\boldsymbol{u\ v\ q}]$ for given directions [11]**.**

2.1.3 Dislocations

In real crystals, a lattice is never perfect in terms of its geometry. There are four main types of imperfections: a) Point defects, b) Line defects c) Planar defects and d) Bulk defects [11]. This work here is concern only with the line defects known as dislocations, which are usually the main transmitter of plastic deformation. When sufficient shear stress is applied on the crystal, a dislocation is able to travel through the crystal structure as shown in Figure 3 and once it reaches its free surface of the crystal, a step is produced. Plastic deformation is due to flow of many such dislocations [11].

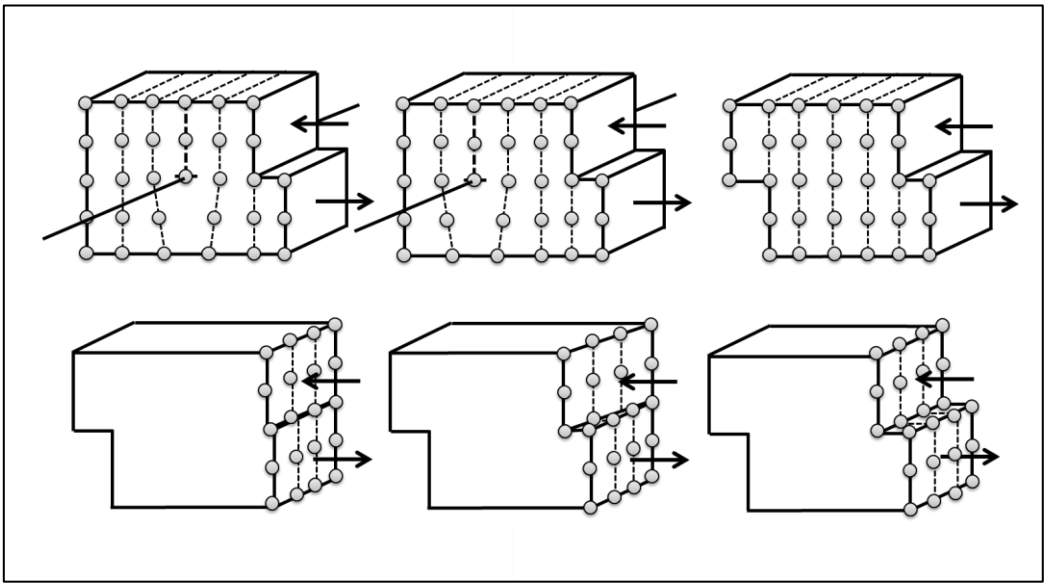

Figure 3 – Representation of the dislocation traveling through the crystalline matter due to applied shear force (upper part is slip of edge dislocation and lower part is slip of screw dislocation) [11]**.**

The shifted and un-shifted parts in the lattice are separated by the dislocation line and the vector describing the direction of dislocation motion is called the Burgers vector [11]. Based on the mutual position of the Burgers vector and dislocation line, the dislocations are sorted in three types, see Figure 4 [11]:

a) Edge dislocation, where the Burgers vector is perpendicular to the dislocation line.
b) Screw dislocation, where the Burgers vector is parallel to the dislocation line.

c) Mix of a) and b), mostly observed in reality.

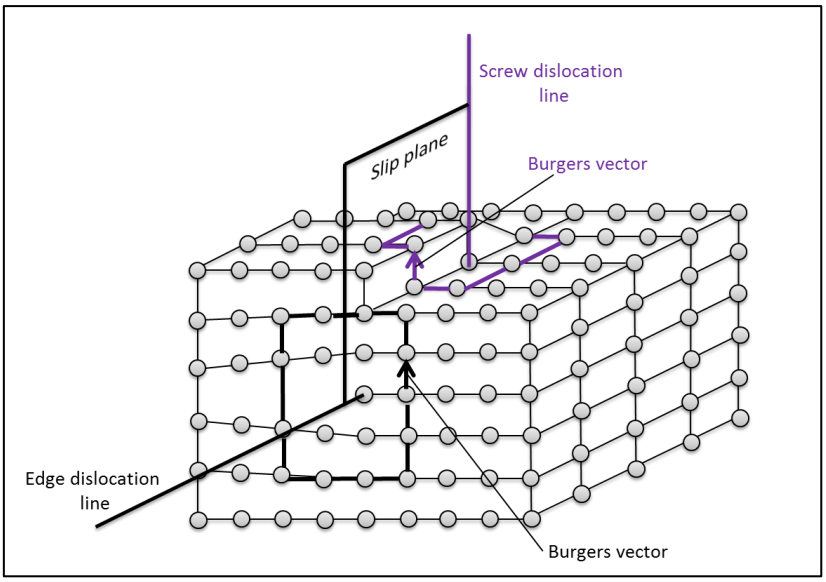

Figure 4 – The edge dislocation together with the screw dislocation described by their Burgers vectors and dislocation lines [11]**.**

2.2 Deformation of a Single Crystal

When external forces are applied on a crystal, stress occurs as a consequence of inner forces which are trying to keep atoms in stable position. This stress is causing change in crystal shape and size - such a phenomena is called deformation. Deformation can be divided in three parts: elastic deformation, elastic plastic deformation and fracture [11].

2.2.1 Elastic Deformation

During the elastic deformation, atoms within their lattice are deflected from the stable position due to external forces. But when the load is reduced, the atoms return back as a consequence of intermolecular forces. In terms of the macroscopic scale, in elastic deformation metals temporarily change their proportions [11].

Elastic properties of crystals are anisotropic and are given by relating stress σ_{ij} and strain ε_{kl} through the generalized Hooke's law [11]:

$$\sigma_{ij} = C_{ijkl} \cdot \varepsilon_{kl}, \tag{2-1}$$

where C_{ijkl} is a fourth order symmetric tensor called the stiffness matrix. Equation (2-1) can be written in Voigt notation as:

$$\begin{bmatrix}\sigma_1\\ \sigma_2\\ \sigma_3\\ \sigma_4\\ \sigma_5\\ \sigma_6\end{bmatrix} = \begin{bmatrix}C_{11} & C_{12} & C_{13} & C_{14} & C_{15} & C_{16}\\ C_{21} & C_{22} & C_{23} & C_{24} & C_{25} & C_{26}\\ C_{31} & C_{32} & C_{33} & C_{34} & C_{35} & C_{36}\\ C_{41} & C_{42} & C_{43} & C_{44} & C_{45} & C_{46}\\ C_{51} & C_{52} & C_{53} & C_{54} & C_{55} & C_{56}\\ C_{61} & C_{62} & C_{63} & C_{64} & C_{65} & C_{66}\end{bmatrix}\begin{bmatrix}\varepsilon_1\\ \varepsilon_2\\ \varepsilon_3\\ \varepsilon_4\\ \varepsilon_5\\ \varepsilon_6\end{bmatrix}, \tag{2-2}$$

Cubic crystals have only three independents components in their stiffness matrices because of their symmetric planes [11]:

$$\begin{bmatrix}\sigma_1\\ \sigma_2\\ \sigma_3\\ \sigma_4\\ \sigma_5\\ \sigma_6\end{bmatrix} = \begin{bmatrix}C_{11} & C_{12} & C_{12} & 0 & 0 & 0\\ C_{12} & C_{11} & C_{12} & 0 & 0 & 0\\ C_{12} & C_{12} & C_{11} & 0 & 0 & 0\\ 0 & 0 & 0 & C_{44} & 0 & 0\\ 0 & 0 & 0 & 0 & C_{44} & 0\\ 0 & 0 & 0 & 0 & 0 & C_{44}\end{bmatrix}\begin{bmatrix}\varepsilon_1\\ \varepsilon_2\\ \varepsilon_3\\ \varepsilon_4\\ \varepsilon_5\\ \varepsilon_6\end{bmatrix}, \tag{2-3}$$

The explanation of why in some circumstances polycrystalline aggregates have isotropic behaviour lies in the superposition of large number of randomly orientated crystals inside the aggregate, where the fairly uniform distribution of the individual anisotropic crystals is averaged over the volume [11].

2.2.2 Plastic Deformation

2.2.2.1 Deformation by Slip in Perfect Lattice

Deformation of a crystal is caused by a crystal slip (the translation of one plane of atoms over another) which happens on the planes with highest atomic density (slip planes) and in the close packed atomic directions (slip directions) [11]. In other words, slip occurs in the directions where least energy is required to move. A specific slip plane with a specific slip direction is called a slip system [11], with the number of slip systems depending on the crystallographic structure. This project is interested in FCC structure with 12 slip systems (see Figure 5) and BCC structure with 48 slip systems (see Section 1.1.2).

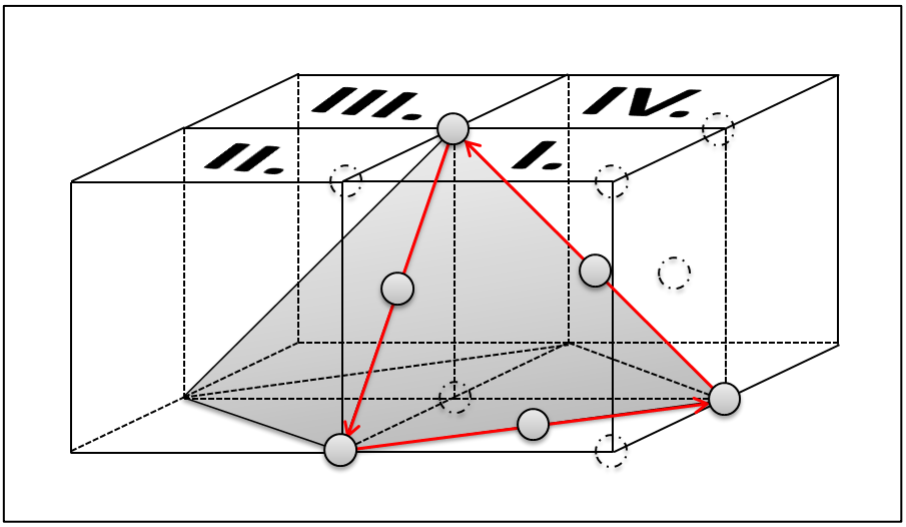

Figure 5 – Slip in the crystal lattice can occur on a family of the slip planes {1 1 1} in the slip directions <1 1 0>, together called slip systems. FCC structure has 4 slip planes (grey triangles in quadrants I., II., III., IV) and each is having 3 slip direction (red arrows), that gives 12 slip systems (reduced from 24 to 12 due to its symmetry) [11]**.**

The plastic deformation due to a single slip can be in a very simplified way illustrated as a distortion of a pack of playing cards when it is pushed from one direction [5], see Figure 6.

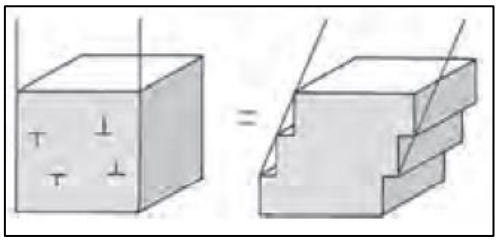

Figure 6 – Plastic deformation of a metal due to a single slip [5]**.**

2.2.2.2 Dislocation Slip

In reality the distortion energy, which is required to plastically deform a crystal is much lower than the energy which would be needed to deform a crystal with a perfect lattice. The reason lies in lattice imperfections, namely the dislocations [1]. In a real crystal lattice slip does not occur through motion of an entire plane, but results from motion of dislocations through the lattice. The massive flow of dislocations in the crystal is the main plastic deformation mechanism [1]. Note,

that plastic deformation does not change crystal volume and that the crystal lattice stays undistorted after a dislocation pass through it.

There also different mechanisms of plastic deformation, e.g. diffusionless deformation types as martensite deformation and mechanical twinning. For more details see reference [1].

2.2.2.3 Resolved shear stress

When stress occurs within a crystal, it can be resolved on each slip system α. When the resolved shear stress in a particular slip system α reaches a critical value (known as the critical resolved shear stress τ_c^{α}) then the dislocations will start to move in the same slip system α. A slip system, which is undergoing slip, is called an active slip system [1].

Let force $\boldsymbol{P}$ be applied on a single crystal containing only one slip system defined by slip direction $\boldsymbol{S}$, normal to the slip plane $\boldsymbol{N}$ and cross-sectional area $\boldsymbol{A_0}$ (see Figure 7). The cross-sectional area of slip surface $\boldsymbol{A}$ can be derived from $\boldsymbol{A_0}$:

$$\boldsymbol{A_s} = \frac{\boldsymbol{A_0}}{cos\,\emptyset}, \tag{2-4}$$

where $\emptyset$ is the angle between $\boldsymbol{N}$ and the load axis. The component of force $\boldsymbol{P}$ acting in the slip direction can be obtained as:

$$\boldsymbol{F_s} = \boldsymbol{P}\,cos\,\varphi, \tag{2-5}$$

where φ is angle between $\boldsymbol{S}$ and load axis. Finally the resolved shear stress τ is obtained:

$$\tau = \frac{\boldsymbol{F_s}}{\boldsymbol{A_s}} = \frac{\boldsymbol{P}}{\boldsymbol{A_0}}\,cos\,\emptyset\,cos\,\varphi. \tag{2-6}$$

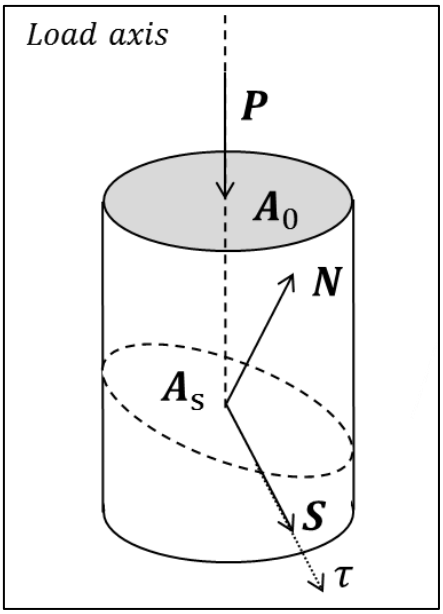

Figure 7 – Derivation of the resolved shear stress in a single crystal with one slip system [1]**.**

From the relation (2-6) it is obvious that the resolved shear stress has the highest value when angles ∅ and φ are equal to $\frac{1}{4}\pi$.

2.2.2.4 Crystal Rotation

Let us again consider a single crystal in tension with one active slip system described by $\boldsymbol{N}$ and $\boldsymbol{S}$ and where the tension axis is defined by the line segment AB, see Figure 8. Assume that the crystal is modelled as a plastic-rigid, since here the elasticity can be ignored. When the slip occurs, it can be seen that the tension axis rotates with respect to the slip system orientation which stays preserved. But as in most of tensile machines, the loading axis is constrained in horizontal direction, the crystal has to undergo rotation in the way that the line segment AB returns to its vertical position [11].

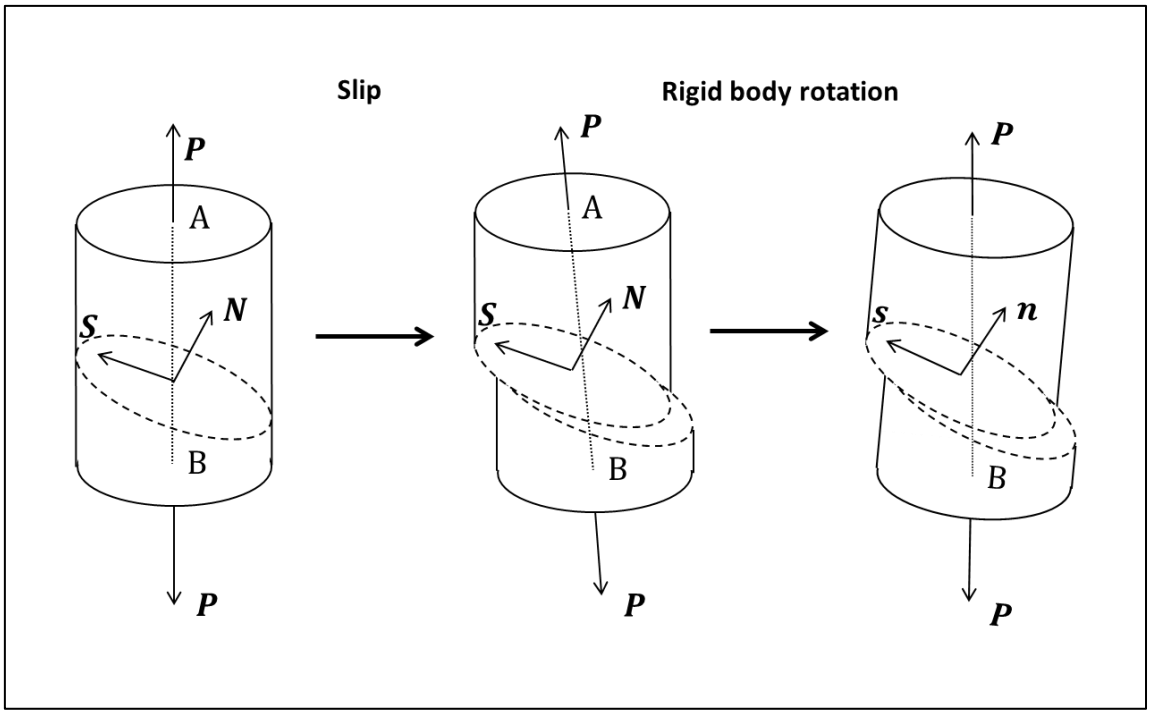

Figure 8 – Rigid body rotation of a single crystal during plastic deformation due to constrains of a tensile machine.

The conclusion is that when the crystal is constrained (e.g. in a crystalline aggregate), the massive flow of dislocations can cause crystal lattice rotation due to the plastic deformation [11].

2.2.2.5 Evolution of plastic deformation in a single crystal

Slip deformation in a single crystal starts when the resolved shear stress in the most favourable orientated slip system reach the value of the critical resolved shear stress. The plastic deformation in an annealed FCC crystal can be dived into three stages (for a specific direction of load, when at the beginning only one slip system starts to slip), see Figure 9.

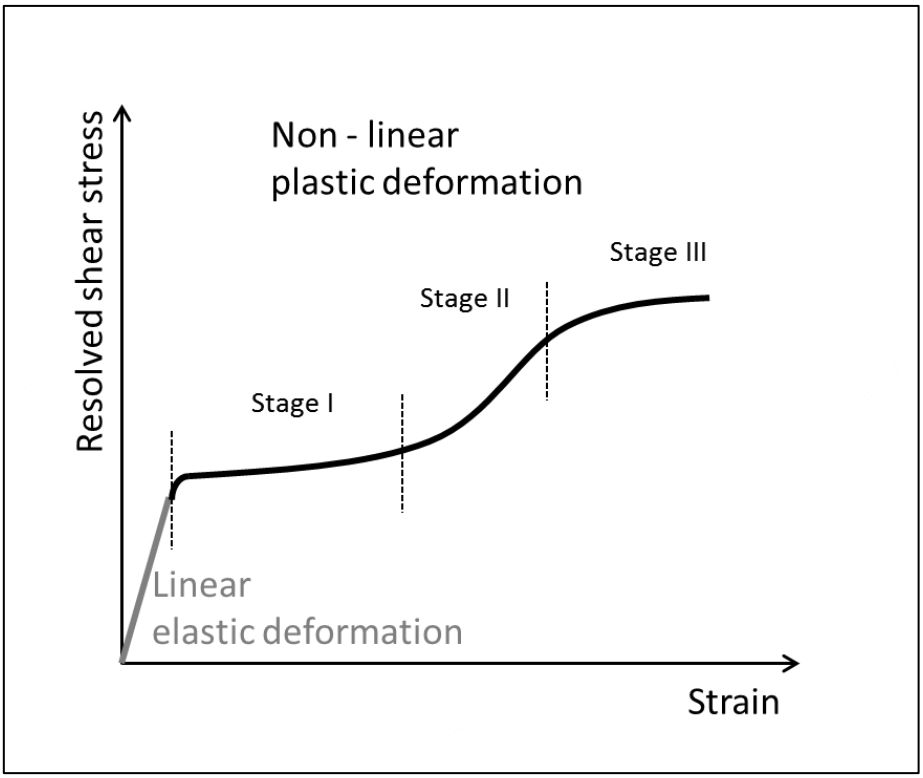

Figure 9 – Uniaxial stress strain curve for an annealed single FCC crystal [1]**.**

The first stage is called easy glide (or laminar flow) [1] where only one slip system is active, dislocations during their slip do not cross each other's path, therefore deformation grows fast even for a small increase of the resolved shear stress. In this stage new dislocations arise. The crystal rotates during deformation and as a consequence, the critical resolved shear stress is reached in other slip systems.

That is when the laminar flow change to the turbulent flow (second stage) [1], where the dislocation slips cross each other and the density of dislocations is rapidly growing (new dislocations arise). As a consequence the crystal hardens – more energy is required to increase the level of the plastic deformation.

The stage number three is called the dynamic recovery [1]. The stresses within the crystal are high enough for the dislocations to overcome different kind of obstacles (e.g. another active slip system, some imperfections in the lattice). In this stage the rate of strain hardening is decreased.

2.3 Deformation of a Polycrystalline Aggregate

A polycrystalline aggregate is composed of a certain number of grains. The mechanical elastic-plastic properties are strongly influenced by the orientation of these grains [1]. Aggregates can have isotropic properties, when they comprise of a large number of randomly orientated crystals and their superposition leads to isotropic response to mechanical loading. However, during finite deformation, the orientation of the crystals changes and that give rise to a certain preferable texture (distribution of the crystallographic orientations) which is the cause of the anisotropy in the polycrystalline aggregate.

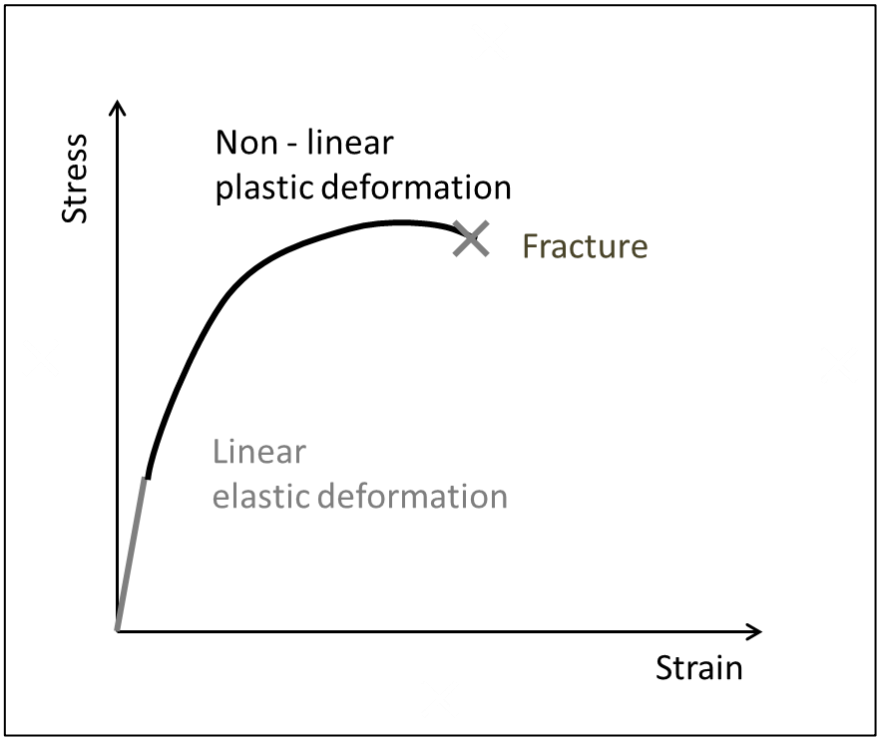

Figure 10 – Uniaxial stress strain curve for polycrystalline aggregate, which hardens since the beginning of the plastic deformation [1]**.**

During the plastic deformation, polycrystalline aggregate exhibits stress heterogeneity at the grain scale due to grains mechanical interaction.

From the beginning of the plastic deformation process more slip systems are active and dislocations are piling-up on the grain boundaries due to their difficult

penetrability [1]. All that leads to the turbulent flow and to the strain hardening since the beginning of the plastic deformation [1], see Figure 10.

2.4 Plasticity in Engineering

Plasticity in metals describes permanent deformation, which occurs when the level of deformation crosses the yielding point. Plasticity is in particular fields of engineering desirable, e.g. industrial forging but in cases where metallic structures are designed to withstand a certain load before yielding occurs, plasticity is unacceptable. Either way, understanding of the plasticity nature and ability to predict material behaviour during elastic-plastic deformation is crucial in the modern world, where engineering structures are inseparable part of our daily life.

2.4.1 Yielding criterions for ductile metals

The problem with determining when material (polycrystalline aggregate) starts to yield upon various combination of stress can be approximate by using yield surface, which is in the three dimensional space of the principal stresses set of yield points which define the boundary between elastic and plastic deformation [1].

2.4.1.1 Maximum shear stress criterion

The first yield criteria, which can define such a surface was established by Henri Tresca, Saint-Venant, Otto Mohr and James Guest during the 19th century [4]. Maximum shear stress criterion “assumes that yielding occurs when the maximum shear stress reaches the value of the shear stress in the uniaxial-tension test” [1]:

$$\frac{\sigma_1 - \sigma_3}{2} = \frac{\sigma_0}{2} \tag{2-7}$$

where $\sigma_1$is the largest and $\sigma_3$is the smallest principal stress and $\frac{\sigma_0}{2}$ is the shear stress when in the uniaxial-tension test the material starts to yield.

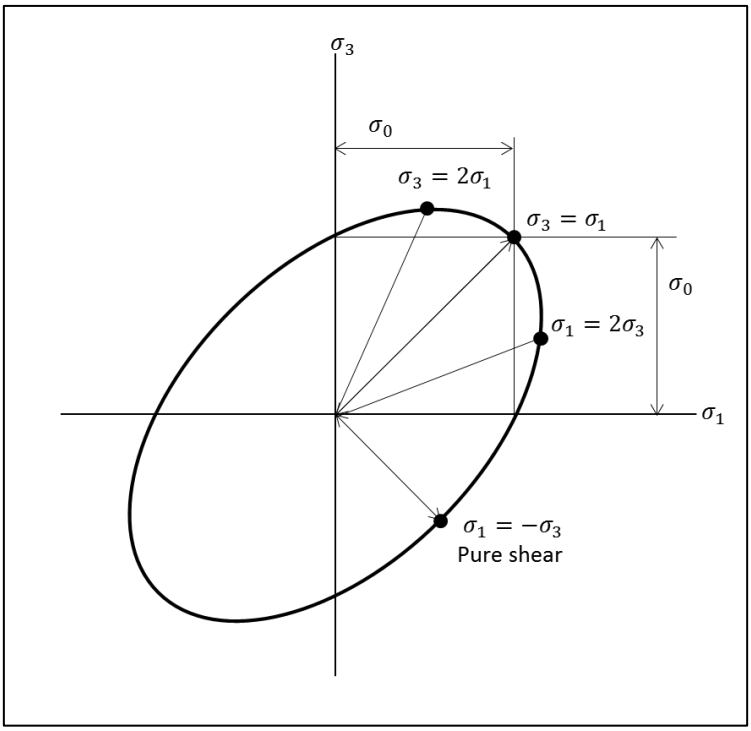

Figure 11 – The representation of the Von Mises criterion for plane stress deformation of an isotropic material [1]**.**

2.4.1.2 Von Mises yield criterion

In the early 20th century Von Mises suggested a new criterion based on the second invariant of the stress tensor J_2 and stated that if J_2 reaches a critical value, material will start to yield [1]. The Von Mises criterion is usually written in the following form:

$$\sigma_0 = \frac{1}{2}[(\sigma_1-\sigma_2)^2 + (\sigma_2-\sigma_3)^2 + (\sigma_3-\sigma_1)^2]^{1/2} \tag{2-8}$$

where σ_0 is the yield stress for uniaxial tension and σ_1, σ_2, σ_3 are the principal stresses. One of the physical interpretation of the Eq (2-8) is that the yielding occurs once the distortion energy (energy which is causing material shearing, not volume change) gets at critical value [1]. Now consider a material undergoing plane stress deformation. Then Eq (2-8) can be rewritten in a form that represents an ellipse:

$$\sigma_0{}^2 = \sigma_1{}^2+\sigma_3{}^2 - \sigma_1\sigma_3 \tag{2-9}$$

such an ellipse is called the yield locus [1], see Figure 11.

The main distinction between the Von Mises and Maximum shear stress yield criterion is that the latter does not take into account the middle principal stress and it has been proven that the intermediate principal stress influences yield condition of e.g. copper or aluminium [4]. Therefore the Von Mises criterion provides in some cases better approximation for determining material yielding. Note that both criterions are just empirical approximations and do not take in consideration anisotropic materials, where their response to mechanical loading is dependent on the direction of the load and boundary conditions.

2.4.1.3 Anisotropy in Yielding

Rodney Hill in 1948 proposed new formulation of the Von Mises yield criterion for an orthotropic material (special case of anisotropy):

$$1 = F(\sigma_1-\sigma_2)^2 + G(\sigma_2-\sigma_3)^2 + H(\sigma_3-\sigma_1)^2 \tag{2-10}$$

where F, G and H are constants that define the level of anisotropy. Yield locus for anisotropic material is distorted and is not symmetric as the isotropic yield locus in Figure 11.

Many improvements and suggestions of the Hill criterion have been lately proposed [2], but with an assumption, that the level of anisotropy in a metal is fixed throughout the calculation. However, this supposition in some particular cases can cause insufficient accuracy in predicting material (e.g. springback effect after the sheet metal stamping process [3]) and does not allow us to fully predict physical phenomena of metal deformation. That is why there is vast intention of development new methods such as CPFEM.

2.5 Pole Figures

Pole figures [1] are discussed here, because the data (precisely, crystals orientation) extracted from an experiment can be compared directly with a numerical analysis and its accuracy can be verified.

The information about crystals orientation can be obtained by X-ray irradiation of polycrystalline aggregate using a diffractometer. A beam of X-rays strikes a polycrystalline aggregate. After an impact, the beam of the light is spread into many specific directions and from the angles and intensities of these diffracted beams, 2D representation of crystals orientation is obtained, which is called the pole figure. There two main methods of obtaining the pole figure: the stereographic projection (used in this project to generate pole diagrams) and the equal-are projection [1]. In Figure 12 is illustrated how the orientation of one face for a single cubic crystal [1 0 0] is obtained by using stereographic projection. Let's have a single cubic crystal surrounded by an imaginary sphere which is cut in the middle by a plane. When a vector, which is normal to the crystal face, meets sphere, point A is obtained. Then, the point A is connected to the most southerly point of the sphere S and the point X is obtained, which is the intersection of line AS and the middle plane. This point X is then projected in the 2D pole figure. Normally pole figure represents family of directions such as <1 0 0>, <1 1 0 >, or <1 1 1> and for all crystals within the crystal aggregate (for an example see Figure 25).

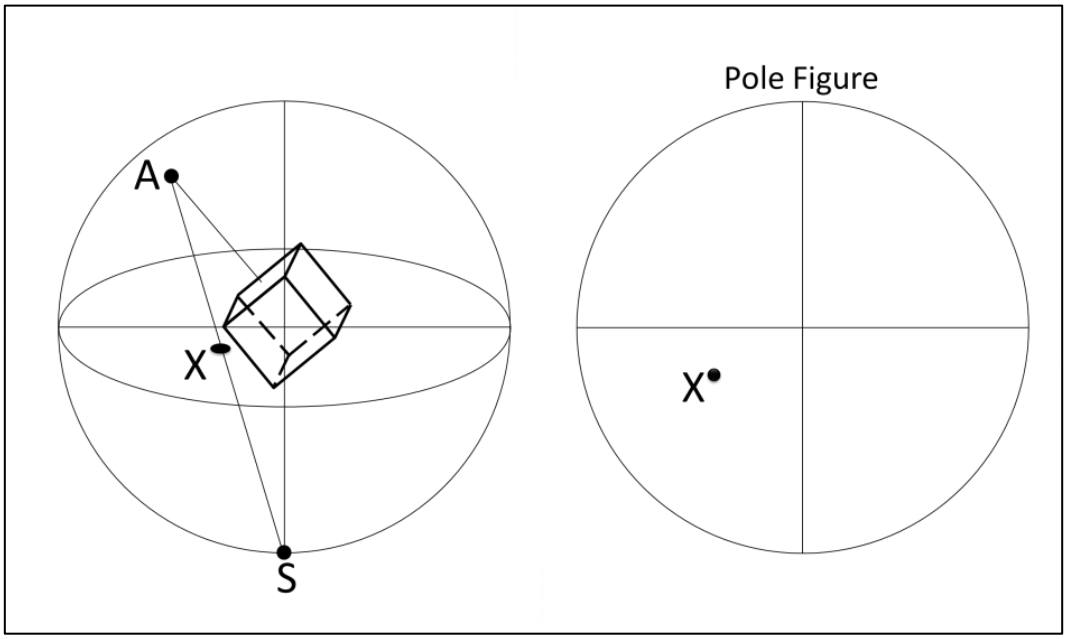

Figure 12 – Crystallographic projection of a single face of cubic crystal [1 0 0].

2.6 Conclusion

This section introduces the atomistic theory of metals and their behaviour during the elastic-plastic deformation, where the composition and structure of a single crystal and a crystal aggregate are presented together with elastic plastic deformation mechanisms. Afterward, common assumptions and their limitations when modelling plasticity in metals are discussed. At the end, the crystallographic projection is briefly explained as a method to obtain information about crystal distribution within a polycrystalline aggregate.

The theory covered in this section provides a physical explanation of deformation in ductile metals. The following chapter will describe this behaviour in terms of continuum mechanics, which is used for solving of many engineering problems, including large deformations of metals.

3 REVIEW OF CONTINUUM MECHANICS

Continuum mechanics description is used for solving engineering problems as working with material on the atomistic level is not in the engineering scale applicable. In this approximation, the behaviour of a large number of particles is simplified into a continuum mass with physical quantities that characterize averages over a volume. This chapter introduces the basic concepts of continuum mechanics, which should allow the reader to understand the continuum theory of Crystal Plasticity covered in this work. For more details of continuum mechanics, please see Reference [12], where following is a summary from this reference.

3.1 Kinematics

Kinematics is in this case a part of the continuum mechanics, which is concern with displacement and motion of a material body regardless to its cause [12].

3.1.1 Continuum body and motion

Consider the deformable body $\mathcal{B}$ in the three dimensional Euclidean space having a continuum mass over its volume and described by continuum particles (material points) $X \in \mathcal{B}$ [12]. This body $\mathcal{B}$ occupies territory Ω_0 called reference configuration at time t_0 and region Ω called current configuration at time t and it is related to the fixed Cartesian coordinate system with its origin O and basis vectors $\boldsymbol{e}_1, \boldsymbol{e}_2, \boldsymbol{e}_3$. The motion of the body $\mathcal{B}$ from the reference configuration Ω_0 to the current configuration Ω is described by $\boldsymbol{\chi}$ [12]:

$$\boldsymbol{x} = \boldsymbol{\chi}(\boldsymbol{X}, t) \tag{3-1}$$

where $\boldsymbol{x}$ is the position vector of a material point x in Ω and $\boldsymbol{X}$ is the position vector of the same material point X in Ω_0. The displacement between the configurations is represented by $\boldsymbol{U}$ in the Langrangian form [12]:

$$\boldsymbol{U}(\boldsymbol{X}, t) = \boldsymbol{x}(\boldsymbol{X}, t) - \boldsymbol{X} \tag{3-2}$$

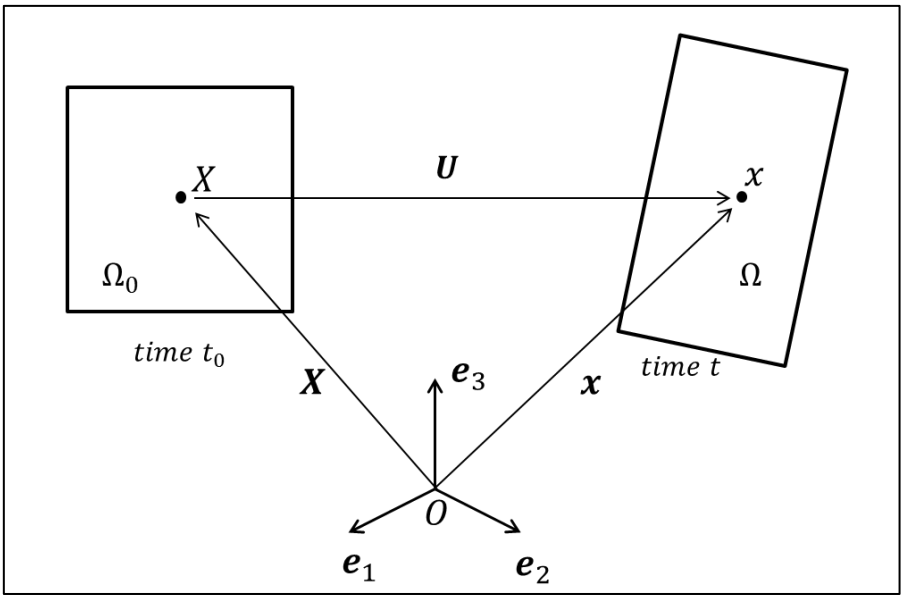

Figure 13 – Motion of the continuum body $\mathcal{B}$ from the reference configuration Ω_0 to the current configuration Ω [12]**.**

3.1.2 Deformation gradient

Let's consider the same deformation as in Figure 13 and introduce material fibre $d\boldsymbol{X}$ in the reference configuration as it is shown in Figure 14, which can be homogenously map to the current configuration as $d\boldsymbol{x}$ [12]:

$$d\boldsymbol{x} = \frac{\partial \boldsymbol{x}}{\partial \boldsymbol{X}} \cdot d\boldsymbol{X}, \tag{3-3}$$

where the partial differentiation is called the material deformation gradient $\mathbf{F}$ [12]:

$$\mathbf{F} = \frac{\partial \boldsymbol{x}}{\partial \boldsymbol{X}} = \mathrm{Grad}\boldsymbol{x}(\boldsymbol{X}, t) \tag{3-4}$$

This second order tensor is description of the change of shape and size of the neighbourhood of the material point during the motion from the reference configuration Ω_0 to the current configuration Ω [12].

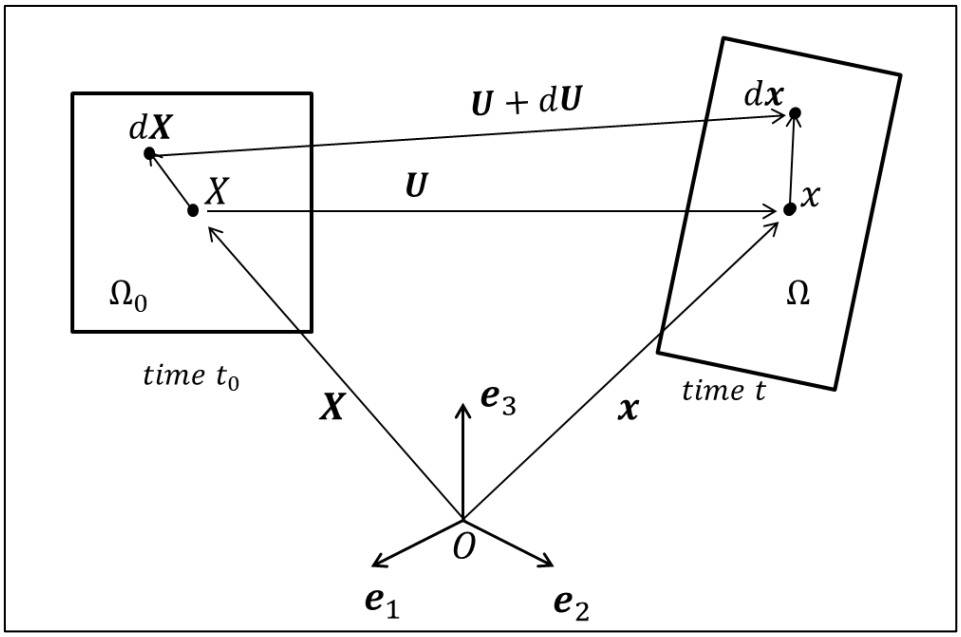

Figure 14 - Motion of the material fibre dX from the reference configuration Ω_0 to the current configuration Ω [12]**.**

The determinant of the deformation gradient $\mathbf{F}$ is known as Jacobian determinant and it represents volume ratio between reference and current configuration [12]:

$$J = \det\mathbf{F} = \frac{dV}{dV_0} \tag{3-5}$$

3.1.3 Strain tensor

There is a wide range of different definitions of the strain. Here is considered only one, namely the Green-Lagrange strain tensor [12]. By considering change of square of the magnitude of the material fibre $d\boldsymbol{X}$ it can be written that:

$$\begin{aligned} |d\boldsymbol{x}|^2 - |d\boldsymbol{X}|^2 &= (\mathbf{F}\cdot d\boldsymbol{X})(\mathbf{F}\cdot d\boldsymbol{X}) - d\boldsymbol{X}\cdot d\boldsymbol{X} = d\boldsymbol{X}(\mathbf{F}^{\mathrm{T}}\cdot\mathbf{F})d\boldsymbol{X} - d\boldsymbol{X}\cdot d\boldsymbol{X} \\ &= d\boldsymbol{X}(\mathbf{F}^{\mathrm{T}}\cdot\mathbf{F}-\mathbf{I})d\boldsymbol{X} = 2d\boldsymbol{X}\cdot\mathbf{E}\cdot d\boldsymbol{X} \end{aligned} \tag{3-6}$$

and from here, the Green Lagrange symmetric strain tensor is defined:

$$\mathbf{E} = \frac{1}{2}(\mathbf{F}^{\mathrm{T}}\cdot\mathbf{F}-\mathbf{I}), \tag{3-7}$$

where $\mathbf{I}$ is identity tensor and $\mathbf{E}$ is defined with respect to the reference configuration [12].

3.1.4 Deformation rates

Next is the outline of how the position, shape and size vary with time during the motion $\boldsymbol{x} = \boldsymbol{\chi}(\boldsymbol{X}, t)$ [12].

3.1.4.1 Material velocity gradient

The rate of the deformation gradient is called material velocity gradient [12] and is defined as follows:

$$\dot{\mathbf{F}} = \frac{\partial}{\partial t}\frac{\partial \boldsymbol{x}}{\partial \boldsymbol{X}} = \frac{\partial}{\partial \boldsymbol{X}}\frac{\partial \boldsymbol{x}}{\partial t} = \frac{\partial \dot{\boldsymbol{x}}}{\partial \boldsymbol{X}} = \mathrm{Grad}\boldsymbol{V}(\boldsymbol{X}, t) \tag{3-8}$$

or in index notation [12]:

$$\dot{F}_{ij} = \frac{\partial \dot{x}_i}{\partial X_j}. \tag{3-9}$$

The rate of the deformation gradient represents relative velocity between two locations in the reference configuration Ω_0 [12].

3.1.4.2 Spatial velocity gradient

The velocity field is given as:

$$\boldsymbol{v}(\boldsymbol{x}, t) = \frac{\partial \boldsymbol{x}}{\partial t} \tag{3-10}$$

and the spatial velocity gradient $\mathbf{l}$ [12] is derivative of a velocity field $\boldsymbol{v}$ with respect to the current configuration:

$$\mathbf{l}(\mathbf{x}, t) = \frac{\partial \boldsymbol{v}}{\partial \boldsymbol{x}}, \tag{3-11}$$

which represents relative velocity between two locations in the current configuration Ω.

The relation between the velocity gradient $\mathbf{l}$ and the deformation gradient $\mathbf{F}$ is [12]:

$$\mathbf{l} = \frac{\partial \boldsymbol{v}(\boldsymbol{x}, t)}{\partial \boldsymbol{x}} = \frac{\partial \dot{\boldsymbol{x}}}{\partial \boldsymbol{x}} = \frac{d}{dt}\frac{\partial \boldsymbol{x}}{\partial \boldsymbol{X}}\frac{\partial \boldsymbol{X}}{\partial \boldsymbol{x}} = \dot{\mathbf{F}}\mathbf{F}^{(-1)} \tag{3-12}$$

3.2 The Concept of Stress

The motion and deformation described in previous section is caused by external and internal forces acting on the deformable body. These forces produce within the body a stress, which is defined as a force per unit area [12].

Let us use the same kinematic framework as in Section 3.1 with an arbitrary external forces acting on the surface of the body and internal forces acting within the body. Let us consider the body cut by an imaginary plane into two parts as can be seen in Figure 15 and consider the lower part. Infinite small force $d\boldsymbol{f}$ acting on the surface element is the same for the current configuration and for the reference configuration [12]:

$$d\boldsymbol{f} = \boldsymbol{t}ds = \boldsymbol{T}dS\,, \tag{3-13}$$

$$\boldsymbol{t} = \boldsymbol{t}(\boldsymbol{x}, t, \boldsymbol{n}), \boldsymbol{T} = \boldsymbol{T}(\boldsymbol{X}, t, \boldsymbol{N})$$

The Cauchy stress $\boldsymbol{\sigma}$ and the Cauchy traction vector $\boldsymbol{t}$ [12] acting on a surface ds with its normal unit vector $\boldsymbol{n}$ are defined in the current configuration.

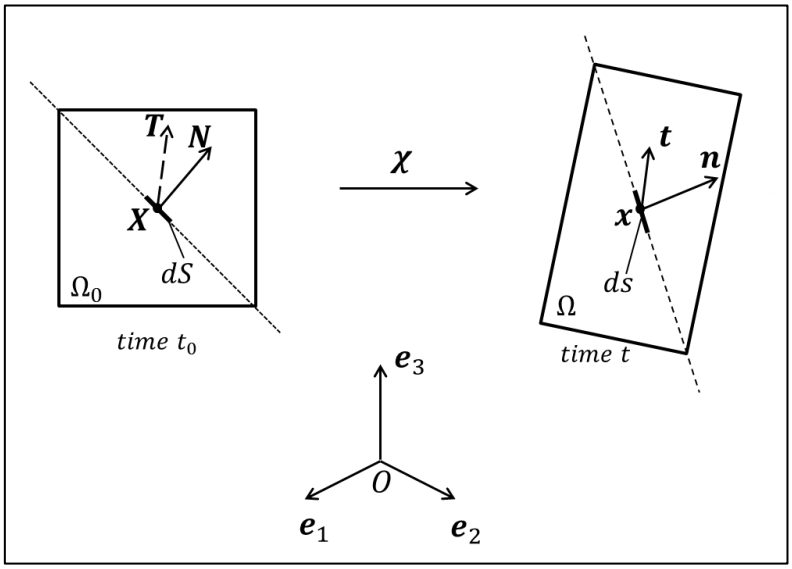

Figure 15 – Stress occurring due to traction vectors acting on infinitesimal surface elements [12]**.**

In the reference configuration is defined the first Piola-Kirchhoff stress $\mathbf{P}$ and the first Piola-Kirchhoff traction vector $\boldsymbol{T}$ (has the same direction as $\boldsymbol{t}$, but different magnitude [12]) acting on a surface dS with its normal unit vector $\boldsymbol{N}$. Here the Cauchy's stress theorem is introduced:

$$\boldsymbol{t}(\boldsymbol{x}, t, \boldsymbol{n}) = \boldsymbol{\sigma}(\boldsymbol{x}, t)\, \boldsymbol{n}, \tag{3-14}$$

$$\boldsymbol{T}(\boldsymbol{X}, t, \boldsymbol{N}) = \mathbf{P}(\boldsymbol{X}, t)\, \boldsymbol{N}$$

The first Piola-Kirchhoff stress can be pushed forward to the current configuration:

$$\boldsymbol{\sigma} = J^{-1}\mathbf{P}\mathbf{F}^{\mathrm{T}} = \boldsymbol{\sigma}^{\mathrm{T}}\,, \tag{3-15}$$

or the symmetric Cauchy stress pulled back [12]:

$$\mathbf{P} = J\boldsymbol{\sigma}\mathbf{F}^{-\mathrm{T}}. \tag{3-16}$$

The first Piola-Kirchhoff stress $\mathbf{P}$ is not a symmetric tensor, which is not convenient for the use in constitute models. For that reason the second Piola-Kirchhoff stress $\mathbf{S}$ [12] was introduced:

$$\mathbf{S} = J\mathbf{F}^{-1}\boldsymbol{\sigma}\mathbf{F}^{-\mathrm{T}} = \mathbf{S}^{\mathrm{T}}\,, \tag{3-17}$$

where $\mathbf{S}$ is fully defined in the reference configuration. Another alternative stress tensor widely used is the Kirchhoff stress tensor $\boldsymbol{\tau}$ termed in the current configuration and differs from Cauchy stress only by the volume ratio J [12]:

$$\boldsymbol{\tau} = J\boldsymbol{\sigma} = \boldsymbol{\tau}^{\mathrm{T}}\,. \tag{3-18}$$

3.3 Objective Rates

The constitutive laws are mostly expressed in terms of increments and it is important to introduce objective time derivatives of stresses [12].

3.3.1 Jaumann rate of the Cauchy stress

Euclidean transformation of the Cauchy stress tensor $\boldsymbol{\sigma}$ [12] is given by equation (3-19) and fulfils the requirement of objectivity.

$$\boldsymbol{\sigma}^{+} = \mathbf{Q} \cdot \boldsymbol{\sigma} \cdot \mathbf{Q}^{\mathbf{T}}, \tag{3-19}$$

where $\mathbf{Q}$ is the proper orthogonal tensor [12]:

$$\mathbf{Q} \cdot \mathbf{Q}^{\mathbf{T}} = \mathbf{1}; \det\mathbf{Q} = +\mathbf{1}. \tag{3-20}$$

However the stress rate is not objective:

$$\dot{\boldsymbol{\sigma}}^{+} \neq \mathbf{Q} \cdot \dot{\boldsymbol{\sigma}} \cdot \mathbf{Q}^{\mathbf{T}}, \tag{3-21}$$

and is derived by the product rule of differentiation:

$$\frac{\mathbf{d}}{\mathbf{dt}}(\boldsymbol{\sigma}^{+}) = \dot{\boldsymbol{\sigma}}^{+} = \dot{\mathbf{Q}} \cdot \boldsymbol{\sigma} \cdot \mathbf{Q}^{\mathbf{T}} + \mathbf{Q} \cdot \dot{\boldsymbol{\sigma}} \cdot \mathbf{Q}^{\mathbf{T}} + \mathbf{Q} \cdot \boldsymbol{\sigma} \cdot \dot{\mathbf{Q}}^{\mathbf{T}}. \tag{3-22}$$

Rigid body rotation involves the transformation of the spin tensor $\mathbf{w}$, the skew-symmetric part of the spatial velocity gradient $\mathbf{l}$ [12]:

$$\mathbf{w}^{+} = \dot{\mathbf{Q}}\mathbf{Q}^{\mathbf{T}} + \mathbf{Q}\mathbf{w}\mathbf{Q}^{\mathbf{T}}. \tag{3-23}$$

Proof of Eq (3-23):

Euclidean transformation of the deformation gradient $\mathbf{F}$:

$$\mathbf{F}^{+} = \frac{\partial \mathbf{x}^{+}}{\partial \mathbf{X}} = \mathbf{Q}\frac{\partial \mathbf{x}}{\partial \mathbf{X}} = \mathbf{Q}\mathbf{F} \tag{3-24}$$

and of the spatial velocity gradient $\mathbf{l}$ are written as follows:

$$\mathbf{l}^{+} = (\dot{\mathbf{F}}\mathbf{F}^{-\mathbf{1}})^{+} = \dot{\mathbf{F}}^{+}(\mathbf{F}^{+})^{-\mathbf{1}} = (\dot{\mathbf{Q}}\mathbf{F} + \mathbf{Q}\dot{\mathbf{F}})(\mathbf{F}^{-\mathbf{1}}\mathbf{Q}^{\mathbf{T}}) = \dot{\mathbf{Q}}\mathbf{Q}^{\mathbf{T}} + \mathbf{Q}\mathbf{l}\mathbf{Q}^{\mathbf{T}}, \tag{3-25}$$

The spatial velocity gradient can be decomposed to the symmetric and skew-symmetric part:

$$\mathbf{l}(\mathbf{x}, \mathrm{t}) = \mathbf{d}(\mathbf{x}, \mathrm{t}) + \mathbf{w}(\mathbf{x}, \mathrm{t}), \tag{3-26}$$

where the $\mathbf{d}$ is the stretch rate tensor and $\mathbf{w}$ is the spin tensor [12]:

$$\mathbf{d} = \frac{1}{2}(\mathbf{l} + \mathbf{l}^{\mathbf{T}}) = \mathbf{d}^{\mathbf{T}}, \tag{3-27}$$

$$\mathbf{w} = \frac{\mathbf{1}}{\mathbf{2}}(\mathbf{l} - \mathbf{l}^{\mathbf{T}}) = -\mathbf{w}^{\mathbf{T}}. \tag{3-28}$$

Note that $\mathbf{d}$ is not a pure rate of plastic strain and $\boldsymbol{\omega}$ is not a pure rate of rotation [12].

By using Eq's (3-25),(3-26), (3-28) the Eq (3-23) the equation can be proven:

$$\mathbf{w}^{+} = \left[\frac{\mathbf{1}}{\mathbf{2}}(\mathbf{l} - \mathbf{l}^{\mathbf{T}})\right]^{+} = \frac{\mathbf{1}}{\mathbf{2}}\mathbf{l}^{*} - \frac{\mathbf{1}}{\mathbf{2}}(\mathbf{l}^{+})^{\mathbf{T}} \tag{3-29}$$

$$= \frac{\mathbf{1}}{\mathbf{2}}\left(\dot{\mathbf{Q}}\mathbf{Q}^{\mathbf{T}} + \mathbf{Q}\mathbf{d}\mathbf{Q}^{\mathbf{T}} + \mathbf{Q}\mathbf{w}\mathbf{Q}^{\mathbf{T}}\right) - \frac{\mathbf{1}}{\mathbf{2}}\{(-\dot{\mathbf{Q}}\mathbf{Q}^{\mathbf{T}}) + [\mathbf{Q}(\mathbf{d} + \mathbf{w})\mathbf{Q}^{\mathbf{T}}]^{\mathbf{T}}$$

$$= \dot{\mathbf{Q}}\mathbf{Q}^{\mathbf{T}} + \mathbf{Q}\mathbf{w}\mathbf{Q}^{\mathbf{T}}..$$

Now from Eq (3-23) it is possible to express rate of the orthogonal tensor $\mathbf{Q}$ and its transpose $\mathbf{Q}^{\mathbf{T}}$ [12]:

$$\dot{\mathbf{Q}} = \mathbf{w}^{+}\mathbf{Q} - \mathbf{Q}\mathbf{w} \tag{3-30}$$

$$(\dot{\mathbf{Q}^{\mathbf{T}}}) = -\mathbf{Q}^{\mathbf{T}}\mathbf{w}^{+} + \mathbf{w}\mathbf{Q}^{\mathbf{T}}. \tag{3-31}$$

By implementing Eq's (3-30) and (3-31) into Eq (3-22) following expression is obtained:

$$\dot{\boldsymbol{\sigma}}^{+} = (\mathbf{w}^{+}\mathbf{Q} - \mathbf{Q}\mathbf{w}) \cdot \boldsymbol{\sigma} \cdot \mathbf{Q}^{\mathbf{T}} + \mathbf{Q} \cdot \dot{\boldsymbol{\sigma}} \cdot \mathbf{Q}^{\mathbf{T}} + \mathbf{Q} \cdot \boldsymbol{\sigma} \cdot (-\mathbf{Q}^{\mathbf{T}}\mathbf{w}^{+} + \mathbf{w}\mathbf{Q}^{\mathbf{T}}), \tag{3-32}$$

then the relation can be written that:

$$(\dot{\boldsymbol{\sigma}} - \mathbf{w}\boldsymbol{\sigma} + \boldsymbol{\sigma}\mathbf{w})^{+} = \mathbf{Q}(\dot{\boldsymbol{\sigma}} - \mathbf{w}\boldsymbol{\sigma} + \boldsymbol{\sigma}\mathbf{w})\mathbf{Q}^{\mathbf{T}} \tag{3-33}$$

and the Jaumann rate of Cauchy stress $\boldsymbol{\sigma}^{\boldsymbol{\nabla}}$ [12] which is the term in the brackets can be introduced**:**

$$\boldsymbol{\sigma}^{\boldsymbol{\nabla}} = \dot{\boldsymbol{\sigma}} - \mathbf{w}\boldsymbol{\sigma} + \boldsymbol{\sigma}\mathbf{w}. \tag{3-34}$$

Finally, its objectivity can be proved:

$$\boldsymbol{\sigma}^{\boldsymbol{\nabla}^{+}} = \mathbf{Q}\boldsymbol{\sigma}^{\boldsymbol{\nabla}}\mathbf{Q}^{\mathbf{T}}. \tag{3-35}$$

3.3.2 Jaumann rate of the Kirchhoff stress

Euclidean transformation of the Kirchhoff stress tensor $\boldsymbol{\tau}$ [12] is given by equation (3-36) and fulfils the requirement of objectivity [12].

$$\boldsymbol{\tau}^{+} = \mathbf{Q} \cdot \boldsymbol{\tau} \cdot \mathbf{Q}^{\mathbf{T}}, \tag{3-36}$$

where $\mathbf{Q}$ is the proper orthogonal tensor [12]:

$$\mathbf{Q} \cdot \mathbf{Q}^{\mathbf{T}} = \mathbf{1}; \det\mathbf{Q} = +\mathbf{1}. \tag{3-37}$$

However the stress rate is not objective:

$$\dot{\boldsymbol{\tau}}^{+} \neq \mathbf{Q} \cdot \dot{\boldsymbol{\tau}} \cdot \mathbf{Q}^{\mathbf{T}} \tag{3-38}$$

and is derived by the product rule of differentiation:

$$\frac{\mathbf{d}}{\mathbf{dt}}(\boldsymbol{\tau}^{+}) = \dot{\boldsymbol{\tau}}^{+} = \dot{\mathbf{Q}} \cdot \boldsymbol{\tau} \cdot \mathbf{Q}^{\mathbf{T}} + \mathbf{Q} \cdot \dot{\boldsymbol{\tau}} \cdot \mathbf{Q}^{\mathbf{T}} + \mathbf{Q} \cdot \boldsymbol{\tau} \cdot \dot{\mathbf{Q}}^{\mathbf{T}}. \tag{3-39}$$

which can be written in terms of Cauchy stress [12]:

$$\frac{\mathbf{d}}{\mathbf{dt}}(\mathrm{J}\boldsymbol{\sigma}^{+}) = \dot{\mathbf{Q}} \cdot \mathrm{J}\boldsymbol{\sigma} \cdot \mathbf{Q}^{\mathbf{T}} + \mathbf{Q} \cdot \dot{\mathrm{J}}\boldsymbol{\sigma} \cdot \mathbf{Q}^{\mathbf{T}} + \mathbf{Q} \cdot \mathrm{J}\boldsymbol{\sigma} \cdot \dot{\mathbf{Q}}^{\mathbf{T}}. \tag{3-40}$$

By implementing Eq's (3-30) and (3-31) into Eq (3-40) and with defining the material time derivative of the volume ratio $\dot{J} = J\mathrm{tr}(\mathbf{d})$ the following can be written:

$$\dot{\mathrm{J}}\boldsymbol{\sigma}^{+} + \mathrm{J}\dot{\boldsymbol{\sigma}}^{+} = (\mathbf{w}^{+}\mathbf{Q} - \mathbf{Q}\mathbf{w}) \cdot \mathrm{J}\boldsymbol{\sigma} \cdot \mathbf{Q}^{\mathbf{T}} + \mathbf{Q} \cdot \mathrm{J}\dot{\boldsymbol{\sigma}} \cdot \mathbf{Q}^{\mathbf{T}} + \mathbf{Q} \cdot \dot{\mathrm{J}}\boldsymbol{\sigma} \cdot \mathbf{Q}^{\mathbf{T}} + \mathbf{Q} \cdot \mathrm{J}\boldsymbol{\sigma} \cdot (-\mathbf{Q}^{\mathbf{T}}\mathbf{w}^{+} + \mathbf{w}\mathbf{Q}^{\mathbf{T}}) \tag{3-41}$$

and then following expression obtained:

$$(\dot{\boldsymbol{\sigma}} + \mathrm{tr}(\mathbf{d})\boldsymbol{\sigma} + -\mathbf{w}\boldsymbol{\sigma} + \boldsymbol{\sigma}\mathbf{w})^{+} = \mathbf{Q}(\dot{\boldsymbol{\sigma}} + \mathrm{tr}(\mathbf{d})\boldsymbol{\sigma} - \mathbf{w}\boldsymbol{\sigma} + \boldsymbol{\sigma}\mathbf{w})\mathbf{Q}^{\mathbf{T}}. \tag{3-42}$$

Finally the Jaumann rate of Kirchhoff stress $\boldsymbol{\tau}^{\boldsymbol{\nabla}}$ [12] in terms of Cauchy stress can be introduced**:**

$$\boldsymbol{\tau}^{\boldsymbol{\nabla}} = \dot{\boldsymbol{\sigma}} + \mathrm{tr}(\mathbf{d})\boldsymbol{\sigma} + -\mathbf{w}\boldsymbol{\sigma} + \boldsymbol{\sigma}\mathbf{w} \tag{3-43}$$

and by using Equation (3-34) one get relation as:

$$\boldsymbol{\tau}^{\nabla^+} = \boldsymbol{\sigma}^{\nabla} + \mathrm{tr}(\mathbf{d})\boldsymbol{\sigma} = \boldsymbol{\sigma}^{\nabla} + \boldsymbol{\sigma}(\mathbf{I} : \mathbf{d}). \tag{3-44}$$

3.4 Single Crystal Strength Model Theory

The atomistic nature of metals and its behaviour during mechanical deformation can be described by numerous crystal plasticity models which are based on continuum mechanics. Following gives their brief review, for broader overview please see reference [3].

The main distinctions between crystal plasticity models are in:

1. Solving problems with different material microstructure (FCC [6; 9; 13], BCC [14], HCP crystal systems [15][16]).
2. Different representation of the crystallographic texture:
    a. Discrete mapping, where each integration point in the finite element mesh is representing a single crystal or a grain [7; 10; 15].
    b. Homogenization, where averaged material properties over volume are used [17; 18].
3. Solving problems with different deformation mechanisms (crystal slip [10], twinning [16; 19], martensite formation or damage [3]).
4. Using different types of constitutive models:
    a. Phenomenological - the constitutive laws are based on empirical observations [20; 21].
    b. Microstructure-based approach - the constitutive laws capture more precisely nature of plastic deformation; an example is a model which is built on the dislocation density theory [22-24].

In this research has been chosen the Single Crystal Strength Model, because it is able to predict deformation of FCC and BCC structures [20] with different strain rate setting and its details description is available as it has been used by many other researchers [7; 10; 21; 25-27].

The bases of the Single Crystal Strength Model theory were laid by Taylor [28]. Later, Rice [29] and Hill and Rice [30] developed general framework for the

finite elastic-plastic deformations for the rate independent materials, which was extended by the rate dependent constitutive law by Peirce et al [31]. Many researches made vital contribution to the crystal plasticity theory and following is a summary of their work [3; 27; 32-35].

3.4.1 Kinematics of Plastic Deformation

Dislocation slip is introduced in this work as the only plastic deformation mechanism and is presented in the context of continuum mechanics. The consequence is that the atomistic representation of the structure is lost, but the slip system geometry and stress notion are preserved. First, theoretical description of a single slip for kinematics with small deformations will be introduced and later it will be extended for finite deformation caused by the multislip.

Let's assume that a single crystal element is a deformable continuum body, denoted by $\mathcal{B}$, which is composed of a set of material points, represented by $P \in \mathcal{B}$ and is considered in the three-dimensional Euclidean space at a given time t. Further, a fixed reference frame described by Cartesian coordinate system in three dimension with a fixed origin O and basis vectors $\boldsymbol{e}_1, \boldsymbol{e}_2, \boldsymbol{e}_3$ *(*where $\boldsymbol{e}_1$ is perpendicular to the paper) is introduced. Let's presume that this crystal element has only one crystal slip plane (one slip system) defined by the crystallographic direction represented by two unit vectors: $\boldsymbol{N}$ as a normal to the slip plane and $\boldsymbol{S}$ as a slip direction of the dislocation flow. These vectors remain during plastic shearing unchanged, as well as the volume of the crystal [20], see Figure 16.

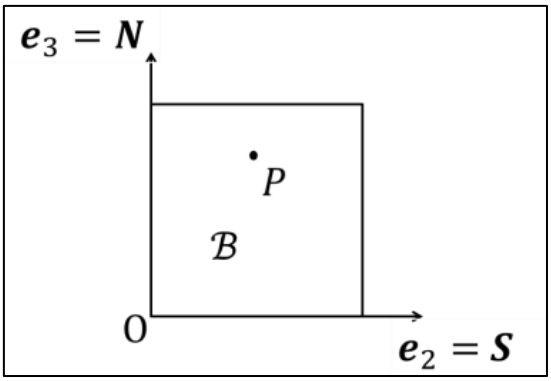

Figure 16 – Single crystal element with one slip system described in sense of continuum mechanics [27]**.**

3.4.1.1 Small plastic deformation of a single crystal

Now, consider a crystal element $\mathcal{B}$ (with the same properties as described above) with a material point $\mathrm{X} \in d\mathcal{B}$ at time $t = 0$, where its position is defined by a material vector $d\boldsymbol{X}$ in the reference configuration Ω_0. During plastic shearing given by a shear γ, the material point X moves to a point x that is termed in the current configuration Ω at time Δt. Position of x is described by a spatial vector $d\boldsymbol{x}$. This shearing is given by motion $\boldsymbol{\chi}$:

$$d\boldsymbol{x} = \boldsymbol{\chi}(d\boldsymbol{X}, \mathrm{d}t). \tag{3-45}$$

Finally, $d\mathbf{U}$ represents in Figure 17 the displacement between points X and x. That is described as follows (in Lagrangian form):

$$d\boldsymbol{U}(d\boldsymbol{X}, dt) = d\boldsymbol{x}(\boldsymbol{X}, t) - d\boldsymbol{X} \tag{3-46}$$

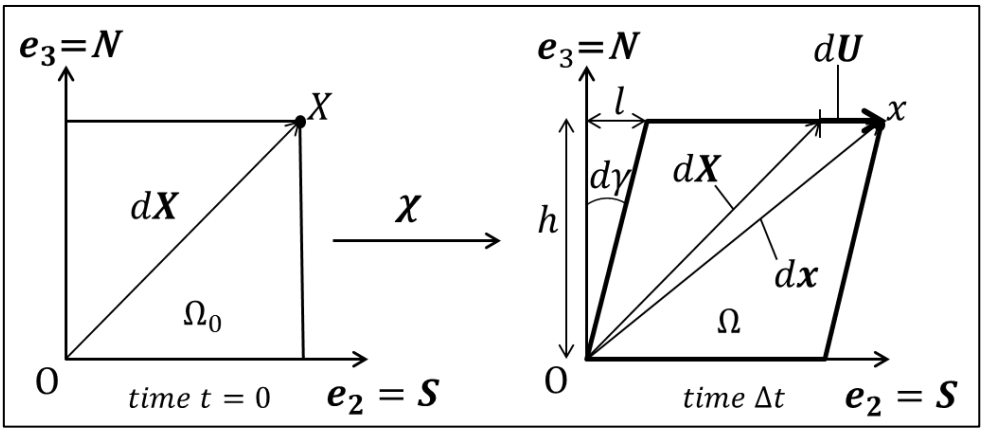

Figure 17 – Plastic shearing on a slip system [27].

When assumption of small rotations ($\tan\alpha = \alpha$) and stretching is applied, it can be written that:

$$\frac{l}{h} = \gamma, \tag{3-47}$$

$$h = \boldsymbol{N} \cdot d\boldsymbol{X}, \tag{3-48}$$

$$l = \gamma \boldsymbol{N} \cdot d\boldsymbol{X}. \tag{3-49}$$

It can be seen that:

$$l = |d\boldsymbol{U}|, \tag{3-50}$$

$$|d\boldsymbol{U}| = \gamma \boldsymbol{N} \cdot d\boldsymbol{X} \tag{3-51}$$

Now:

$$d\boldsymbol{U} = |d\boldsymbol{U}|\boldsymbol{S}, \tag{3-52}$$

$$d\boldsymbol{U} = d\boldsymbol{x}(\boldsymbol{X}, t) - d\boldsymbol{X} = \gamma \boldsymbol{S}(\boldsymbol{N} \cdot d\boldsymbol{X}), \tag{3-53}$$

And in index notation:

$$dx_i - dX_i = \gamma S_i N_j dX_j, \tag{3-54}$$

After differentiating both sides with respect to the time one gets following:

$$\frac{d}{dt}\frac{dx_i}{dX_j} = \frac{d}{dt}\gamma S_i N_j, \tag{3-55}$$

Expressed in Newton's notation:

$$\frac{d\dot{x}_i}{dX_j} = \dot{\gamma} S_i N_j, \tag{3-56}$$

Next, chain rule is applied:

$$\frac{\frac{\partial \dot{x}_i}{\partial X_j} dX_j}{dX_j} = \dot{\gamma} S_i N_j, \tag{3-57}$$

And finally:

$$\frac{\partial \dot{x}_i}{\partial X_j} = \dot{\gamma} S_i N_j, \tag{3-58}$$

where the left side of the equation is the material velocity gradient defined with respect to the reference configuration, $\boldsymbol{S}\otimes\boldsymbol{N}$ is the tensor product between the slip direction and normal to the slip.

In the case of multislip, the total plastic deformation is a superposition of shear strains in each active slip system α and Equation (3-58) can be re-written for n slip systems, then it stands that:

$$\mathbf{L}^{\mathrm{p}} = \sum_{\alpha=1}^{n} \dot{\gamma}^{\alpha} \boldsymbol{S}^{\alpha} \otimes \boldsymbol{N}^{\alpha}, \tag{3-59}$$

where superscript p is always since now associated with the plastic deformation. Note that the calculations above are summary from the reference [27].

3.4.1.2 Finite plastic deformation of a single crystal

Rice [29] extended theoretical description of a slip for cases of finite deformation. Procedure from section above becomes valid for a large deformation (small rotations and finite stretching) if it is considered as a sequence of small deformations, i.e. small microstructural rearrangements governed by its associated forces.

If in the same framework (Figure 17), the crystal element undergoes again plastic deformation, where the shear is considered small, from deformed configuration at time t to further deformed state at time $t + \Delta t$, the material point X and x are substituted by x_t and $x_{t+\Delta t}$ and if the same process as for small deformation is followed, one can write:

$$d\dot{\boldsymbol{x}} = \dot{\gamma}\boldsymbol{s}(\boldsymbol{n} \cdot d\boldsymbol{x}), \tag{3-60}$$

$$\frac{d\dot{\boldsymbol{x}}}{d\boldsymbol{x}} = \dot{\gamma}\boldsymbol{s}\otimes\boldsymbol{n}, \tag{3-61}$$

where the left side of the Equation (3-61) is the spatial velocity gradient $\mathbf{l}^{\mathrm{p}}$ (the incremental deformation happened this time in the current configuration) and where $\boldsymbol{s}$ is a slip direction of the dislocation flow and $\boldsymbol{n}$ is the normal to the slip plane, both defined with respect to the current configuration. For the case of multislip, the total plastic deformation is a superposition of shear strains in each active slip system α and it can be stated that [27]:

$$\mathbf{l}^{\mathrm{p}} = \sum_{\alpha=1}^{\mathrm{n}} \dot{\gamma}^{\alpha} \boldsymbol{s}^{\alpha} \otimes \boldsymbol{n}^{\alpha}. \tag{3-62}$$

This spatial velocity gradient can be decomposed into the plastic symmetric and skew-symmetric part which is rate of deformation sometimes called stretch rate tensor or simply stretch tensor $\mathbf{d}^{\mathrm{p}}$ and spin tensor $\boldsymbol{\omega}^{\mathrm{p}}$ respectively:

$$\mathbf{l}^{\mathrm{p}} = \frac{1}{2}(\mathbf{l}^{p} + \mathbf{l}^{\mathrm{pT}}) + \frac{1}{2}(\mathbf{l}^{p} - \mathbf{l}^{\mathrm{pT}}) = \mathbf{d}^{\mathrm{p}} + \boldsymbol{\omega}^{\mathrm{p}}. \tag{3-63}$$

As it was mentioned before $\mathbf{d}^{\mathrm{p}}$ is not a pure rate of plastic strain and $\boldsymbol{\omega}^{\mathrm{p}}$ is not a pure rate of rotation [12].

Considering ideal plastic deformation due to a single slip on the crystal element it can be showed that:

$$\mathbf{F}^{\mathrm{p}} = \begin{bmatrix} 1 & 0 & 0 \\ 0 & 1 & \gamma \\ 0 & 0 & 1 \end{bmatrix} \Rightarrow \mathbf{l}_{\mathbf{p}} = \begin{bmatrix} 0 & 0 & 0 \\ 0 & 0 & \dot{\gamma} \\ 0 & 0 & 0 \end{bmatrix} \Rightarrow \mathbf{d}^{\mathrm{p}} = \begin{bmatrix} 0 & 0 & 0 \\ 0 & 0 & \dot{\gamma}/2 \\ 0 & \dot{\gamma}/2 & 0 \end{bmatrix}, \boldsymbol{\omega}^{\mathrm{p}} = \begin{bmatrix} 0 & 0 & 0 \\ 0 & 0 & \dot{\gamma}/2 \\ 0 & -\dot{\gamma}/2 & 0 \end{bmatrix} \tag{3-64}$$

where $\mathbf{F}^{\mathrm{p}}$ is the deformation gradient. This decomposition of the plastic shearing can be illustrated such as in Figure 18.

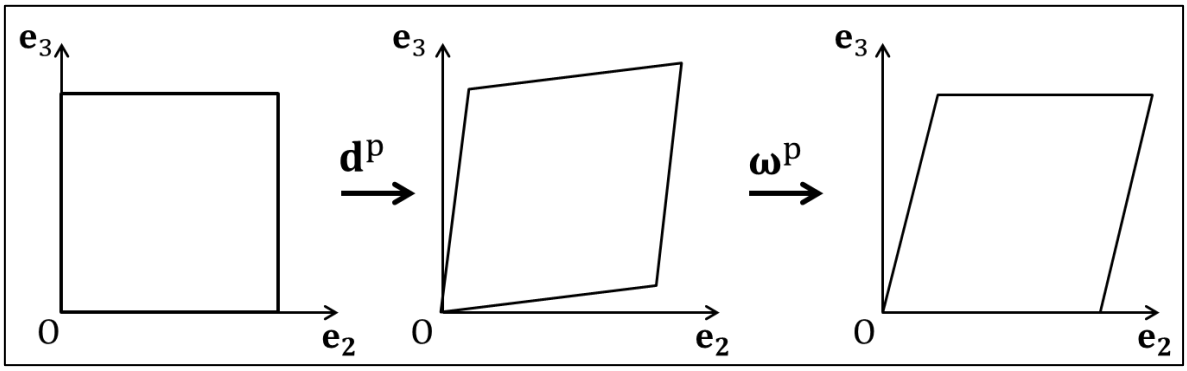

Figure 18 – Simple plastic shear decomposed into pure shear and rotation [27].

3.4.2 Kinematics of Finite Elastic Plastic Deformation

Now, consider a finite elastic-plastic deformation of a crystal element (as defined in Section 3.4.1), where the deformation gradient $\mathbf{F}$ can be decomposed into to the lattice part (superscript *) and the plastic part (superscript p) [3]:

$$\mathbf{F} = \mathbf{F}^{*}\mathbf{F}^{\mathrm{p}}. \tag{3-65}$$

This multiplicative decomposition is done in order to express the deformation in two steps (see Figure 19):

After applying certain amount of external forces on the crystal element in the reference configuration Ω_0, plastic shearing occurs denoted by shear γ and last until the intermediate configuration Ω_{int} is reached. This permanent material deformation leaves the crystallographic orientation and elastic properties unchanged and is driven by the plastic part of the deformation gradient $\mathbf{F}^{\mathrm{p}}$. This shearing happens on a slip system defined by a pair of unit vectors: normal to the slip plane $\boldsymbol{N}$ and its slip directions $\boldsymbol{S}$. In the case of multislip, the total plastic shear γ is a superposition of shear strains in each active slip system.

The plastic shearing is followed by an elastic stretching and an elastic/rigid body rotation denoted by $\mathbf{F}^{*}$, until the current configuration Ω is reached. The reason of the rigid body rotation is explained in Figure 8. Note that the slip system move together with the lattice and is characterized by the slip direction $\boldsymbol{s}$ and normal to the slip planes $\boldsymbol{n}$, both termed in the deformed configuration and for n number of slip systems α it can be stated that [21]:

$$\boldsymbol{s}^{(\alpha)} = \mathbf{F}^{*} \cdot \boldsymbol{S}^{(\alpha)} \tag{3-66}$$

$$\boldsymbol{n}^{(\alpha)} = \boldsymbol{N}^{(\alpha)} \cdot \mathbf{F}^{*(-1)} \tag{3-67}$$

In reality both deformations are happening at the same time.

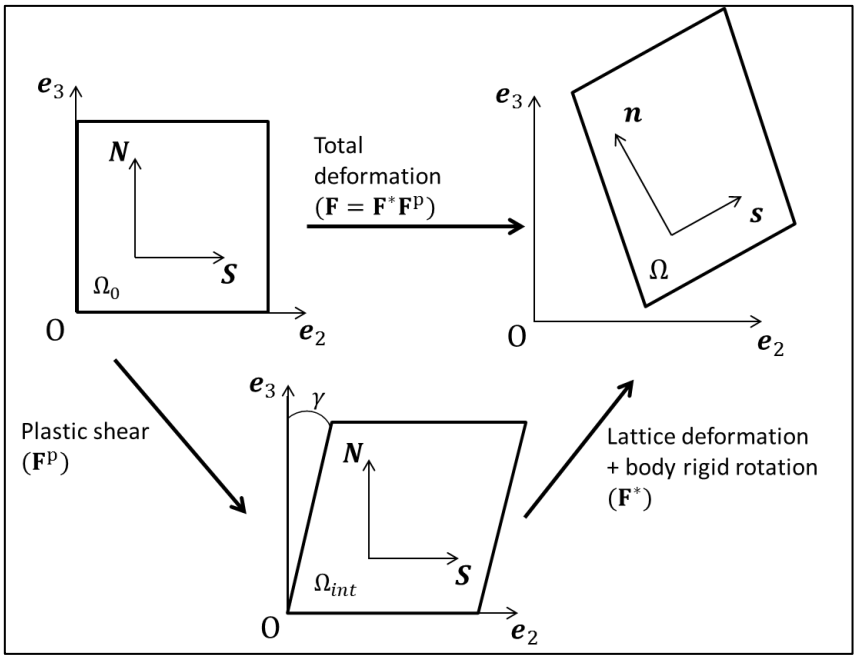

Figure 19 – 3.2 Kinematics of finite elastic plastic deformation of the single crystal element [3].

For constitutive models it is necessary to express the crystal element deformation as a sequence of small deformations governed by spatial velocity gradient $\mathbf{l}$ and time increment Δt [27]. The relation between the velocity gradient $\mathbf{l}$ and the deformation gradient $\mathbf{F}$ is:

$$\mathbf{l} = \frac{\partial \boldsymbol{v}(\boldsymbol{x}, t)}{\partial \boldsymbol{x}} = \frac{\partial \dot{\boldsymbol{x}}}{\partial \boldsymbol{x}} = \frac{d}{dt}\frac{\partial \boldsymbol{x}}{\partial \boldsymbol{X}}\frac{\partial \boldsymbol{X}}{\partial \boldsymbol{x}} = \dot{\mathbf{F}}\mathbf{F}^{(-1)} \tag{3-68}$$

and by substituting Equation (3-65) into (3-68) one gets following relation:

$$\dot{\mathbf{F}}\mathbf{F}^{(-1)} = \dot{\mathbf{F}}^*\mathbf{F}^{*(-1)} + \mathbf{F}^*\dot{\mathbf{F}}^p\mathbf{F}^{p(-1)}\mathbf{F}^{*(-1)} \tag{3-69}$$

In addition, $\boldsymbol{l}$ can be additively decomposed as in Equation (3-63) into the symmetric and anti-symmetric part:

$$\mathbf{l} = \frac{1}{2}(\mathbf{l} + \mathbf{l}^{\mathbf{T}}) + \frac{1}{2}(\mathbf{l} - \mathbf{l}^{\mathbf{T}}) = \mathbf{d} + \boldsymbol{\omega}. \tag{3-70}$$

Note that $\mathbf{d}$ is not a pure rate of plastic strain and $\boldsymbol{\omega}$ is not a pure rate of rotation [12].

Furthermore the stretch rate tensor $\mathbf{d}$ and spin tensor $\boldsymbol{\omega}$ can be broke down to lattice part and plastic part for the same reason as it was done for the deformation gradient:

$$\mathbf{d} = \mathbf{d}^{*} + \mathbf{d}^{\mathrm{p}}, \tag{3-71}$$

$$\boldsymbol{\omega} = \boldsymbol{\omega}^{*} + \boldsymbol{\omega}^{\mathrm{p}}, \tag{3-72}$$

where the plastic part of the stretch rate tensor $\mathbf{d}^{\mathrm{p}}$ and the spin tensor $\boldsymbol{\omega}^{\mathbf{p}}$ are the only contribution to the plastic shearing [27]. They can be related to the deformation tensor due to Equation (3-69) [27]:

$$\mathbf{d}^{\mathrm{p}} + \boldsymbol{\omega}^{\mathrm{p}} = \mathbf{F}^{*}\dot{\mathbf{F}}^{\mathbf{p}}\mathbf{F}^{\mathbf{p}(-1)}\mathbf{F}^{*(-1)} \tag{3-73}$$

and are explicitly given with respect to the current configuration as it was shown in Equation (3-62):

$$\mathbf{d}^{\mathrm{p}} + \boldsymbol{\omega}^{\mathrm{p}} = \sum_{\alpha=1}^{\mathrm{n}} \dot{\gamma}^{\alpha} \boldsymbol{s}^{(\alpha)} \otimes \boldsymbol{n}^{(\alpha)} \tag{3-74}$$

or with respect to the intermediate configuration, the rate of residual deformation can be expressed by combining Equations (3-66), (3-67), (3-73) and (3-74):

$$\dot{\mathbf{F}}^{\mathbf{p}}\mathbf{F}^{\mathbf{p}(-1)} = \sum_{\alpha=1}^{\mathrm{n}} \dot{\gamma}^{\alpha} \boldsymbol{S}^{\alpha} \otimes \boldsymbol{N}^{\alpha} \tag{3-75}$$

Now for convenience, two second rank tensors for each slip system α are defined according to additive decomposition in $(3\text{-}63)_2$ and Equation (3-62) [27]:

$$\mathbf{H}^{(\alpha)} = \frac{1}{2}(\boldsymbol{s}^{(\alpha)} \otimes \boldsymbol{n}^{(\alpha)} + \boldsymbol{n}^{(\alpha)} \otimes \boldsymbol{s}^{(\alpha)}) \tag{3-76}$$

$$\mathbf{W}^{(\alpha)} = \frac{1}{2}(\boldsymbol{s}^{(\alpha)} \otimes \boldsymbol{n}^{(\alpha)} - \boldsymbol{n}^{(\alpha)} \otimes \boldsymbol{s}^{(\alpha)}) \tag{3-77}$$

where:

$$\mathbf{d}^{\mathrm{p}} = \sum_{\alpha=1}^{n} \mathbf{H}^{(\alpha)} \dot{\gamma}^{\alpha} \tag{3-78}$$

and:

$$\boldsymbol{\omega}^{\mathrm{p}} = \sum_{\alpha=1}^{n} \mathbf{W}^{(\alpha)} \dot{\gamma}^{\alpha}. \tag{3-79}$$

3.4.3 Constitutive laws

In Figure 7 it has been shown how stress for each slip system α in a single crystal can be resolved in particular slip direction $\boldsymbol{s}$ on given slip plane $\boldsymbol{n}$.

The Equation (2-6) represents well-known Schmid's law [1] and can be represented in convenient tensorial form for each slip system α in the current configuration. Assuming that elastic deformation is negligible it can be written that [34]:

$$\tau^{(\alpha)} = \boldsymbol{n}^{(\alpha)} \cdot \boldsymbol{\tau} \cdot \boldsymbol{s}^{(\alpha)} \tag{3-80}$$

where $\boldsymbol{\tau}$, the symmetric Kirchhoff stress tensor, which is defined with respect to the current configuration.

Rate of the resolved shear stress can be obtained by using differentiation of (3-80):

$$\dot{\tau}^{(\alpha)} = \dot{\boldsymbol{n}}^{(\alpha)} \cdot \boldsymbol{\tau} \cdot \boldsymbol{s}^{(\alpha)} + \boldsymbol{n}^{(\alpha)} \cdot \dot{\boldsymbol{\tau}} \cdot \boldsymbol{s}^{(\alpha)} + \boldsymbol{n}^{(\alpha)} \cdot \boldsymbol{\tau} \cdot \dot{\boldsymbol{s}}^{(\alpha)}, \tag{3-81}$$

employing next two rate Equations:

$$\dot{\boldsymbol{s}}^{(\alpha)} = (\mathbf{d}^{*} + \boldsymbol{\omega}^{*}) \cdot \boldsymbol{s}^{(\alpha)} \tag{3-82}$$

$$\dot{\boldsymbol{n}}^{(\alpha)} = -\boldsymbol{n}^{(\alpha)} \cdot (\mathbf{d}^{*} + \boldsymbol{\omega}^{*}) \tag{3-83}$$

and by definition of the Jaumann rate of Kirchhoff stress (see section 3.3.1), finally the rate is obtained:

$$\dot{\boldsymbol{\tau}}^{(\alpha)} = \boldsymbol{n}^{(\alpha)} \cdot (\boldsymbol{\tau}^{\boldsymbol{\nabla}*} - \mathbf{d}^{*} \cdot \boldsymbol{\tau} + \boldsymbol{\tau} \cdot \mathbf{d}^{*}) \cdot \boldsymbol{s}^{(\alpha)}, \tag{3-84}$$

where $\boldsymbol{\tau}^{\boldsymbol{\nabla}*}$ is the Jaumann rate of Kirchhoff stress based on axes that rotate with the crystal lattice.

When the resolved shear stress occurs on the slip system α, it still doesn't mean that the shearing will follow. The stress has to reach or pass over a

certain level, named the slip system critical resolved shear stress τ_c^α [3] and in such a case, the slip system is called active:

$$if: \tau^\alpha \geq \tau_c^\alpha \tag{3-85}$$

$$then: \dot{\gamma}^\alpha \neq 0. \tag{3-86}$$

In this work is used the rate dependent viscoplastic power law introduced by Hutchinson [36] which is relating the strain rate of the slip system $\dot{\gamma}^\alpha$ with the ratio of the resolved shear stress τ^α and the critical resolved shear stress g^α:

$$\dot{\gamma}^\alpha = \dot{\gamma}_0 \left|\frac{\tau^\alpha}{\tau_c^\alpha}\right|^m sgn(\tau^\alpha), \tag{3-87}$$

where $\dot{\gamma}_0$ is the reference strain rate on the slip system α and m is the rate sensitivity exponent. Rate dependency is useful when dealing with creep, with material at high temperature or with dynamic problems at high deformation rate. The rate independency can be set as the rate sensitivity exponent goes to infinity $\mathrm{n} \to \infty$, then the material is considered to have rate independent behaviour. Note, that by using this approach every slip system is considered to be active. But for rate independent material ($\mathrm{n} \to \infty$) and for low resolved shear stress it is obvious that:

$$if: \tau^\alpha < \tau_c^\alpha \tag{3-88}$$

$$then: \dot{\gamma}^\alpha \cong 0. \tag{3-89}$$

As it was shown, plastic deformation is described in terms of the rate of shear strain $\dot{\gamma}^\alpha$ and the resolved shear stress τ^α. These two variables were chosen so that they satisfy work conjugacy: $\tau^\alpha \cdot \dot{\gamma}^\alpha$ is equal to the rate of work as a result of slip on slip system α per unit of reference volume [27].

3.4.4 Strain Hardening

During plastic deformation the metal is hardening. That is due to complexity of dislocation flow throughout the polycrystalline structure and dislocation generation itself [1]. Here is used phenomenological description developed by Hutchinson [36], which has been proven as sufficient approach by numerous

researchers [7; 8; 20] and it is widely used, although it lacks from some physical aspects (grain size dependency, dislocation interaction with grain boundary).

The strain hardening on a given slip system α is expressed by the evolution of the critical resolved shear stress τ_c^α through the incremental relation:

$$\dot{\tau}_c^\alpha = \sum_{\beta=1}^{n} h^{\alpha\beta} \left|\dot{\gamma}^\beta\right|, \tag{3-90}$$

where n is the number of slip systems and $h_{\alpha\beta}$ is the hardening matrix [37]:

$$h^{\alpha\beta} = q^{\alpha\beta}\left[h_0\left(1 - \frac{\tau_c^\beta}{\tau_s}\right)^a\right], \tag{3-91}$$

In the Equation (3-91) h_0 is the initial hardening, τ_s is the saturation stress, a is slip system hardening parameters and $q^{\alpha\beta}$ is for FCC metals with 12 slip systems a 12 by 12 matrix, where the diagonal values are equal 1 (self-hardening) and the rest are the ratios of latent-hardening to self-hardening (usually between 1 and 1.4 [33]).

The Equation (3-91) captures:

1) self-hardening (influence of hardening of slip system α on slip in α),
2) latent-hardening (influence of hardening of slip system α on slip in β).

3.4.5 Overall Constitutive law

Keeping in mind that the crystallographic slip does not affect elasticity and by following Hill and Rice [30], the Jaumann rate of Kirchhoff stress $\boldsymbol{\tau}^{\nabla *}$ can be related to the lattice part of the stretch rate tensor $\mathbf{d}^*$ as the elastic law [21]:

$$\boldsymbol{\tau}^{\nabla *} = \mathbb{C} : \mathbf{d}^*, \tag{3-92}$$

or in terms of Cauchy stress (for proof see Section 3.3.2):

$$\boldsymbol{\sigma}^{\nabla *} + \boldsymbol{\sigma}(\mathbf{I} : \mathbf{d}^*) = \mathbb{C} : \mathbf{d}^*, \tag{3-93}$$

where $\mathbb{C}$ is the four-rank tensor of elastic moduli in the spatial description with minor and major symmetries (21 independent components) and $\boldsymbol{\sigma}^{\nabla *}$ is the stress rate on axes which rotate with the crystal lattice [21]:

$$\boldsymbol{\sigma}^{\nabla *} = \dot{\boldsymbol{\sigma}} - \boldsymbol{\omega}^{*} \cdot \boldsymbol{\sigma} + \boldsymbol{\sigma} \cdot \boldsymbol{\omega}^{*}, \tag{3-94}$$

with $\dot{\boldsymbol{\tau}}$ the material derivative of Kirchhoff stress. The Jaumann rate of Kirchhoff stress $\boldsymbol{\tau}^{\nabla}$ can be based on axes which rotate with the material, then:

$$\boldsymbol{\sigma}^{\boldsymbol{\nabla}} = \dot{\boldsymbol{\sigma}} - \boldsymbol{\omega} \cdot \boldsymbol{\sigma} + \boldsymbol{\sigma} \cdot \boldsymbol{\omega}, \tag{3-95}$$

where the difference is:

$$\boldsymbol{\sigma}^{\nabla *} - \boldsymbol{\sigma}^{\nabla} = \boldsymbol{\omega}^{\mathrm{p}} \cdot \boldsymbol{\sigma} - \boldsymbol{\sigma} \cdot \boldsymbol{\omega}^{\mathrm{p}} = \sum_{\alpha=1}^{\mathrm{n}} \boldsymbol{\beta}^{(\alpha)} \dot{\gamma}^{\alpha}, \tag{3-96}$$

where:

$$\boldsymbol{\beta}^{(\alpha)} = \mathbf{W}^{(\alpha)} \cdot \boldsymbol{\sigma} - \boldsymbol{\sigma} \cdot \mathbf{W}^{(\alpha)}. \tag{3-97}$$

Finally, by using Equations (3-71), (3-78), (3-92) and (3-96) one can derive constitutive law [21]:

$$\boldsymbol{\sigma}^{\nabla} = \mathbb{C} : \mathbf{d} - \boldsymbol{\sigma}(\mathbf{I} : \mathbf{d}^{*}) - \sum_{\alpha=1}^{\mathrm{n}} \left[\mathbb{C} : \mathbf{H}^{(\alpha)} + \boldsymbol{\beta}^{(\alpha)}\right] \dot{\gamma}^{(\alpha)}. \tag{3-98}$$

3.4.6 Simplification to 1D Problem

To illustrate the multiplicative decomposition of the deformation gradient and the relation expressed in Equation (3-98), one can think of a crystal specimen in tension test which is deform up to strain ε and is simplified as 1D problem (1D stress state together with 1D strain state – considering not real material properties). In Voigt notation, strain ε_1 can be decomposed into the elastic and plastic part:

$$\varepsilon_1 = \varepsilon_1^{e} + \varepsilon_1^{p} \tag{3-99}$$

and so its rate:

$$\dot{\varepsilon}_1 = \dot{\varepsilon}_1^e + \dot{\varepsilon}_1^p. \tag{3-100}$$

It was stated that stress is determined solely from the elastic part of the deformation and then it can be written that:

$$\sigma_1 = C_{11} \cdot \varepsilon_1^e, \tag{3-101}$$

where C_{11} is a component of the stiffness matrix. Further, by substituting Eq (3-99) into Eq (3-101) it can be written that:

$$\dot{\sigma}_1 = C_{11} \cdot \dot{\varepsilon}_1 - C_{11} \cdot \dot{\varepsilon}_1^p \tag{3-102}$$

and in case of the crystal multislip:

$$\dot{\sigma}_1 = C_{11} \cdot \dot{\varepsilon}_1 - \sum_{\alpha=1}^{n} C_{11} \cdot \dot{\varepsilon}_1^{p(\alpha)}, \tag{3-103}$$

where the sum is over the n active slip systems α. The Eq (3-103) express the same as the Eq (3-98) but in simplified approach, that can help to understand and appreciate the main constitutive law in the single crystal strength model [27].

3.5 Conclusion

In Section 3 the basic theory of continuum mechanics, which includes kinematics of deformation, concept of stress and time objective derivatives has been introduced together with the single crystal strength theory, which sits on these parts of the continuum mechanics.

It has been demonstrated, how the physical understanding of elastic-plastic deformation can be represented as a mathematical model in terms of continuum mechanics theory. This mathematical description, the single crystal strength model, will be in following section implemented into the finite element code and used in computational analysis of large deformation of crystals and their aggregates.

4 MODEL IMPLEMENTATION AND PRE/POST PROCESS SOFTWARE DEVELOPMENT

Continuum mechanics is a tool that allows interpreting nature of specific materials and their behaviour during deformation process into a simplified mathematical model. Then such a model can be implemented into Finite Element (FE) framework as a material model and used to perform computational analysis and solve particular engineering problems.

Commercial FEA software products do not provide crystal plasticity (CP) material models. But users can write their own constitutive models and subroutines by using special interfaces (e.g. in Abaqus®/Standart such interface is called UMAT), or if the source code of a FEA software is available, by implementing CP material models directly into the programmes, which is the case of this project.

In this work the single crystal strength model (described in Section 3.4) is implemented as material model directly into the explicit FE solver LLNL - DYNA3D® [38] by following implicit FE solver ABAQUS®/Standard User Material Subroutine (UMAT) developed by Huang [21] and schematic layout done by Harewood [39]. The reason why the model is incorporating into the explicit FE solver is that the future intention is to study dynamic engineering problems.

Furthermore, new methodologies including new software for pre-processing and post-processing were developed.

4.1 Explicit vs. Implicit FEM

DYNA3D® is an explicit FE solver which is design to run dynamic simulations, while Abaqus®/Standard is an implicit solver dealing with quasi-static simulations. In a simplified way it means that DYNA3D® uses very small times steps to hold force and displacement equilibriums. The Abaqus®/Standard implementation allows large time steps but in order to solve for equilibrium it

uses an iterative method. For more information about comparison of the implicit and explicit FE methods see reference [25]

4.2 Model Implementation

For description of the DYNA3D® software architecture see Reference [40].

4.2.1 Incremental Formulation

The implemented CP material model within the FEM framework DYNA3D® has five main functions [21]:

1) Calculate increment of the critical resolved shear stress τ_c^α in each slip system of a single crystal.

$$\Delta\tau_c^\alpha = \sum_{\beta=1}^{n} h^{\alpha\beta}\left|\Delta\gamma^\beta\right| \tag{4-1}$$

2) Calculate increment of the resolved shear stress $\Delta\tau^\alpha$ in each slip system of a single crystal. Using Equations (3-84), (3-43), (3-93), (3-71), (3-72) and (3-74) following is obtained:

$$\Delta\tau^\alpha = \left[c_{ijkl}H_{kl}^{(\alpha)} + W_{ik}^{(\alpha)}\sigma_{jk} + W_{jk}^{(\alpha)}\sigma_{ik}\right]\cdot\left[\Delta\varepsilon_{ij} - \sum_{\beta=1}^{n} H_{kl}^{(\beta)}\,\Delta\gamma^{(\beta)}\right] \tag{4-2}$$

where $\Delta\varepsilon_{ij}$ is total strain increment in the deformation, c_{ijkl} is the tensor of elastic moduli, σ_{ij} is the current stress tensor, $H_{ij}^{(\alpha)}$ and $W_{ij}^{(\alpha)}$ are second order tensors related with the rate of stretching, respectively with the spin tensor (see Equations (3-76) and (3-77)).

3) Calculate increment of the corotational stress increment $\Delta\sigma_{ij}$ of a single crystal using Equation (3-98):

$$\Delta\sigma_{ij} = c_{ijkl}\,\Delta\varepsilon_{kl} - \sigma_{ij}\Delta\varepsilon_{kk} - \sum_{\alpha=1}^{n}\left[c_{ijkl}\,H_{kl}^{(\alpha)} + W_{ik}^{(\alpha)}\sigma_{jk} + W_{jk}^{(\alpha)}\sigma_{ik}\right]\Delta\gamma^{(\alpha)} \tag{4-3}$$

4) Calculate increment of shear strain $\Delta\gamma^{(\alpha)}$ in each slip system

$$\Delta\gamma^{(\alpha)} = \dot{\gamma}^{(\alpha)}\Delta t. \tag{4-4}$$

where Δt is the time increment $\dot{\gamma}^{(\alpha)}$ can be carried out from Equation (3-87).

5) Rotate the crystal lattice, which is deformed only due to elastic deformation. Equations (3-82) and (3-83) can be re-written in the incremental form:

$$\Delta s_i^{(\alpha)} = \left\{ \Delta\varepsilon_{ij} + \omega_{ij}\Delta t - \sum_{\beta=1}^{n} \left[H_{ij}^{(\beta)} + W_{ij}^{(\alpha)} \right] \Delta\gamma^{(\beta)} \right\} \cdot s_j^{(\alpha)} \tag{4-5}$$

$$\Delta n_i = -n_j^{(\alpha)} \left\{ \Delta\varepsilon_{ji} + \omega_{ji}\Delta t - \sum_{\beta=1}^{n} \left[H_{ji}^{(\beta)} + W_{ji}^{(\alpha)} \right] \Delta\gamma^{(\beta)} \right\} \tag{4-6}$$

where $s_i^{(\alpha)}$ and $n_i^{(\alpha)}$ are the slip direction of the slip system α and normal to the slip plane respectively.

4.2.2 CP Material Model in DYNA3D® as Subroutines

The CP material model is implemented into DYNA3D® as four subroutines:

1) f3dm94.f is the main subroutine which is called by DYNA3D® for every integration point, which represents a single crystal, and for each iteration. At the beginning the FE solver provides the subroutine with the strain and time increment (Δt, $\Delta\boldsymbol{\varepsilon}$), the stress tensor ($\boldsymbol{\sigma}$) and the material data as the crystallographic orientation, the elastic stiffness tensor, the critical resolved shear stress (τ_c^{α}) and the shear strain (γ^{α}) for each slip system. All these quantities are at the begging denoted at the time t (except the strain and time increment). Then they are updated according to the model and forward Euler explicit integration scheme (e.g. $\boldsymbol{\sigma}_{t+\Delta t} = \boldsymbol{\sigma}_t + \dot{\boldsymbol{\sigma}} \cdot \Delta t$). Then they are passed back to the FE solver. Note that all calculations are done in global coordinate system (CS).
2) slipsys.f subroutine generates all slip systems in material coordinate system (for FCC 12 slip systems and for BCC 48 slip systems).

3) inse94.f is called by DYNA3D® just at the beginning of a simulation and for each integration point. This subroutine determines initial values of the material coordinate system, the critical resolved shear stress on each slip system and the crystal orientation matrix $\mathbf{T}$ (which transform material CS to global CS). Then it calls slipsys.f and afterward it rotates slip systems from material CS to global CS.
4) m2g_stif94.f is a subroutine which transform the elastic stiffness matrix from material CS to global CS using crystal orientation matrix $\mathbf{T}$**.** This subroutine is called in each f3dm94.f.

4.2.3 Algorithms for the single crystal strength model

Note that an initial implementation of UMAT [21] into DYNA3D® was available at the beginning of this project.

Simplified scheme of the algorithm is as follows:

4.2.3.1 Initialization (inse94.f)

This subroutine is called only at the beginning of each simulation for each integration point.

1) Calculating crystal orientation in the global CS – these data are obtained from the input file in the Card 6 (Material Type 94 – Crystal Plasticity) which is provided by the user when running DYNA3D® simulation, see Appendix B.
2) Calculating the second order transformation tensor $\mathbf{T}$, this is later used for converting the stiffness matrix from material CS to global CS and is also used for tracking the evolution of crystal rotation during deformation:

$$\mathbf{T} = \mathbf{G}\mathbf{M}^{-1} \tag{4-7}$$

where $\mathbf{G}$ is a second order tensor defining global CS and $\mathbf{M}$ is the second order tensor defining material CS in global CS. Here note that this tensor $\mathbf{T}$ was implemented later, when need of trace of crystallographic orientation was discovered.

3) Setting up slip systems in the material CS.

a. For FCC 12 slip systems.
b. For BCC 48 slip systems.

4) Rotating slip directions and slip planes into the global CS using transformation tensor $\mathbf{T}$.
5) Initializing values of the current strength of each slip system h_0^α, which is obtained from the input file in the Card 6 (Material Type 94 – Crystal Plasticity), see Appendix B.

4.2.3.2 Main subroutine

The main subroutine progress as follows:

1) Calculating the second order tensor $\mathbf{H}^{(\alpha)}$ from Eq (3-76), using values of $\boldsymbol{s}$ and $\boldsymbol{n}$ from previous increment. These values are stored in vector slpdef:

$$\mathrm{slpdef}[6,\alpha] = \begin{bmatrix} H_{11} \\ H_{22} \\ H_{33} \\ 2H_{12} \\ 2H_{23} \\ 2H_{13} \end{bmatrix} \tag{4-8}$$

2) Calculating spin tensor $\mathbf{W}^{(\alpha)}$ from Eq (3-77).

$$\mathrm{slpspn}[3,\alpha] = \begin{bmatrix} W_{12} \\ W_{23} \\ W_{13} \end{bmatrix} \tag{4-9}$$

3) Calculating shear strain rate $\dot{\gamma}^\alpha$ (fslip[α]) in each slip system according to Eq (3-87) by calling function strainrate.
4) The orientation matrix $\mathbf{T}$ can be rotated as it was done by Raphanel et al. [41]. This rotation is happening only due to elastic deformation of the crystal.

$$\mathbf{T}_{t+\Delta t} = e^{\boldsymbol{\omega}^* \Delta t} \mathbf{T}_t \tag{4-10}$$

where “the exponential of an anti-symmetric second-order tensor is an orthogonal tensor that can be determined by the Rodrigues formula” [41]:

$$e^{\boldsymbol{\omega}^*\Delta t} = \mathbf{I} + \frac{\sin(w^e \Delta t)}{w^e}\boldsymbol{\omega}^* + \frac{1-\cos(w^e \Delta t)}{(w^e)^2}(\boldsymbol{\omega}^*)^2 \tag{4-11}$$

where $w^e = \sqrt{\omega_{ij}^* \omega_{ij}^*/2}$. The details about the code of updating orientation matrix can be found in Appendix A.1.

5) Rotating the fourth order elastic stiffness matrix $c_{ijkl}$from the material CS to the global CS by using matrix $\mathbf{T}$, the main subroutine is calling for this operation the subroutine m2g_stif94.f.
6) Calculating ddemsd which is used in the calculation of the increment of the resolved shear stress

$$\mathrm{ddemsd} = \left[c_{ijkl} H_{kl}^{(\alpha)} + W_{ik}^{(\alpha)} \sigma_{jk} + W_{jk}^{(\alpha)} \sigma_{ik}\right] \tag{4-12}$$

7) Calculating of the hardening matrix $\mathrm{h}_{\alpha\beta}$ (in the code it is written as $h[\alpha, \alpha]$) for each slip system according to Eq (3-91). The main subroutine is calling function latentharden(). To choose hardening as in UMAT developed by Huang [21] choose in the material card in column 51-60 value 1.0. (see Appendix B), other value will implement hardening as in Kalidindi [20], also described in Eq (3-91) which code implementation can be seen in Appendix A.2.
8) Calculating the increment of the shear strain $\mathrm{d\_gamma}[\alpha]$ as in Equation (4-4).
9) Updating the shear strain γ^{α} for each slip system.

$$\mathrm{gamma\_a}[\alpha] = \mathrm{gamma\_a}[\alpha] + \mathrm{d\_gamma}[\alpha] \tag{4-13}$$

10) Calculating the increment of the current strength of each slip system ($\mathrm{delta\_g\_a}[\alpha]$) by according to Equation (3-90).
11) Updating the current strength in each slip system

$$\mathrm{g\_a}[\alpha] = \mathrm{g\_a}[\alpha] + \mathrm{delta\_g\_a}[\alpha] \tag{4-14}$$

12) Calculating dvgrad, which is lately used to rotate the slip systems

$$\mathrm{dvgrad}[3,3] = \left\{ \Delta\varepsilon_{ij} + \omega_{ij}\Delta t - \sum_{\beta=1}^{n} \left[H_{ij}^{(\beta)} + W_{ij}^{(\alpha)} \right] \Delta\gamma^{(\beta)} \right\}$$

13) Calculating increment of the resolved shear stress in each slip system ($\mathrm{dtau\_a}[\alpha]$) according to Equation (4-2).
14) Updating resolved shear stress τ^{α} in each slip system.

$$\mathrm{tau\_a}[\alpha] = \mathrm{tau\_a}[\alpha] + \mathrm{dtau\_a}[\alpha] \tag{4-15}$$

15) Calculating the increment of the stress tensor ($\mathrm{deltasig}[6,6]$) based on Equation (4-3).
16) Updating the stress tensor

$$\mathrm{sig}[6,6] = \mathrm{sig}[6,6] + \mathrm{deltasig}[6,6] \tag{4-16}$$

17) Calculating the increments for slip directions ($\mathrm{d\_slipdir}[3,\alpha]$) and the normal to the slip plane ($\mathrm{d\_slipnor}[3,\alpha]$) as in Equations (4-5) and (4-6).
18) Updating slip directions $\mathbf{s}^{\alpha}$ and normals $\mathbf{n}^{\alpha}$ for each slip system.

$$\mathrm{slipdir}[3,\alpha] = \mathrm{slipdir}[3,\alpha] + \mathrm{d\_slipdir}[3,\alpha] \tag{4-17}$$

$$\mathrm{slipnor}[3,\alpha] = \mathrm{slipnor}[3,\alpha] + \mathrm{d\_slipnor}[3,\alpha] \tag{4-18}$$

The subroutine f3dm94.f is called for each integration point and for each iteration.

4.3 Debugging of the new Implementation

Testing of the initial implementation of the UMAT-Single Crystal Plasticity [21] to DYNA3D® during simulation of a metal deformation showed that the model results were unrealistic. Therefore a methodology to debug the code was developed.

The debugging process of the new CPFEM was done by comparing results from a set of simulations obtained by using UMAT-Single Crystal Plasticity [21] and the new CPFEM. This was a long process where each value included in the code was saved for each iteration in a specific file and compared. This allowed

to find differences and to track a bug in the code. For an example see Appendix A.1.

4.4 Generating Material Input File for DYNA3D®

At the beginning of a simulation DYNA3D® reads the material properties of a model from the material cards in the input file, see Appendix B. When a model is composed from many crystals with varied orientation, each crystal has to have its own material card. To write these cards manually would be very inconvenient and would not be realistic in a case of modelling initially annealed material represented by a large number of randomly orientated crystals. Therefore a new script written in Fortran 90 was developed to generate material cards and assign to each of them fairly random orientation. For detailed description of the script please see Appendix A.3.

4.5 Plotting Stress Strain Curves

A stress strain curve is in engineering used as a way to define material behaviour during a deformation (as it can be seen in Section 6) and it implicitly relates force which deforms material with the level of deformation. It is also one of the ways how to validate a computational model by making comparison with experimental data (etc. as it was done in this work in Section 5).

However DYNA3D® does not provide a tool that would be able to plot stress strain curves. What DYNA3D® can provide are reaction forces of each node in the model (when in the input file for DYNA3D® seventh option in the card 3 is set to one, see Appendix B). Then, after a simulation, file named forrct is generated. A script written in Visual Basic Application (VBA) was developed to plot the stress strain curve by using data from a file forrct. User defines in a Microsoft Office - Excel interface size of a computational model, speed of the nodes which are constrained to a motion, time step for which DYNA3D® plots data to forrct and termination time of the simulation. After a single click on the button “Stress-Strain Curve” user will be asked to select location of a forrct file and then the script will plot stress strain curves. This script allowed very fast analysis of the material properties and their evolution during a simulation. All

stress strain curves plotted in this work were done by using this script. For more details see Appendix A.4.

4.6 Tracing an Evolution of Crystallographic Orientation

In order to be able to enhance understanding of anisotropy in metals by using CPFEM (see Section Aims and Objectives) it is very important to be able to investigate an evolution of crystallographic orientation in any time during a deformation and to determinate a level of anisotropy within a testing material. A method crystallographic projection, which provides the information about crystallographic orientation (see Section 2.5), was chosen for this work, because the data extracted from an experiment can be compared directly with a numerical analysis and accuracy of an experimental prediction can be obtained (etc. as it is done in Section 5.2.). However, DYNA3D® does not provide a tool to obtain crystallographic projection and plot pole figures. Therefore, new method was developed.

4.6.1 MATLAB® Toolbox for Quantitative Texture Analysis

MTEX [42] is a tool that is able to plot pole figures (see Section 2.5) if data about crystal orientation are available. This toolbox was review and considered as convenient for determining a level of anisotropy within a computational model.

To fully define a crystal orientation in a fixed Cartesian coordinate system with orthonormal base vectors $\boldsymbol{e_1}, \boldsymbol{e_2}$ and $\boldsymbol{e_3}$, three vectors are required $\boldsymbol{e_1^c}, \boldsymbol{e_2^c}$ and $\boldsymbol{e_3^c}$, which denote an orthonormal basis of a crystal. Each vector $\boldsymbol{e_1^c}, \boldsymbol{e_2^c}$ and $\boldsymbol{e_3^c}$ has three components in the fixed Cartesian coordinate system, so if only one crystal is taken into consideration, MTEX require an array 3×3 to plot its pole figure (each column represents each vector $\boldsymbol{e_i^c}$). For k crystals, MTEX has to be provided by an array $(3 \cdot k) \times 3$. This array can be extracted from the CP model, see following section.

4.6.2 Extraction of Crystal Orientation from the CP Model

With the initial implementation of the UMAT into DYNA3D® it was inconvenient to extract information about orientation of crystals. Therefore a new crystal rotation treatment was implemented, for more information see Section 4.2.3.2 and Appendix A.1.

In the CP model the information about a crystal orientation is provided by the orientation matrix $\mathbf{T}$ (3×3) in terms of <1 0 0> directions. This matrix is updated in every time increment, see Equation (4-10). Each column in this matrix represents an orthonormal base of a crystal $\boldsymbol{e}_i^c$. This matrix $\mathbf{T}$ and its evolution during deformation is passed to the d3plot file, which can be open by post-processing software Ls-PrePost [43]. The information of the crystal orientation (expressed as 9 components of the matrix $\mathbf{T}$) can be found under the history of an element as variables “history var#1 – history var#9”.

4.6.3 Formatting Extracted Data from the CP Model

Data about crystal orientation extracted from the CP model from LS-PrePost (history var#1 – history var#9) has to be saved and formatted in order to plot pole figures by using the toolbox MTEX. This formatting was done by developing an algorithm in in Matlab®, which gather data (9 components of the $\mathbf{T}$ matrix for a single crystal) and pass them to the toolbox MTEX which plots a pole figure (see for example Figure 25). For detailed description of the saving process and the algorithm see Appendix A.5.

4.7 Conclusions

In this section was shown how the CP material model was implemented into the explicit FE solver DYNA3D® based on the work of Huang [21]. This implementation will allow prediction of a finite metal deformation as it is shown in the following sections. The reason why it was decided to implement UMAT into an explicit FE solver is that the future intention will be to investigate material response to dynamic mechanical loading.

5 MODEL VALIDATION

After development of the new CPFEM tool in previous section, the objective of this section is to show its validation in terms of:

- Demonstrating the CPFEM ability to predict large deformation of a single crystal or polycrystalline aggregates of particular metals.
- Recognizing accuracy of such prediction.
- Identifying limits and imperfections of the CPFEM.
- Identifying possible improvements.

5.1 Comparison with User-material Subroutine (UMAT)-ABAQUS®

UMAT is a user interface in Abaqus®/Standard [44] that allows defining material models, which were not included in the commercial pack. In 1991 Huang [21] incorporated the single crystal plasticity theory into the FEA solver Abaqus® and this work is its implementation. Therefore, first validations of the material model were done by comparing results from various simulations obtained from UMAT-Single Crystal Plasticity [21], (which was already used by other researcher with reasonable results [7]) and DYNA3D®.

5.2 Comparison with Experimental Data

A broad survey of experiments done by other researchers [7; 10; 26; 45] was done in order to find suitable data to validate the CP model by re-running these experiments and by comparing their results. Experiments done by Kalidindi [20] using copper material were reviewed and chosen for our validation. Some of the experiments done by Kalidindi were repeated by using the CPFEM developed in this work and results were compared. The outcome was that the results were not in agreement, for an example see Figure 20. That has been assessed and it was discovered that the discrepancy is due to the different strain hardening approach which was used by Huang [21] and Kalidindi [20]. Therefore new hardening was implemented, for more details see Section 3.4.4 and Appendix A.2. These simulations were repeated with a new strain hardening, results can be seen in following sections.

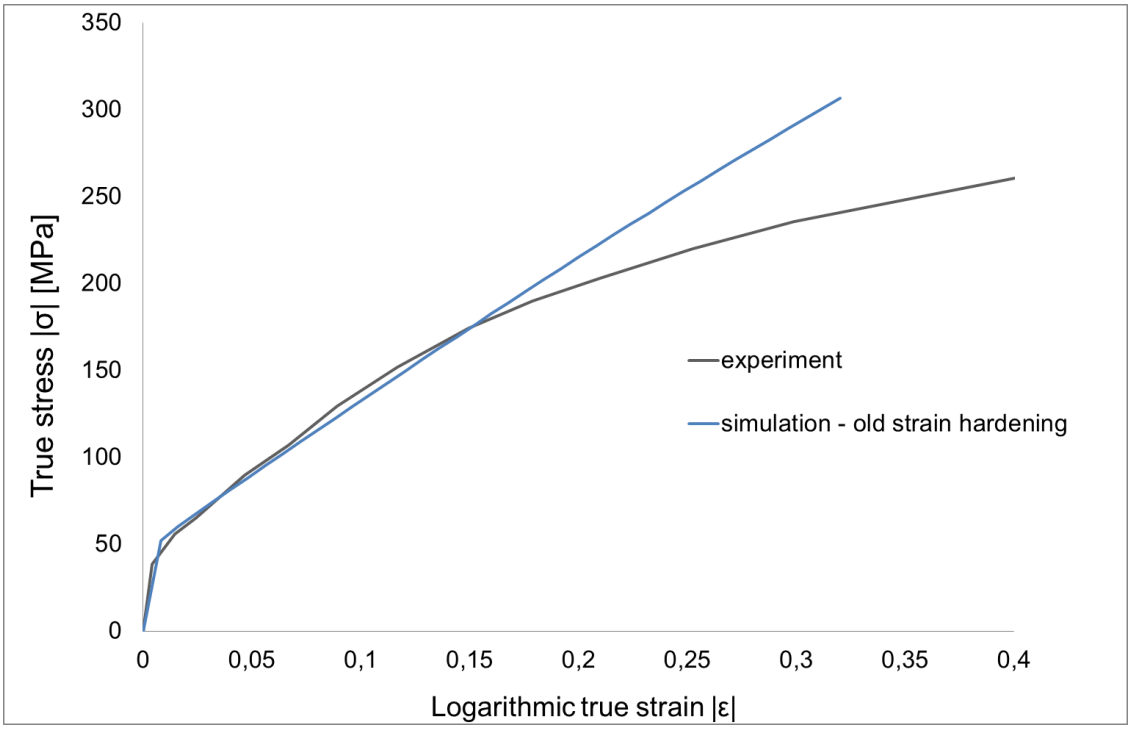

Figure 20 – Comparison of stress strain curves of experiment done by Kalidindi [20] **(compression of a single crystal, the same experiment as in Section 5.2.1) and the new CPFEM method with the strain hardening proposed by Huang** [21]**.**

5.2.1 Large Deformation of a Single Crystal

To validate the CP material model and its integration into the FE framework, simulation of a large deformation of a single crystal OFHC copper at room temperature was performed and the results were compared with experimental measurements [20].

5.2.1.1 Material Data

The material used in the simulation was an annealed single crystal of OFHC copper, where the components of its stiffness matrix are shown in Table 1 [14], or in terms of elastic modulus, shear modulus and Poisson's ratio in Table 2.

Table 1 – Components of the stiffness matrix as illustrated in Equation (2-3), for an annealed single crystal of OFHC copper [20]**.**

C_{11}	C_{12}	C_{44}
170 GPa	124 GPa	75 GPa

Table 2 – The elastic modulus E for cubic symmetry is the same for the longitudinal direction, transverse direction and normal direction. G is the shear modulus and ν is the poisson's ration.

E	G	ν
67 GPa	75 GPa	0.42

The relations between the stiffness matrix components and elastic modulus, shear modulus and Poisson's ratio for a material with the cubic symmetry can be seen by comparing Equations (2-1) and (5-1).

$$\begin{bmatrix}\sigma_1\\ \sigma_2\\ \sigma_3\\ \sigma_4\\ \sigma_5\\ \sigma_6\end{bmatrix} = \begin{bmatrix}\hat{E}(1-\nu) & \hat{E}\nu & \hat{E}\nu & 0 & 0 & 0\\ \hat{E}\nu & \hat{E}(1-\nu) & \hat{E}\nu & 0 & 0 & 0\\ \hat{E}\nu & \hat{E}\nu & \hat{E}(1-\nu) & 0 & 0 & 0\\ 0 & 0 & 0 & G & 0 & 0\\ 0 & 0 & 0 & 0 & G & 0\\ 0 & 0 & 0 & 0 & 0 & G\end{bmatrix}\begin{bmatrix}\varepsilon_1\\ \varepsilon_2\\ \varepsilon_3\\ \varepsilon_4\\ \varepsilon_5\\ \varepsilon_6\end{bmatrix} \tag{5-1}$$

where $\hat{E}$ is elastic modulus modified by poisson's ratio:

$$\hat{E} = \frac{E}{(1-2\nu)(1+\nu)} \tag{5-2}$$

Hardening of the slip systems in the simulation happens according to the Equation (3-91), where h_0 is the initial hardening, τ_s is the saturation stress, a is slip system hardening parameters, m is the rate sensitivity parameter, $\dot{\gamma}_0$ is the reference strain rate on the slip system α and $q^{\alpha\beta}$ is for FCC metals with 12 slip systems a 12 by 12 matrix, where the diagonal values are equal 1 (self-hardening) and the rest are the ratios of latent-hardening to self-hardening choose in this case as 1.4 [46]. The values for the slip hardening are given in Table 3.

Table 3 – Slip hardening values used in the simulation are the same as used by Kalidindi [20]**.**

h_0	τ_s	τ_c^k	a	m	$\dot{\gamma}_0$
250 MPa	190 MPa	16 MPa	2.5	83.33	0.001 s^{-1}

5.2.1.2 Boundary Conditions and Mesh

Let the orthonormal base vectors $\boldsymbol{e_1}, \boldsymbol{e_2}$ and $\boldsymbol{e_3}$ define a fixed global Cartesian CS; and let $\boldsymbol{e_1^c}, \boldsymbol{e_2^c}$ and $\boldsymbol{e_3^c}$ denote an orthonormal basis of a FCC crystal in terms of <100> directions.

One element (solid three-dimensional hexahedral element with one integration point [38]) of volume 1 mm^3 (grain size dependency is not taken into an account in our model) representing a single crystal was compressed with the crystallographic direction [011] align with the global CS, specifically with the vector $\boldsymbol{e_3}$, see Figure 21. The bottom face of the crystal was restricted in the motion in the $\boldsymbol{e_3}$ direction and to the top face of the crystal was assigned velocity in the way that the crystal was deformed with the axial strain rate equal to 0.001/s up to the true strain equal 0.5, see Figure 22.

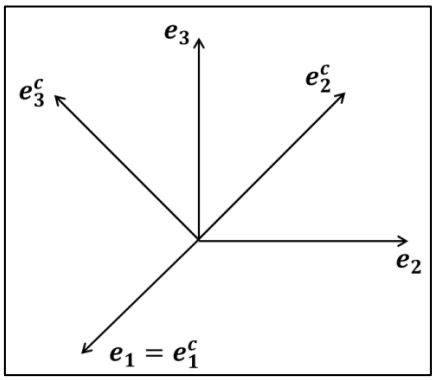

Figure 21 – An FCC single crystal orientated with its crystallographic direction [011] align with the base vector of the global CS e_3.

5.2.1.3 Results

It can be seen from Figure 22 that the length of the model in $\boldsymbol{e_2}$ direction was during the deformation due to crystal anisotropy unchanged, which in agreement with the experiment [20]. The reason why the crystal underwent plane strain deformation can be seen once the slip rate of each slip system is examined closer, see Table 4. It can be observed that only four slip systems out of twelve are active. Using values from Table 4, the spatial velocity gradient according to Equation (3-62) can be calculated:

$$[\mathbf{l}^{\mathrm{p}}] = \dot{\gamma}\begin{bmatrix} 2\sqrt{\frac{2}{3}} & 0 & 0 \\ 0 & 0 & 0 \\ 0 & 0 & -2\sqrt{\frac{2}{3}} \end{bmatrix} \quad (5\text{-}3)$$

The matrix above shows that the plastic deformation in the uniaxial compression of the single crystal with specific orientation is plane strain.

Table 4 – The slip system α is defined in the crystal and global CS by its slip direction s^c and it's normal to the slip plane s^c, s and n respectively. During the compression the stress within the crystal is resolved on each slip system α as resolved shear stress τ. When the resolved shear stress reach critical value (critical resolved shear stress) slip occurs donated by the strain rate $\dot{\gamma}$ [20]**.**

α	s^c	n^c	s	n	τ	$\dot{\gamma}$
1	$\frac{1}{\sqrt{2}}\ -\frac{1}{\sqrt{2}}\ 0$	$\frac{1}{\sqrt{3}}\ \frac{1}{\sqrt{3}}\ \frac{1}{\sqrt{3}}$	$\frac{1}{\sqrt{2}}\ -\frac{1}{2}\ -\frac{1}{2}$	$\frac{1}{\sqrt{3}}\ 0\ \sqrt{\frac{2}{3}}$	$\frac{\sigma}{\sqrt{6}}$	$\dot{\gamma}$
2	$-\frac{1}{\sqrt{2}}\ 0\ \frac{1}{\sqrt{2}}$	$\frac{1}{\sqrt{3}}\ \frac{1}{\sqrt{3}}\ \frac{1}{\sqrt{3}}$	$-\frac{1}{\sqrt{2}}\ -\frac{1}{2}\ \frac{1}{2}$	$\frac{1}{\sqrt{3}}\ 0\ \sqrt{\frac{2}{3}}$	$-\frac{\sigma}{\sqrt{6}}$	$-\dot{\gamma}$
3	$0\ \frac{1}{\sqrt{2}}\ -\frac{1}{\sqrt{2}}$	$\frac{1}{\sqrt{3}}\ \frac{1}{\sqrt{3}}\ \frac{1}{\sqrt{3}}$	0 1 0	$\frac{1}{\sqrt{3}}\ 0\ \sqrt{\frac{2}{3}}$	0	0
4	$\frac{1}{\sqrt{2}}\ 0\ \frac{1}{\sqrt{2}}$	$-\frac{1}{\sqrt{3}}\ \frac{1}{\sqrt{3}}\ \frac{1}{\sqrt{3}}$	$\frac{1}{\sqrt{2}}\ -\frac{1}{2}\ \frac{1}{2}$	$-\frac{1}{\sqrt{3}}\ 0\ \sqrt{\frac{2}{3}}$	$-\frac{\sigma}{\sqrt{6}}$	$-\dot{\gamma}$
5	$-\frac{1}{\sqrt{2}}\ -\frac{1}{\sqrt{2}}\ 0$	$-\frac{1}{\sqrt{3}}\ \frac{1}{\sqrt{3}}\ \frac{1}{\sqrt{3}}$	$-\frac{1}{\sqrt{2}}\ -\frac{1}{2}\ -\frac{1}{2}$	$-\frac{1}{\sqrt{3}}\ 0\ \sqrt{\frac{2}{3}}$	$\frac{\sigma}{\sqrt{6}}$	$\dot{\gamma}$
6	$0\ \frac{1}{\sqrt{2}}\ -\frac{1}{\sqrt{2}}$	$-\frac{1}{\sqrt{3}}\ \frac{1}{\sqrt{3}}\ \frac{1}{\sqrt{3}}$	0 1 0	$-\frac{1}{\sqrt{3}}\ 0\ \sqrt{\frac{2}{3}}$	0	0
7	$-\frac{1}{\sqrt{2}}\ 0\ \frac{1}{\sqrt{2}}$	$\frac{1}{\sqrt{3}}\ -\frac{1}{\sqrt{3}}\ \frac{1}{\sqrt{3}}$	$-\frac{1}{\sqrt{2}}\ -\frac{1}{2}\ \frac{1}{2}$	$\frac{1}{\sqrt{3}}\ -\sqrt{\frac{2}{3}}\ 0$	0	0
8	$0\ -\frac{1}{\sqrt{2}}\ -\frac{1}{\sqrt{2}}$	$\frac{1}{\sqrt{3}}\ -\frac{1}{\sqrt{3}}\ \frac{1}{\sqrt{3}}$	0 0 -1	$\frac{1}{\sqrt{3}}\ -\sqrt{\frac{2}{3}}\ 0$	0	0

9	$\frac{1}{\sqrt{2}}\ \frac{1}{\sqrt{2}}\ 0$	$\frac{1}{\sqrt{3}} - \frac{1}{\sqrt{3}}\ \frac{1}{\sqrt{3}}$	$\frac{1}{\sqrt{2}}\ \frac{1}{2}\ \frac{1}{2}$	$\frac{1}{\sqrt{3}} - \sqrt{\frac{2}{3}}\ 0$	0	0
10	$-\frac{1}{\sqrt{2}}\ \frac{1}{\sqrt{2}}\ 0$	$-\frac{1}{\sqrt{3}} - \frac{1}{\sqrt{3}}\ \frac{1}{\sqrt{3}}$	$-\frac{1}{\sqrt{2}}\ \frac{1}{2}\ \frac{1}{2}$	$-\frac{1}{\sqrt{3}} - \sqrt{\frac{2}{3}}\ 0$	0	0
11	$\frac{1}{\sqrt{2}}\ 0\ \frac{1}{\sqrt{2}}$	$-\frac{1}{\sqrt{3}} - \frac{1}{\sqrt{3}}\ \frac{1}{\sqrt{3}}$	$\frac{1}{\sqrt{2}} - \frac{1}{2}\ \frac{1}{2}$	$-\frac{1}{\sqrt{3}} - \sqrt{\frac{2}{3}}\ 0$	0	0
12	$0 - \frac{1}{\sqrt{2}} - \frac{1}{\sqrt{2}}$	$-\frac{1}{\sqrt{3}} - \frac{1}{\sqrt{3}}\ \frac{1}{\sqrt{3}}$	0 0 -1	$-\frac{1}{\sqrt{3}} - \sqrt{\frac{2}{3}}\ 0$	0	0

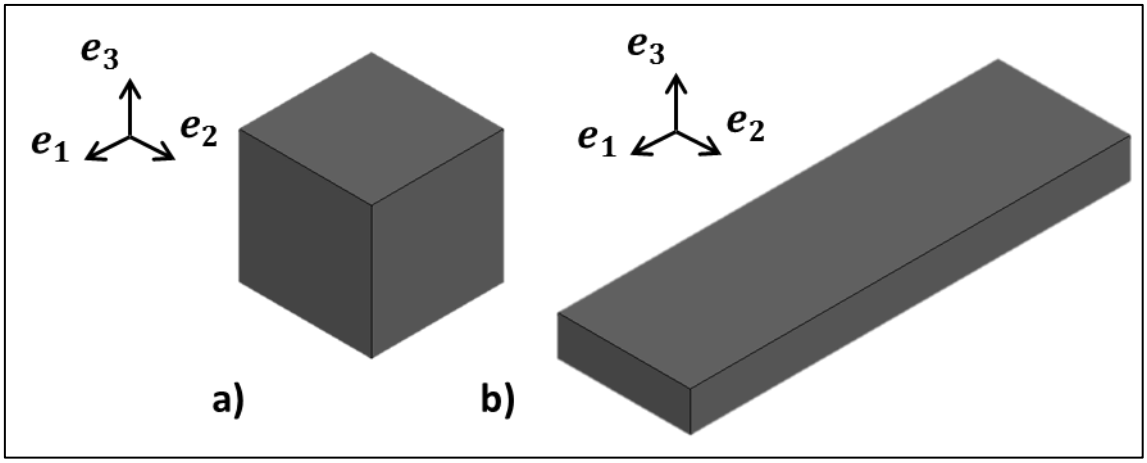

Figure 22 – a) The mesh of the undeformed single crystal. b) The mesh of the single crystal after compression (true strain |ε| = 0.5).

Experimental results for the stress strain curve and the evolution of the crystallographic texture were compared with the simulation, see Figure 23 and Figure 24. The difference in the stress strain curves does not exceed more than 4 %. For this particular crystallographic texture, the orientation of the crystal lattice does not rotate during the experiment, neither during the simulation.

5.2.1.4 Conclusion

It can be concluded that the subroutine for a large elastic-plastic deformations of FCC single crystal is able to reasonable predict the stress flow, macroscopic change of the shape and the evolution of the crystallographic texture.

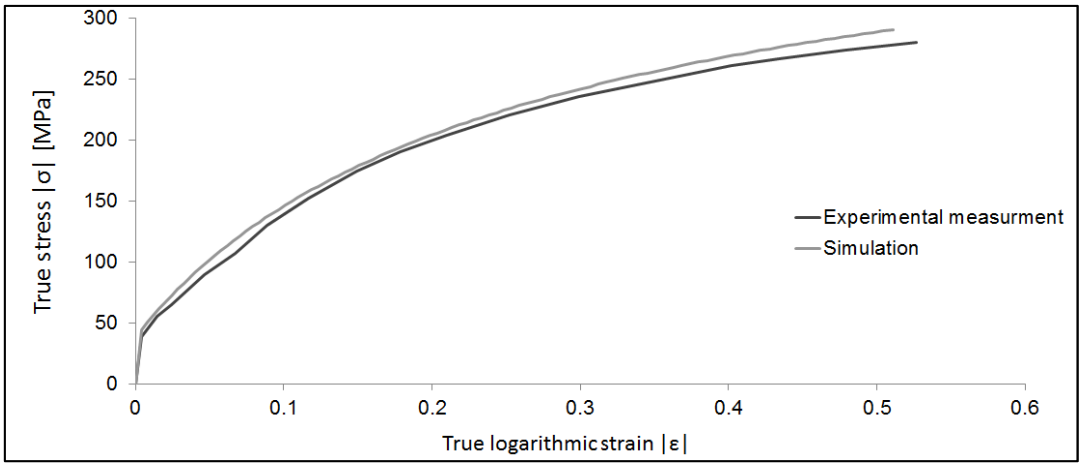

Figure 23 - Axial stress |σ| versus logarithmic axial strain |ε| in the simple compression test at room temperature on single OFHC copper crystal [20]**.**

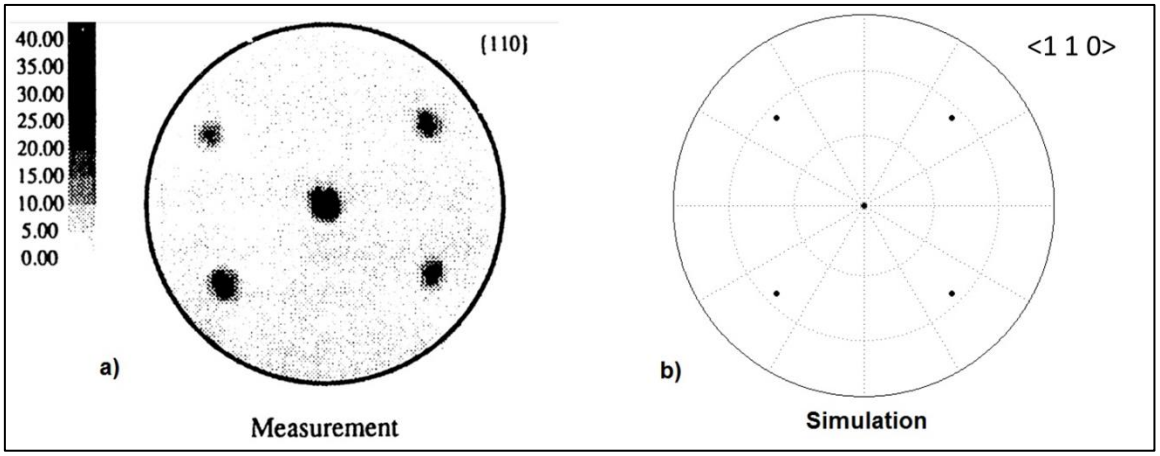

Figure 24 - Initial crystal orientation of a single OFHC copper crystal displayed by using the crystallographic projection in [110] directions: a) experimental specimen where the grey scale represents a number of crystals orientated in particular direction [20]**, b) a single crystal model used in the FE simulation.**

5.2.2 Large deformation of a polycrystalline aggregate

To verify the subroutine reliability on a larger scale model, (1) uniaxial tensile test and (2) uniaxial compression test simulations of an initially isotropic OFHC copper were performed on a representative model (for more information about the representative model assumptions see section below). Results such as the

stress strain curves and evolution of the crystal orientation were compared with the experimental results, for details of the experimental procedures see [47].

5.2.2.1 Representative Model of annealed Polycrystalline Aggregate

In order to be able to represent nearly annealed (isotropic) metal using CPFEM it is needed to make a model composed of a sufficient amount of randomly orientated crystals with a fairly uniform distribution. On the other hand the computational cost of simulation of such model has to be kept low. For this reason sensitive study has been performed and it was discovered that a model composed of 512 crystals is able to represent nearly annealed metal (see Section 6.1) and yet keep low computational cost.

The assumptions for the Representative Model are:

- The Representative Model with volume $1mm^3$ (grain size dependency is not taken into an account in our model) can represent annealed material (with nearly isotropic material properties). The isotropy is obtained due to the superposition of 512 randomly oriented crystals (see Figure 25) inside the model, where the fairly uniform distribution of the individual anisotropic crystals is averaged over the volume.
- Each crystal is represented by a single element (solid hexahedral element with one integration point [38]).
- The FCC micro-structural model with 12 slip systems is incorporated.
- Each crystal retains of both elastic and plastic anisotropy.
- The plastic deformation of crystalline aggregate is solely due to the dislocation slip mechanism.
- The rate viscoplastic power law, slip resistance evolution and material properties of OFHC copper were used as in Kalidindi [20].
- Note that in this model, boundaries between crystals are not explicitly taken into consideration due to the phenomenological approach of the single crystal strength model (hardening of the material is given by equations obtained from empirical observations rather than by defining dislocation density and dislocations “pile-up” [1] on the crystal boundaries which does happen in reality). When using dislocation density

constitutive model, boundaries between crystals can be included, for an example see Reference [48].

5.2.2.2 Uniaxial tension and compression

In order to simulate simple tension and compression, the bottom of the Representative Model was constrained to remain plane during the simulation and initial velocity was prescribed to the each node belonging to the top plane which resulted in axial strain rate of ±60 s^{-1}. This strain rate differs from the one used in the experiment (0.001 s^{-1}). The reason for this is that the DYNA3D is an explicit solver and setting strain rate for such low strain rate would significantly increase computational cost, hence higher strain rate was used and sensitivity study was performed, see Figure 29.

The Representative Model was compressed up to absolute value of the true strain (as it was done in experiment) |ε| = 1.5, respectively pulled |ε| = 0.37 (for larger strain necking has occurred which lead to inaccuracy), see Figure 26.

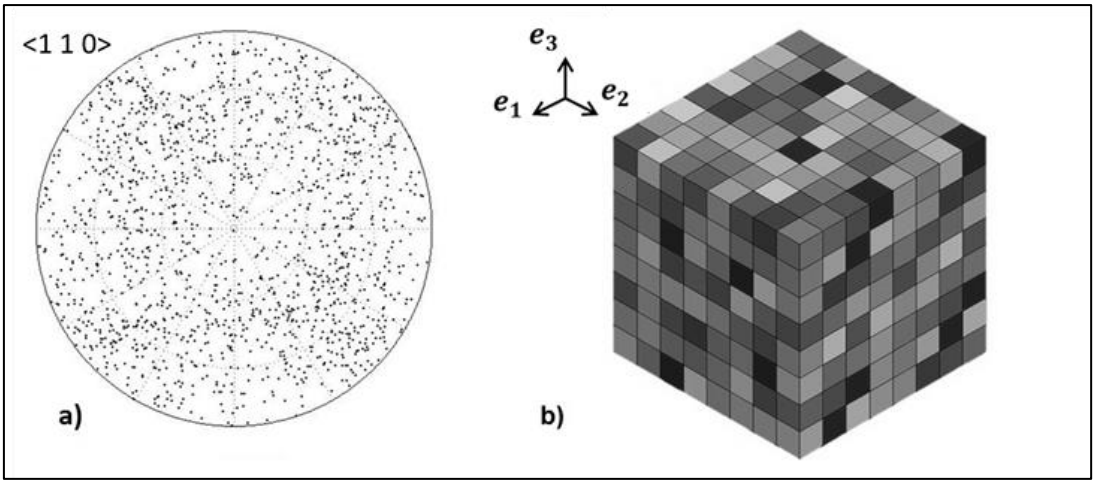

Figure 25 - a) Initial crystals orientation in the Representative Model displayed by using the crystallographic projection - pole figure <1 0 0>. b) The mesh of the Representative Model – one element represents one crystal.

5.2.2.3 Results

Afterward, the stress strain curves were evaluated and compared with the experimental data (Figure 27 and Figure 28). In both cases can be observed that the levels of the stress flow in the plastic zone for the simulations are

slightly higher. That can be explained by the differences in the strain rate, where experiments were run at $\dot{\epsilon}$ = 0.001/s and the simulations were run at $\dot{\epsilon}$ = 0.60/s. The way how the stress flow changes at different strain rate can be seen by comparing stress strain curves for compression of one single element, with decreasing the strain rate decrease also the stress flow, see Figure 29. In compression test (Figure 27) can be noticed, that the yielding point is relatively the same as in experiment, but what differs is the slope in elastic zone (not accurate prediction of the elastic stiffness). For the tension test it is the opposite, the elastic stiffness is in agreement and yielding point is highly overestimated.

Another way of evaluating the accuracy of the computational model is the comparison of evolution of the crystallographic texture in the experiment and in the simulation. The crystallographic texture was plotted after the simulation and matched with the experimental data. From the Figure 30 it is obvious that the experimental and simulation results are not in agreement.

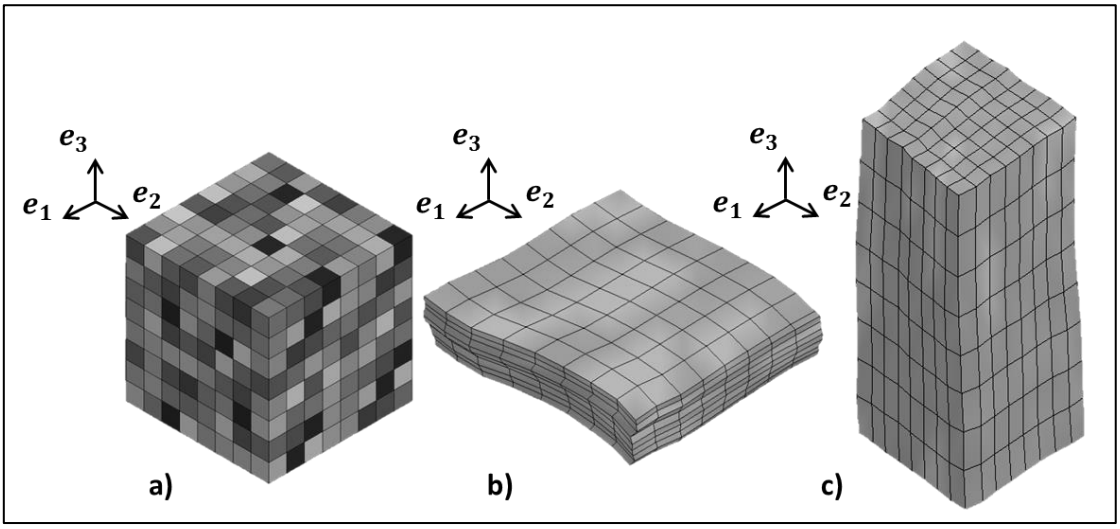

Figure 26 – a) Initial mesh of the Representative Model. b) The mesh of the model after compression c) The mesh of the model after tension.

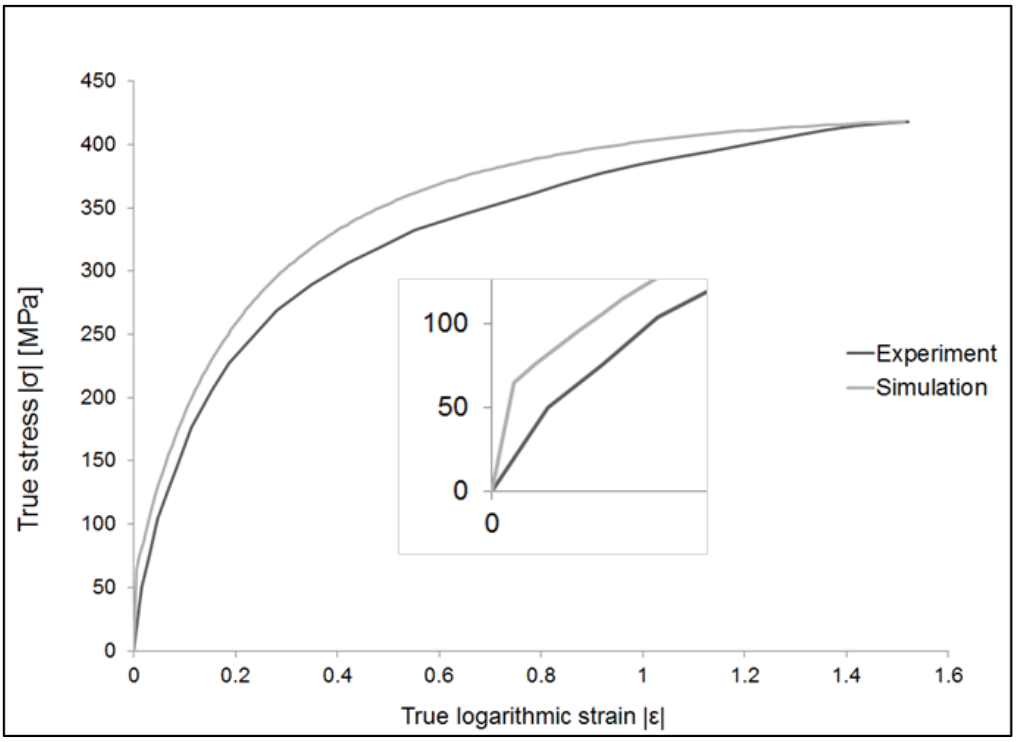

Figure 27 – Comparison of the stress strain curves in the compression derived from the experiment and the simulation.

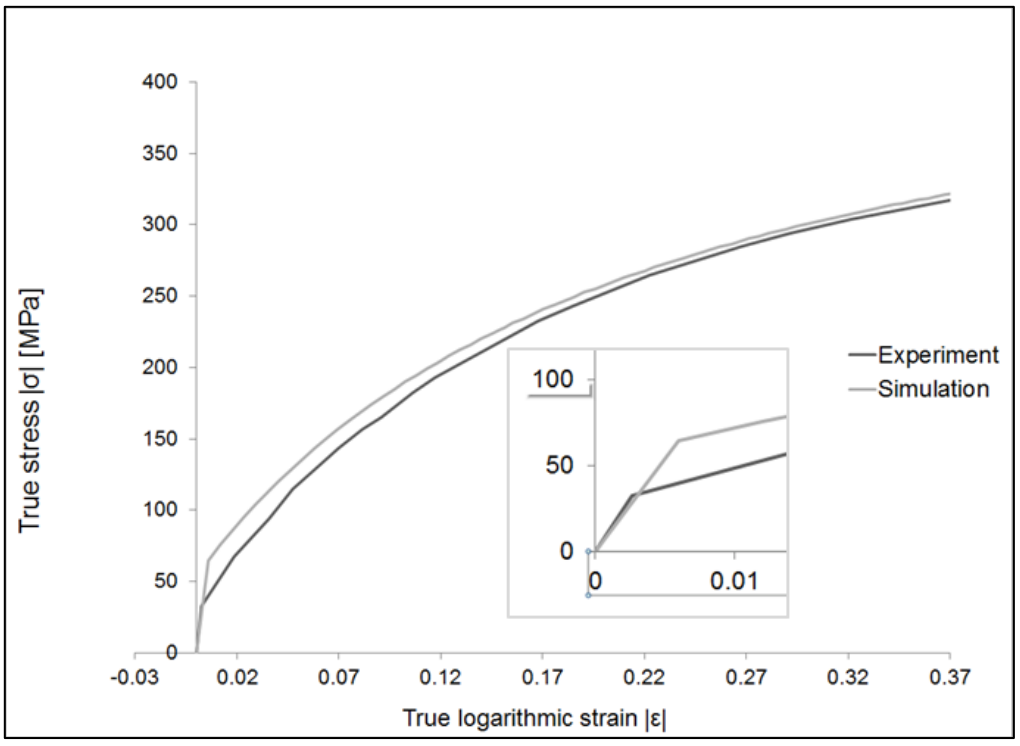

Figure 28 - Comparison of the stress strain curves in the tension derived from the experiment and the simulation.

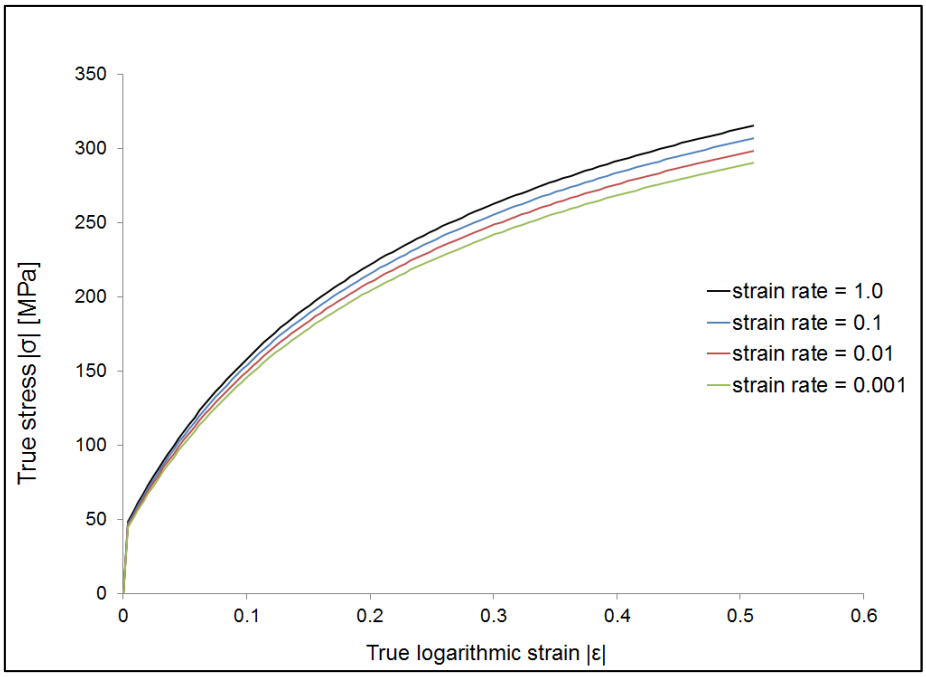

Figure 29 – Comparison of the stress strain curves for compression of single element of OFHC copper with different strain rate setting.

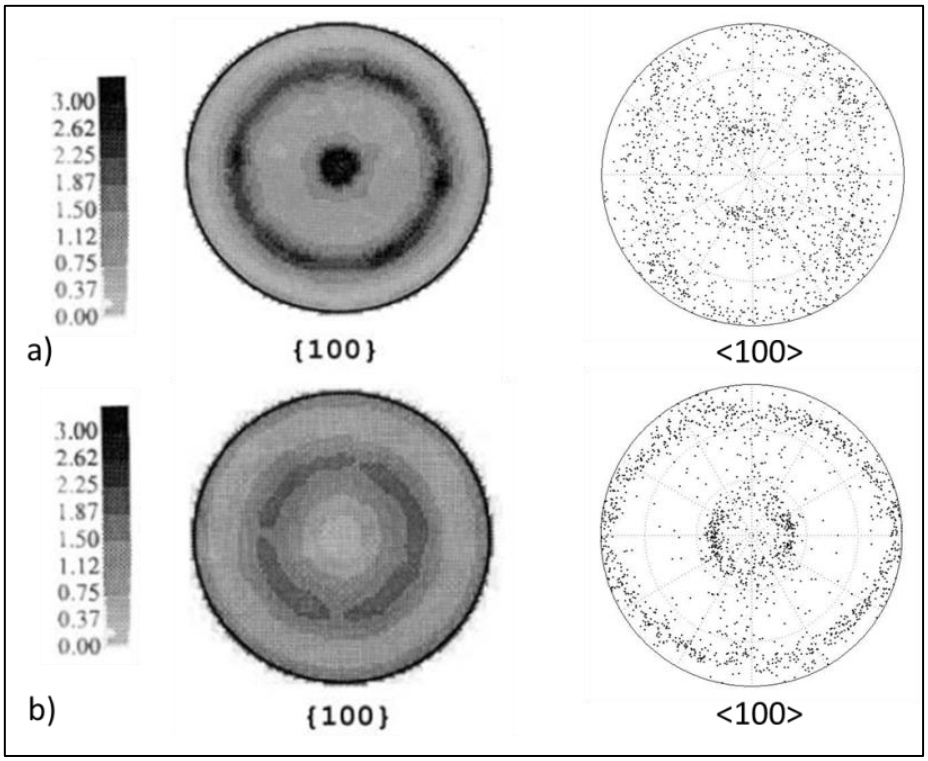

Figure 30 - Experimental [13] **and the numerical crystallographic texture. a) Simple tension of the Representative Model to ε = 0.37. b) Simple compression of the Representative Model to ε = - 1.5.**

5.3 Procedure to Improve Prediction of Large Deformation of FCC Polycrystalline Aggregate

1. An algorithm using MATLAB® code was developed to plot crystallographic texture by using equal-area crystallographic projection, see Section 4.6. Here could be the cause of discrepancy between simulation and experiment. The code and the method have to be investigated.
2. Another cause which could make the simulations results inaccurate could be in a bug in the subroutines code, see Section 4.2.3. The whole subroutine has been already checked step by step by making comparison with Huang implementation [21], but further verification is needed.
3. Origin of the model impreciseness could be in incorrect treatment of the crystal rotation, see Equations (4-5) and (4-6). That also has been already checked, but further investigation is required.
4. Different experimental data could be used for comparison where further literature survey would be needed, or setting up own experiments.

5.4 Proposals for Improvements of the New CPFEM

First, capability of the new CPFEM has to be assessed and necessary improvements has to be identified in terms of ability to predict large deformation of FCC and BCC structures of conditions of interest (e.g. high strain rate).

The new CPFEM is design to predict finite deformations of materials composed of BCC crystals (e.g. tantalum), if appropriate hardening law is implemented. The accuracy of the CPFEM for such prediction has to be investigated and that could be done by comparing data obtained from simulations with experimental data (these data could be acquired from different research sources experiments or by setting up own experiments).

The deformation mechanism incorporated in the new CPFEM accounts only for dislocation slip, but it is well known that in high strain rate deformations other deformation mechanisms can occur, such as twinning [1]. A guide to an

implementation of mechanical twinning as a phenomenological constitutive model can be found in the reference [3]. Another need due to shock wave propagation caused by high strain rate deformation could be to incorporate equation of state of solids at high pressure.

5.5 Conclusion

This chapter shows validation of the CPFEM and its methodology. It also proposes crucial improvements of the CPFEM which can be done in the future projects. The following chapter demonstrates capability of the CPFEM to model deformation of pre-deformed metals and ability to track the anisotropic evolution.

Specific achievements presented in this section are:

- Survey of available material data was done for FCC structures, where it was looked into other research projects. Suitable experimental data to validate the CPFEM were found (Kalidindi 1992 [20]) and new strain hardening law was implemented.
- Accuracy of this model was validated for large deformation of a single crystal of the annealed OFHC copper at room temperature. The change of the macroscopic shape during the deformation, the stress strain curve and evolution of the crystallographic texture obtained from the simple compression are in good agreement (discrepancy less than 5%) with the experiments.
- The model was also tested for large deformation of a polycrystalline aggregate comprised of 512 crystals of annealed anisotropic OFHC copper in the uniaxial compression and tension test. Here sufficient agreement (discrepancy less than 12%) with the experimental data was achieved, except prediction of elastic response for the compression test and yielding point in the tension test:

  Compression test:

  1. The yielding point is in agreement with the experiment.

2. The flow curve is in agreement with slight discrepancy, which could be caused due to different strain rate of the simulation and experiment.
3. The elastic stiffness does not agree with experimental measures (slope of the curve in the elastic zone).

Tension test:

1. The yielding point is highly overestimated in the stress strain curve when comparing with the experimental data.
2. The flow curve is in agreement with slight discrepancy, which could be caused due to different strain rate of the simulation and experiment.
3. The elastic stiffness is in agreement with experimental measures (slope of the curve in the elastic zone).

6 MODELLING BEHAVIOUR OF PRE-DEFORMED METAL

Mechanical properties of a crystal aggregate are significantly influenced by the orientation of the crystals within the aggregate. Piece of metal can have isotropic mechanical properties even if it is composed of anisotropic crystals, see Figure 31. The explanation lies in the superposition of large number of randomly orientated crystals inside the aggregate, where the fairly uniform distribution of the individual anisotropic crystals is averaged over the volume. This behaviour is modelled in Section 6.1. However, during a finite deformation (e.g. cold rolling – see Figure 32), shape and the orientation of the crystals within the isotropic aggregate changes and that give rise to a certain preferable texture (distribution of the crystallographic orientations) which is the cause of anisotropy evolution in a polycrystalline aggregate and change of mechanical material properties.

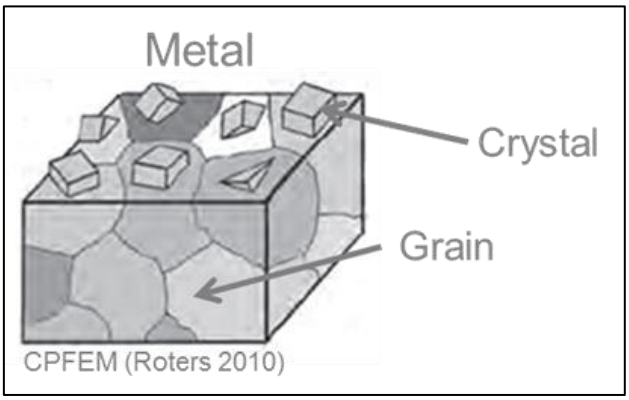

Figure 31 - Metal is made up of grains, where each grain is a single crystal of the material with varied orientation and shape. Usually in engineering calculations because the grains are very small, the behaviour of the metal is homogenized over its volume and its isotropy is assumed (part of the figure were taken from Roters [3]**).**

A demonstration of the ability of the new material model to predict the anisotropic response to mechanical loading of largely pre-deformed metal is shown in the Section 6.2.

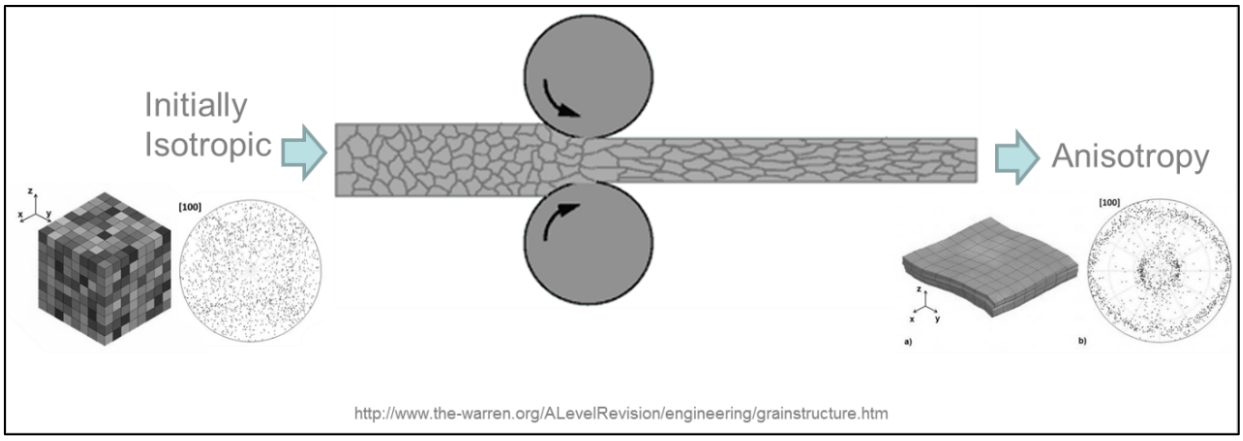

Figure 32 – Processes such as cold rolling, forging or shock loading change the microstructure of the metal and that leads to evolution of the level of anisotropy.

6.1 Isotropic Response to Mechanical Loading

This section demonstrates that the Representative Model from Section 5.2.2.1 has nearly isotropic material properties. To prove it, three identical Representative Models are pulled in three different directions in order to measure their mechanical properties and plot their stress strain curves. These three curves for an isotropic material should be nearly identical.

6.1.1 Methodology

Three undistinguishable Representative Models (with the same definition as in Section 5.2.2.1) are pulled independently in three different directions ($\boldsymbol{e_1}, \boldsymbol{e_2}$ and $\boldsymbol{e_3}$ – see Figure 33) by 10 % of their length with the same strain rate. The Representative Models are deformed in the way that

1) To the face of the first Representative Model (Figure 33a) with an arrow is assigned velocity in the direction $\boldsymbol{e_1}$ and the opposite face is constrained to move in the $\boldsymbol{e_1}$ direction.
2) To the face of the second Representative Model (Figure 33b) with an arrow is assigned velocity in the direction $\boldsymbol{e_2}$ and the opposite face is constrained to move in the $\boldsymbol{e_2}$ direction.
3) To the face of the third Representative Model (Figure 33c) with an arrow is assigned velocity in the direction $\boldsymbol{e_3}$ and the opposite face is constrained to move in the $\boldsymbol{e_3}$ direction.

Then by using script described in Section 4.5 three stress strain curves are plotted and compared.

6.1.2 Results

In Figure 34 can be seen that the material in the tensile test behaves according to the isotropic definition, the response to the tensile loading of Representative Model is nearly independent of its direction. Influence of the rotation of the crystals starts to be significant with much larger deformations. Here it has been proven that the new CPFEM does show isotropic behaviour of a metal Representative Model composed of a large number of randomly orientated anisotropic crystals.

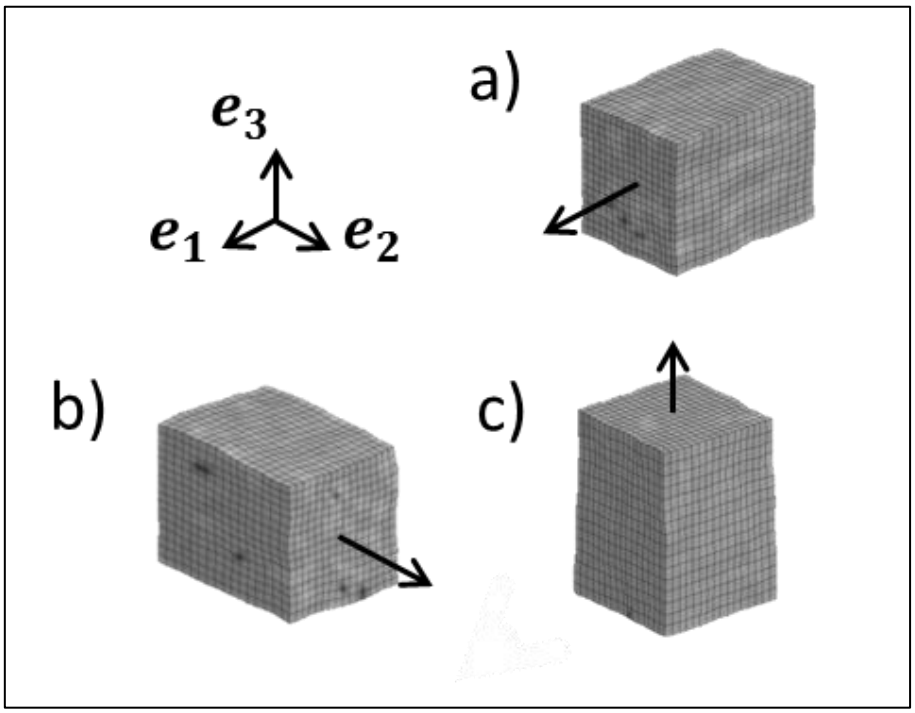

Figure 33 – Methodology of proving isotropic response of the Representative Model by pulling independently in e_1, e_2 and e_3 direction and plotting stress strain curves. The reason why the Representative Model is considered as an isotropic material lies in the superposition of large number of randomly orientated crystals with the fairly uniform distribution of the individual anisotropic crystals.

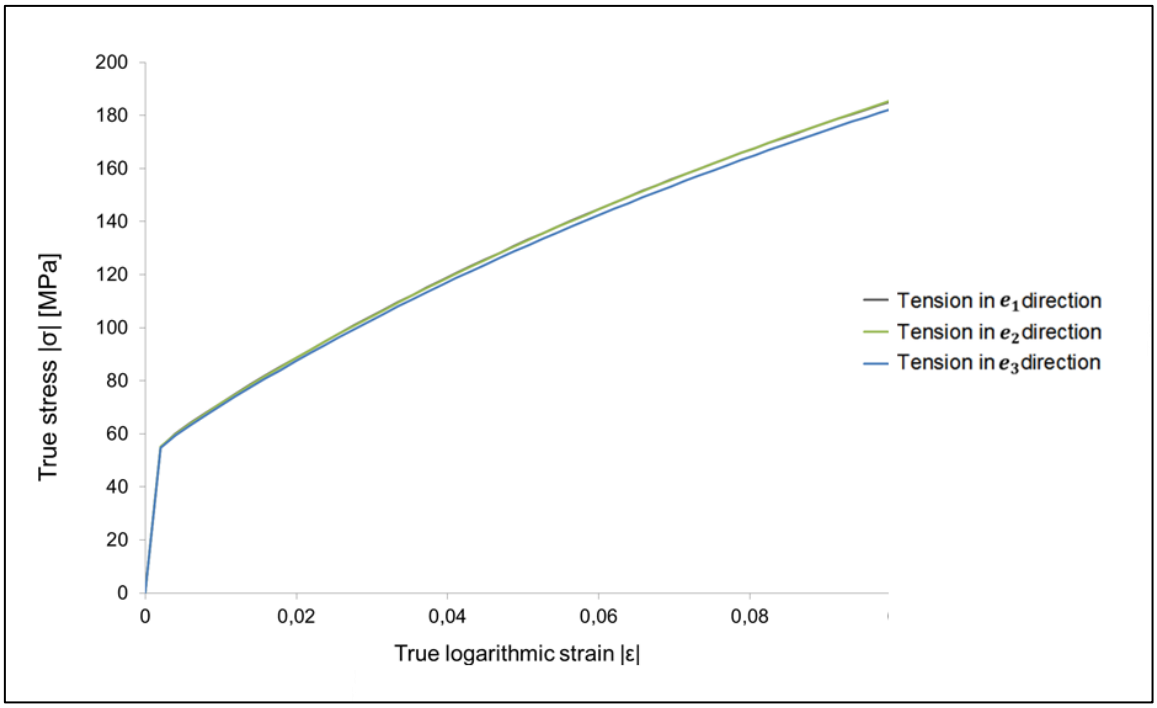

Figure 34 – The stress strain curves of three identical Representative Model in uniaxial tension test pulled independently in e_1, e_2 and e_3 direction.

6.2 Anisotropic Response to Mechanical Loading

This section shows what happened if the same Representative Model as in previous section is first pre-deformed and then the mechanical properties are measured. Anisotropy evolution should be observed and material properties should change during such process.

6.2.1 Methodology

1) An isotropic Representative Model (with the same definition as in Section 5.2.2.1) is firstly pre-deformed by 70 % of its original length in compression in the e_3 direction, such a large deformation change the distribution of the crystallographic orientation (see Figure 35).
2) Approximate elastic deformation in the deformed Representative Model is calculated and an equivalent displacement is applied in the opposite direction as in previous step. If this step is not done, then the removal of the boundary conditions in the next step results in additional inelastic deformation, which influences the results.

3) Then the three models are restarted, with no applied constraints and forces and run to generate a deformed Representative Model in an overall stress-free condition.
4) Afterward, these three pre-deformed Representative Models are pulled independently in three different directions by 10 % such as it was done in Section 6.1 in order to measure mechanical properties. The stress strain curves for each tensile test were carried out and compared.

6.2.2 Results

From stress strain curves (Figure 36) an anisotropic response to the tensile loading of the pre-deformed Representative Models can be observed. The main difference is in their yielding points. Discrepancy in the stress strain curves is caused by the significant re-orientation of the crystals during the pre-deforming process (Figure 35b). The reason why the flow curve in the tension in $\boldsymbol{e_2}$ is lower than in the $\boldsymbol{e_1}$ is not known and further investigation is needed, for some suggestions see Section 5.3.

6.3 Conclusion

One of the objectives of this project is to be able to model anisotropy evolution or in different words, evolution of the mechanical material properties during finite deformation. This section clearly shows that the new CPFEM is able to predict isotropic behaviour of a copper composed of a large number of randomly orientated anisotropic crystals and that is able to capture the change of its mechanical properties during large deformation. Note that the new CPFEM is not able to correctly predict/plot evolution of the crystallographic orientation which is closely related to material properties. Further investigation is needed, for some suggestions see Section 5.3.

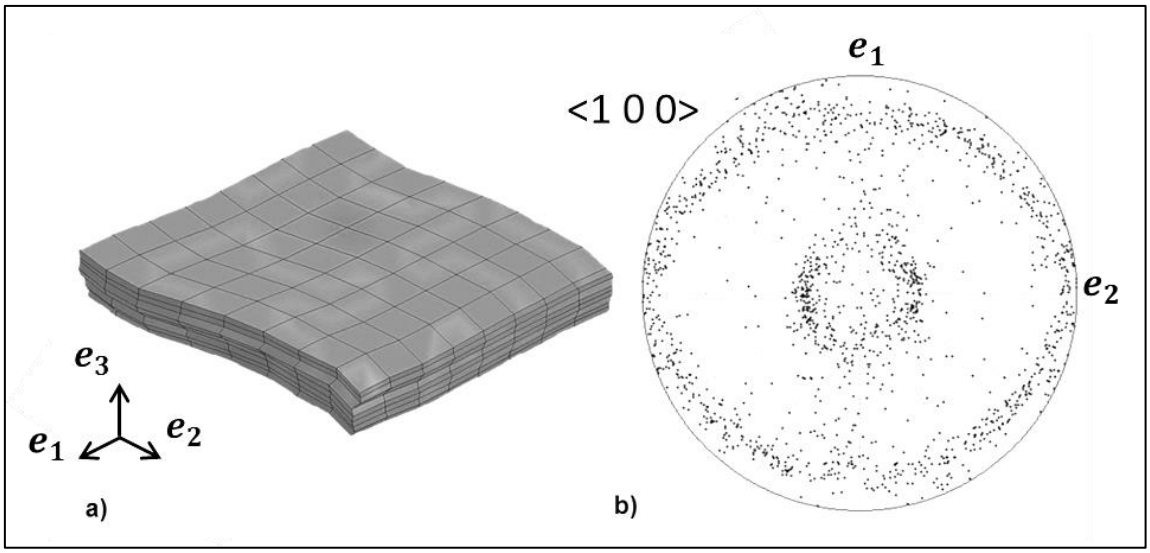

Figure 35 – a) The mesh of the pre-deformed Representative Model after compression in e_3 direction by 70% of its original length. b) Crystals orientation of the pre-deformed Representative Model – the crystallographic projection in [100] direction.

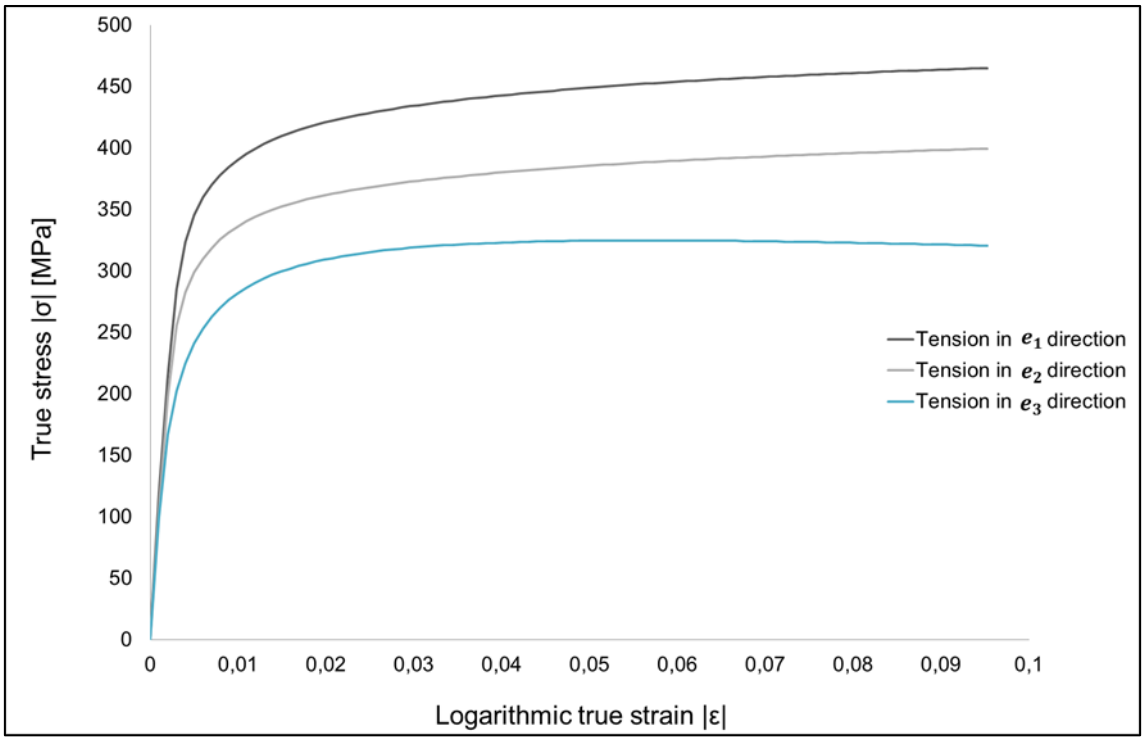

Figure 36 – The stress strain curves of three identical Representative Model (pre-deformed by 70% of their original length) in uniaxial tension test pulled independently in e_1, e_2 and e_3 directions.

7 SUMMARY, CONCLUSION AND FUTURE WORK

7.1 Summary

The aim of this project was to develop a computational capable of predicting large deformations of a single crystal or crystalline aggregate of a metal of interest and ability to trace an evolution of anisotropy within the material. This tool will be used in the future to study the anisotropic evolution in particular metals during dynamic finite deformations. Another aim was validate and assess this tool and its ability to predict a finite deformation and an anisotropy evolution in a polycrystalline aggregate.

In this project a new Crystal Plasticity Finite Element Method tool was developed. This new tool is able to predict large deformations of a single crystal or polycrystalline aggregate of FCC and BCC structures. Furthermore, an accuracy of this model was validated for large deformation of a single crystal of the annealed OFHC copper at room temperature. The change of the macroscopic shape during the deformation, the stress strain curve and evolution of the crystallographic texture obtained from the simple compression are in good agreement (discrepancy less than 5%) with the experiments. Also the model was also tested for large deformation of a polycrystalline aggregate comprised of 512 crystals of annealed anisotropic OFHC copper in uniaxial compression and tension test. Here sufficient agreement with the experimental data was achieved (discrepancy less than 12%), except for the prediction of elastic response for the compression test and yielding point in the tension test. The prediction of the evolution of the crystallographic texture was not accurate. But further investigation was proposed in order to find out the cause of the discrepancy. Note, that the CPFEM tool was not validated for BCC structures due to time constraints. Additionally, behaviour of anisotropic metals during a large deformation was modelled and it was demonstrated that this tool is able to predict and to trace an evolution of anisotropy. Moreover, procedure to improve prediction of a large deformation of FCC polycrystalline aggregate was suggested. Finally, proposals for improvements of the new tool were given and future projects are proposed.

7.2 Conclusion

The main benefit of having this computational tool (the new CPFEM) lies in virtual material testing. This virtual testing has the advantage over experiments in time and cost expenses. This tool and its future improvements will allow studying evolution of anisotropy in FCC and BCC materials during dynamic finite deformations, which can lead to current material models improvement.

7.3 Future Work Proposals

7.3.1 BCC structure validation

The CPFEM was not validated for BCC structures due to project time constraints. Survey of current research papers can be done in order to find experimental data containing information about mechanical response of BCC structures to mechanical loading. Then, these data could be used to re-model the experiment using the CPFEM and finally to perform the model validation.

7.3.2 Evolution laws

With the new CPFEM tool developed in this work, the evolution of anisotropy in particular metals due to a dynamic finite deformation can be investigated and evolution laws proposed. With this evolution laws it will be possible to predict change of elastic and plastic mechanical properties of a metal after its deformation.

7.3.2.1 Evolution of elasticity

Material elastic properties for each crystal are expressed in its stiffness matrix and can be extracted directly from a computational model. However, extracting material elastic properties from a whole aggregate model is not a trivial task. One option is to average individual crystal properties over the volume (homogenization), but there is a risk of losing information about material microstructure. Second option is running set of tests on an aggregate and measure stress strain curves, but this approach is more complex and more complicated than the first option. Choice based on efficiency and accuracy between these two methods has to be made. Then, by running set of simulation

where a material is highly deformed, change of the stiffness matrix can be tracked. The change of the material microstructure can be related with the change of the stiffness matrix and elastic anisotropic evolution law can be developed. Important to note, that such an evolution law has to be linked with an elastic stiffness tensor as a function of a material state parameter, which has to be measurable within the continuum level (could be e.g. rate of the deformation gradient).

7.3.2.2 Evolution of plasticity

Material plastic properties and its anisotropy can be described in simplified way by using its yield locus, which can be obtained by performing a set of virtual tests on a Representative Model (pure shear, uniaxial tension, plain strain, stack compression – see Figure 37) and by interpolating extracted data by using cubic Bezier-spline [8] [50]. Then the Representative Model will undergo prescribed deformations and the modified yield loci will be obtained. This procedure will allow investigating plastic anisotropy evolution in metals during large deformations and an evolution law could be proposed. This evolution law could be a function of a measurable material state parameter within the continuum level.

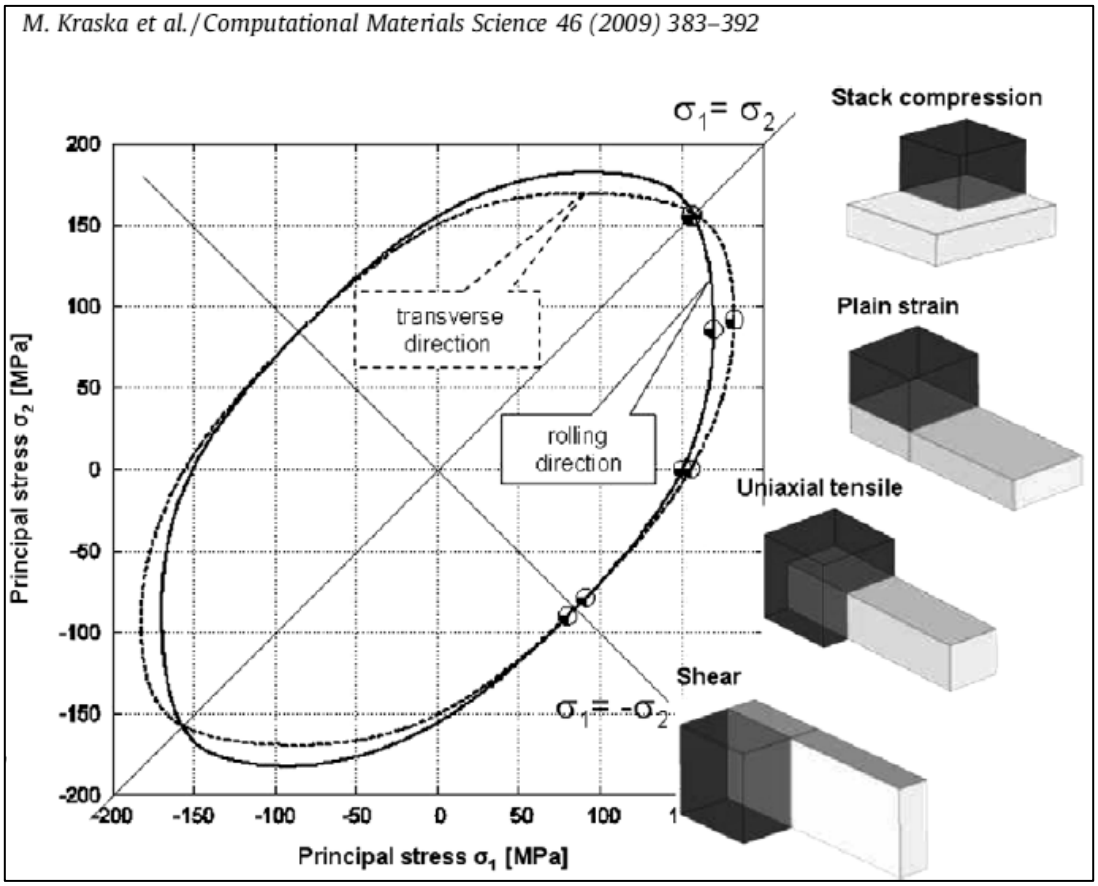

Figure 37 – The Vegter yield locus derived from a virtual test [8]**.**

7.3.3 Elastic projection operators

In 1995 Schreyer [2] proposed a new method where he relates the anisotropic plastic properties with the material elastic anisotropy. By using spectral decompositions of the stiffness matrix (the elasticity matrix) he obtains elastic projection operators which can implicitly describe preferred modes of deformation. Furthermore, the elastic projection operators can be used to define anisotropic yield surface of the material. It will be interesting to use this method to obtain preferred modes of deformation from a particular anisotropic metal and relate them to its microstructure, specifically to crystals orientation.

REFERENCES

[1] Dieter, G. E. (1988), *Mechanical Metallurgy,* SI Metric edition ed, McGraw-Hill Book Co, UK.

[2] Schreyer, H. L. and Zuo, Q. H. (1995), "Anisotropic yield surfaces based on elastic projection operators", *Journal of Applied Mechanics, Transactions ASME,* vol. 62, no. 3, pp. 780-785.

[3] Roters, F., Eisenlohr, P., Bieler, T. R. and Raabe, D. (2010), *Crystal Plasticity Finite Element Methods in Materials Science and Engineering,* WILEY-VCH, Weinheim.

[4] Osakada, K. (2010), "History of plasticity and metal forming analysis", *Journal of Materials Processing Technology,* vol. 210, no. 11, pp. 1436-1454.

[5] Roters, F., Eisenlohr, P., Hantcherli, L., Tjahjanto, D. D., Bieler, T. R. and Raabe, D. (2010), "Overview of constitutive laws, kinematics, homogenization and multiscale methods in crystal plasticity finite-element modeling: Theory, experiments, applications", *Acta Materialia,* vol. 58, no. 4, pp. 1152-1211.

[6] Weber, F., Schestakow, I., Roters, F. and Raaba, D. (2008), "Texture Evolution During Bending of a Single Crystal Copper", *Advanced Engineering Materials,* vol. 10, no. 8.

[7] Savage, P., O'Donnell, B. P., McHugh, P. E., Murphy, B. P. and Quinn, D. F. (2004), "Coronary stent strut size dependent stress-strain response investigated using micromechanical finite element models", *Annals of Biomedical Engineering,* vol. 32, no. 2, pp. 202-211.

[8] Kraska, M., Doig, M., Tikhomirov, D., Raabe, D. and Roters, F. (2009), "Virtual material testing for stamping simulations based on polycrystal plasticity", *Computational Materials Science,* vol. 46, no. 2, pp. 383-392.

[9] Grujicic, M. and Batchu, S. (2002), "Crystal plasticity analysis of earing in deep-drawn OFHC copper cups", *Journal of Materials Science,* vol. 37, no. 4, pp. 753-764.

[10] Zhang, K., Geng, X., Li, J. and Hu, R. (2007), "On the tension necking of copper single crystal specimen under slip deformation mechanism", *Science in China, Series E: Technological Sciences,* vol. 50, no. 3, pp. 308-318.

[11] Macek, K. (1999), *Nauka o Materialu,* 3rd ed, Fakulta strojni, Praha.

[12] Holzapfel, G. A. (2007), *Nonlinear solid mechanics: A continuum approach for engineering,* 6th ed, John Wiley & Sons Ltd., USA.

[13] Kalidindi, S. R., Bronkhorst, C. A. and Anand, L. (1992), "Crystallographic texture evolution in bulk deformation processing of FCC metals", *Journal of the Mechanics and Physics of Solids,* vol. 40, no. 3, pp. 537-569.

[14] Hamelin, C. J., Diak, B. J. and Pilkey, A. K. (2011), "Multiscale modelling of the induced plastic anisotropy in bcc metals", *International Journal of Plasticity,* vol. 27, no. 8, pp. 1185-1202.

[15] HUANG, S., ZHANG, S., LI, D. and PENG, Y. (2011), "Simulation of texture evolution during plastic deformation of FCC, BCC and HCP structured crystals with crystal plasticity based finite element method", *Transactions of Nonferrous Metals Society of China,* vol. 21, no. 8, pp. 1817-1825.

[16] Staroselsky, A. and Anand, L. (2003), "A constitutive model for hcp materials deforming by slip and twinning: Application to magnesium alloy AZ31B", *International Journal of Plasticity,* vol. 19, no. 10, pp. 1843-1864.

[17] Raabe, D. and Roters, F. (2004), "Using texture components in crystal plasticity finite element simulations", *International Journal of Plasticity,* vol. 20, no. 3, pp. 339-361.

[18] Raabe, D., Roters, F. and Wang, Y., (2005), *Simulation of earing during deep drawing of bcc steel by use of a texture component crystal plasticity finite element method*.

[19] Izadbakhsh, A., Inal, K., Mishra, R. K. and Niewczas, M. (2011), "New crystal plasticity constitutive model for large strain deformation in single crystals of magnesium", *Computational Materials Science,* vol. 50, no. 7, pp. 2185-2202.

[20] Kalidindi, S. R. (1992), *Polycrystal plasticity: constitutive modeling and deformation processing* (PhD thesis), Massachusetts Institute of Technology, .

[21] Huang, Y. (1991), "A user material subroutine incorporating single crystal plasticity in the abaqus finete element program", *Mech,* vol. 178.

[22] Ma, A. and Roters, F. (2004), "A constitutive model for fcc single crystals based on dislocation densities and its application to uniaxial compression of aluminium single crystals", *Acta Materialia,* vol. 52, no. 12, pp. 3603-3612.

[23] Ma, A., Roters, F. and Raabe, D. (2006), "Studying the effect of grain boundaries in dislocation density based crystal-plasticity finite element

simulations", *International Journal of Solids and Structures,* vol. 43, no. 24, pp. 7287-7303.

[24] Ma, A., Roters, F. and Raabe, D. (2006), "A dislocation density based constitutive model for crystal plasticity FEM including geometrically necessary dislocations", *Acta Materialia,* vol. 54, no. 8, pp. 2169-2179.

[25] Harewood, F. J. and McHugh, P. E. (2007), "Comparison of the implicit and explicit finite element methods using crystal plasticity", *Computational Materials Science,* vol. 39, no. 2, pp. 481-494.

[26] Li, H. W., Yang, H. and Sun, Z. C. (2008), "A robust integration algorithm for implementing rate dependent crystal plasticity into explicit finite element method", *International Journal of Plasticity,* vol. 24, no. 2, pp. 267-288.

[27] McHugh, P. E. (2004), "Introduction to Crystal Plasticity Theory", *Courses and lectures/ International Centre for Mechanical Sciences,* , no. 464, pp. 125-172.

[28] Taylor, G. I. (1938), "Plastic Strain in Metals", *J. Inst. Metals,* vol. 62, pp. 307.

[29] Rice, J. R. (1971), "Inelastic constitutive relations for solids: An internal-variable theory and its application to metal plasticity", *Journal of the Mechanics and Physics of Solids,* vol. 19, no. 6, pp. 433-455.

[30] Hill, R. and Rice, J. R. (1972), "Constitutive analysis of elastic-plastic crystals at arbitrary strain", *J.Mech.Phys.Solids,* vol. 20, pp. 401.

[31] Peirce, D., Asaro, R. J. and Needleman, A. (1983), "Material rate dependence and localized deformation in crystalline solids", *Acta Metallurgica,* vol. 31, no. 12, pp. 1951-1976.

[32] Asaro, R. J. "Micromechanics of Crystals and Polycrystals", in *Advances in Applied Mechanics,* Elsevier, , pp. 1-115.

[33] Asaro, R. J. (1983), "CRYSTAL PLASTICITY.", *Journal of Applied Mechanics, Transactions ASME,* vol. 50, no. 4 b, pp. 921-934.

[34] Peirce, D., Asaro, R. J. and Needleman, A. (1982), "An analysis of nonuniform and localized deformation in ductile single crystals", *Acta Metallurgica,* vol. 30, no. 6, pp. 1087-1119.

[35] Asaro, R. J. a. R., J.R. (1977), "Strain Localization in Ductile Single Crystals", *J.Mech.Phys.Solids,* vol. 25, pp. 309.

[36] Hutchinson, J. W. (1976), "Bounds and self-consistent estimates for creep of polycrystalline materials.", *Proc. Roy. Soc. London A,* vol. 348, pp. 1001.

[37] Brown, S. B., Kim, K. H. and Anand, L. (1989), "An internal variable constitutive model for hot working of metals", *International Journal of Plasticity,* vol. 5, no. 2, pp. 95-130.

[38] Jerry, I. L. (1999), *DYNA3D: User Manual*.

[39] Harewood, F. J. and McHugh, P. E. (2007), "Comparison of the implicit and explicit finite element methods using crystal plasticity", *Computational Materials Science,* vol. 39, no. 2, pp. 481-494.

[40] Cambell, J. (1998), *Lagrangian Hydrocode Modelling of Hypervelocity Impact on Spacecraft* (unpublished PhD thesis), College of Aeronautics, Cranfield University, Cranfield University.

[41] Raphanel, J. L., Ravichandran, G. and Leroy, Y. M. (2004), "Three-dimensional rate-dependent crystal plasticity based on Runge-Kutta algorithms for update and consistent linearization", *International Journal of Solids and Structures,* vol. 41, no. 22-23, pp. 5995-6021.

[42] Hielscher, R. (2013)*, A MATLAB Toolbox for Quantitative Texture Analysis*, available at: http://code.google.com/p/mtex/.

[43] LSTC (2012)*, LS-PrePost Online documentation*, available at: http://www.lstc.com/lspp/.

[44] ABAQUS (2004), *ABAQUS: Keywords Reference Manual,* .

[45] Zhang, X., Yao, Z., Liu, D., Chen, M. and Chen, Z. (2005), "FEM simulation of the earing of 3104 aluminum sheets", *Xiyou Jinshu Cailiao Yu Gongcheng/Rare Metal Materials and Engineering,* vol. 34, no. 4, pp. 581-585.

[46] Asaro, R. J. and Needleman, A. (1985), "Overview no. 42 Texture development and strain hardening in rate dependent polycrystals", *Acta Metallurgica,* vol. 33, no. 6, pp. 923-953.

[47] Bronkhorst, C. U. (1991), *Plastic deformation and crystallographic texture evolution in face-centered cubic metals* (PhD thesis), Massachusetts Institute of Technology, .

[48] Ma, A., Roters, F. and Raabe, D. (2006), "On the consideration of interactions between dislocations and grain boundaries in crystal plasticity

finite element modeling - Theory, experiments, and simulations", *Acta Materialia,* vol. 54, no. 8, pp. 2181-2194.

[49] LS-DYNA (2007), *LS-DYNA: Keyword User's Manual,* .

[50] Vegter, H., Horn, C.H., Atzema, E.H., An, Y., Pijlman, H.H., Boogaard, T.H. and Huetink, H., (2003), *Characteristaion and modelling of the plastic material behaviour and its application in sheet metal forming simulation*, VII International Conference on Computational Plasticity, Barcelona.

APPENDICES

Appendix A Model Implementation and Software Development

A.1 Debugging

Results obtained from the initial implementation of the UMAT-Single Crystal Plasticity [21] to DYNA3D® during simulation of a metal deformation were unrealistic. Therefore new methodology to debug the code was developed. Here is presented one of the debugging simulations.

A.1.1 Simple shear loading test

In order to check the code concerning the elastic part of Material 94, simple shear loading was chosen (Figure A-1). If the displacement is relatively small, only elastic deformation will occur [3].

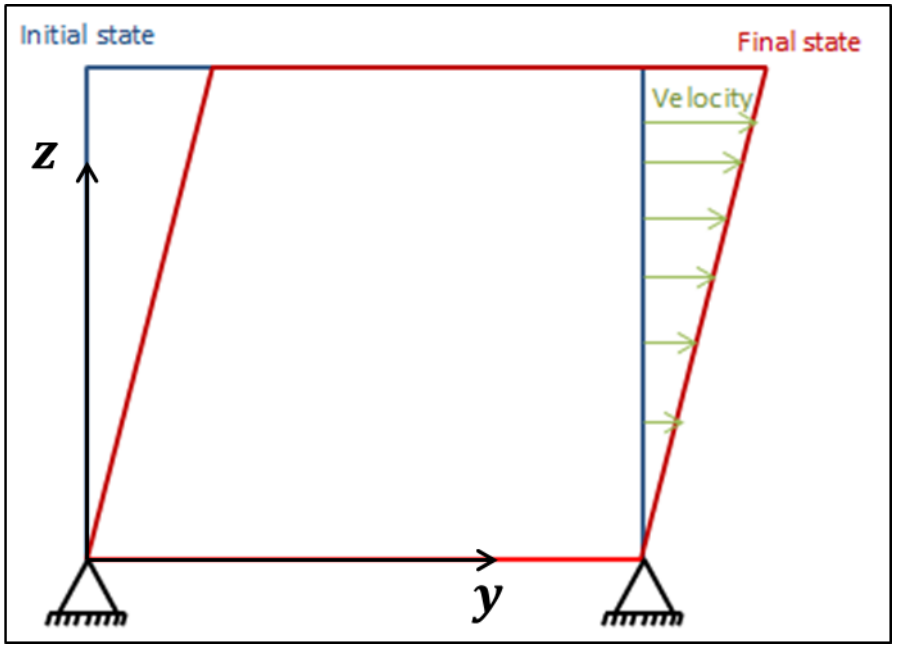

Figure A-1 Illustration of boundary condition for simulation of simple shear deformation test of a single crystal composed of 16 mesh elements.

7.3.4 Methodology

Model of 16 elements (solid three-dimensional hexahedral element with one integration point [49] of volume 1 mm^3) representing a single crystal was

created with copper material properties as in Section 5.2.1.1 and boundary conditions were set as in Figure A-1 (motion of each node was restricted in all directions except the one of velocity). In the aim to compare results: LS-DYNA (material 2 [49]), ABAQUS® (UMAT [21]) and DYNA3D® (material 94, material 2) were used with the same material properties and boundary conditions.

Nine simulations with different crystal orientation for each material model were run in order to see differences in the shear stress (shear strain = 1.25×10^{-3}).

7.3.5 Results

As it can be seen in Table A-1 the only different shear stress was in case of Material 94:

1) If the crystal was orientated as the global coordinate system (GCS) or was turned by 45° by keeping z axis equal to z axis in GCS the results were correct (simulation1, 2, 5, 7).
2) If the crystal was turned by 45° along x axis, respectively y axis (simulation 3, 6 and simulation 4,8) the shear stress differed in Material 94 from others and had value as it would be turned by 45° along y axis, respectively x axis.
3) In the last simulation the result was completely different as the crystal was turned along two axes.

Table A-1 Comparison of results for simple shear loading test for LS-Dyna, Umat and DYNA3D®

			YZ Stress [MPa]			
Simulation	Orientation[1] **a**	Orientation **d**	LS-DYNA	UMAT	DYNA3D® mat 2	DYNA3D® mat 94
1	(1, 0, 0)	(0, 1, 0)	94	94	94	94
2	(1, 1, 0)	(-1, 1,0)	94	94	94	94

[1] Orientation: **a** and **d** are vectors defined in global CS, which identify orientation of the crystal (third vector is calculated and it is perpendicular to a and d).

3	(1, 0, 0)	(0, 1, 1)	29	29	29	94
4	(1, 0, 1)	(1, 0,-1)	94	94	94	29
5	(1, 1, 0)	(-1, 1,0)	94	94	94	94
6	(0, 1, 1)	(0, 1,-1)	29	29	29	94
7	(1, 1, 0)	(1,-1, 0)	94	94	94	94
8	(-1, 0,1)	(-1,0,-1)	94	94	94	29
9	(1, 1, 1)	(1, 0, 1)	15	14	14	-28

7.3.6 Debugging system and conclusion

The bug could be in calculating local coordinate system of the model, stiffness matrix, in reading data from the input file, in passing data on, in storing, etc. Hence, debug system was created. Every variable was plotted at each step in the debug file and compared with UMAT.

It was found out that the problem lies in calculating transformation matrix (from local to global coordinate system, see Section 4.2.3 – Main subroutine) for elastic stiffness matrix. After fixing this bug the simulation was re-run and the results were identical for all four material models.

A.1 Implementation of New Treatment of Crystal Rotation

A new treatment of a crystal rotation was developed in order to be able to track the anisotropy evolution. This code was written in the Fortran 77 as the whole DYNA3D® software

```
c Update of the orientation matrix T
c
c Uprgade orientation matrix T to current the position (old
orientation matrix rotated solely by lattice part (d*+w*)) of
velocity gradient
c (for more information see Raphnel 2004 - "Three-demensional rate-
dependent crystal plasticity based on Runge-Kutta algorithms")
c
      term1 = zero
```

```
      term2 = zero
      term3 = zero
      term4 = zero
      ewedt = zero
      T1 = zero
c
c     Define We+De (elastic part of velocity gradient) - rate!!!!
not increment!!!!
      do i=lft,llt
       do j=1,3
        do k=1,3
         lat_rot(i,j,k) = zero
        enddo
       enddo
      enddo
c
      do i=lft,llt
       delta_s(i,1) = d1(i)
       delta_s(i,2) = d2(i)
       delta_s(i,3) = d3(i)
       delta_s(i,4) = d4(i)
       delta_s(i,5) = d5(i)
       delta_s(i,6) = d6(i)
      enddo
c
      do k=1,6
       do j=1,tnslip
        do i=lft,llt
         delta_s(i,k) = delta_s(i,k) - slpdef(i,k,j)*fslip(i,j)
        enddo
       enddo
      enddo
c
      if (dt1 == zero) then
      else
       do i=lft,llt
        lat_rot(i,1,1) = delta_s(i,1)
        lat_rot(i,2,2) = delta_s(i,2)
        lat_rot(i,3,3) = delta_s(i,3)
        lat_rot(i,1,2) = delta_s(i,4) - wzzdt(i)/dt1
        lat_rot(i,2,1) = delta_s(i,4) + wzzdt(i)/dt1
        lat_rot(i,1,3) = delta_s(i,5) + wyydt(i)/dt1
        lat_rot(i,3,1) = delta_s(i,5) - wyydt(i)/dt1
        lat_rot(i,2,3) = delta_s(i,6) - wxxdt(i)/dt1
        lat_rot(i,3,2) = delta_s(i,6) + wxxdt(i)/dt1
       enddo
      endif
c
      do j=1,tnslip
       do i=lft,llt
        lat_rot(i,1,2) = lat_rot(i,1,2) - slpspn(i,1,j)*fslip(i,j)
        lat_rot(i,2,1) = lat_rot(i,2,1) + slpspn(i,1,j)*fslip(i,j)
        lat_rot(i,1,3) = lat_rot(i,1,3) - slpspn(i,3,j)*fslip(i,j)
        lat_rot(i,3,1) = lat_rot(i,3,1) + slpspn(i,3,j)*fslip(i,j)
        lat_rot(i,2,3) = lat_rot(i,2,3) - slpspn(i,2,j)*fslip(i,j)
        lat_rot(i,3,2) = lat_rot(i,3,2) + slpspn(i,2,j)*fslip(i,j)
```

```
       enddo
      enddo
c
c
c     Calculate term1 = we = sqrt((W:W)/2)
c     Calculate term2 = sin(we*dt)/we
c     Calculate term3 = (1-cos(we*dt)/we**2
      do k=1,3
       do j=1,3
        do i=lft,llt
         term1(i) = term1(i) + lat_rot(i,j,k)*lat_rot(i,j,k)
        enddo
       enddo
      enddo
c
      do i=lft,llt
       term1(i) = sqrt(term1(i)/2)
       if (term1(i) == zero) then
        term2(i) = zero
        term3(i) = zero
       else
        term2(i) = sin(term1(i)*dt1)/term1(i)
        term3(i) = (one-cos(term1(i)*dt1))/term1(i)**2
       endif
      enddo
c     Calculate term4 = We*We, dot product of lat_rot
      do i=1,3
       do j=1,3
        do k=1,3
         do l=lft,llt
          term4(l,i,j) = term4(l,i,j) +
lat_rot(l,i,k)*lat_rot(l,k,j)
         enddo
        enddo
       enddo
      enddo
c
c     Calculate e**(We*dt) = ewedt
      do k=1,3
       do j=1,3
        do i=lft,llt
          ewedt(i,j,k) = Id(j,k) + term2(i)*lat_rot(i,j,k) +
     1                   term3(i)*term4(i,j,k)
        enddo
       enddo
      enddo
c
c     Finally, calculation of the current orientation matrix T' =
ewedt*T
      do i=1,3
       do j=1,3
        do k=1,3
         do l=lft,llt
          T1(l,i,j) = T1(l,i,j) + ewedt(l,i,k)*T(l,k,j)
         enddo
        enddo
```

```
       enddo
      enddo
c
c      Passing back current orientation to T(lnv,3,3)
      T = zero
      do k=1,3
       do j=1,3
        do i=lft,llt
         T(i,j,k) = T1(i,j,k)
        enddo
       enddo
      enddo
c
```

A.2 Implementation of New Strain Hardening

```
c=======================================================================
c
      subroutine latentharden(nset,nslip,tnslip,cm,gamma,g_a,h)
c
c     Routine to calculate strain rate in individual slip systems
c     as in the UMAT the actual expressions are functions and can
be replaced by alternate
c     formulations if required.
c
c
      implicit none
c
      FLOAT hself,hlatent
      external hself,hlatent
      FLOAT hselfk,hlatentk
      external hselfk,hlatentk
c
      integer lnv
      parameter(lnv=VECLEN)
c
      integer lft,llt
      common/aux36/lft,llt
c
      integer nset, nslip(3), tnslip ! no. sets slip systems, no.
slip systems per set, total number of slip systems
      FLOAT gamma                    ! Total element cumulative
shear strain
      FLOAT a                        ! Material parametr
      FLOAT g_a(lnv,48)              ! current slip system strength
      FLOAT h(lnv,48,48)             ! latent and self hardening
moduli for slip systems
      FLOAT cm(*)
c
      integer i,j,latent,k
      integer iself,point
c
      a = cm(41)
      iself = 0
```

```
      do i=1,nset
       point = 19 + 5*i
       do j=1,nslip(i)
        iself = iself + 1
        do latent=1,tnslip
         if(cm(40).eq.1)then      ! Hypersecant hardening law
          if(latent.eq.iself) then
           do k=lft,llt
            h(k,iself,iself) = hself(cm(point),gamma,g_a)
           enddo
          else
           do k=lft,llt
            h(k,latent,iself) = hlatent(i,nslip,iself,latent,
     1                                  cm(point),gamma,g_a)
           enddo
          endif
         else                     ! Kalidindi hardening
          if(latent.eq.iself) then
           do k=lft,llt
            h(k,iself,iself) = hselfk(k,latent,cm(point),g_a,a)
           enddo
          else
           do k=lft,llt
           h(k,latent,iself) = hlatentk(k,i,nslip,iself,latent,
     1                                  cm(point),g_a,a)
           enddo
          endif
         endif
        enddo
       enddo
      enddo
      end

c-----------------------------------------------------------------------
c
c     Hardening law used in Kalidindi 1992 (Crystallographic
texture evolution in bulk deformation processing of FCC Metals)
c
      FLOAT function hselfk(k,latent,cm,g_a,a)
      implicit none
c
      integer lnv
      parameter(lnv=VECLEN)
c
      integer lft,llt
      common/aux36/lft,llt
c
      integer k,latent
      FLOAT gamma                   ! Total element cumulative
shear strain
      FLOAT g_a(lnv,48)             ! current slip system strength
      FLOAT a                       ! material parametr
      FLOAT cm(2)
      FLOAT term1

      term1 = 1.0d+00 - g_a(k, latent)/cm(2)
```

```
      hselfk = cm(1)*(abs(term1))**a*sign(1.0d+00,term1)
      return
      end
c
      FLOAT function hlatentk(k,i,nslip,iself,latent,cm,g_a,a)
      implicit none
c
      integer lnv
      parameter(lnv=VECLEN)
c
      integer lft,llt
      common/aux36/lft,llt
c
      integer k,i,nslip(3),iself,latent
      integer ilower,iupper,j
      FLOAT gamma                    ! Total element cumulative
shear strain
      FLOAT g_a(lnv,48)              ! current slip system strength
      FLOAT a                        ! material parametr
      FLOAT cm(5)
      FLOAT term1,q

      ilower = 1
      iupper = nslip(1)
      if(i.gt.1) then
       do j=2,i
        ilower = ilower + nslip(j-1)
        iupper = iupper + nslip(j)
       enddo
      endif
      if(latent.ge.ilower.and.latent.le.iupper)then
       q = cm(4)
      else
       q=cm(5)
      endif
      term1 = 1.0d+00 - g_a(k, latent)/cm(2)
      hlatentk = cm(1)*q*(abs(term1))**a*sign(1.0d+00,term1)
      return
      end
c=======================================================================
```

A.3 Creating Input File for DYNA3D®

This script reads material card from already existing input material file DYNA3D® (has to be in the same folder) and it creates a new file with n crystals with the same material properties but with different “random” orientation

```
!*************************************************************
**********
```

```
!
!  PROGRAM: Material Card Generator for DYNA3D® - Mat94
!
!  PURPOSE:  Assigning two vectors in the material card to
represent random crystal orientation rotation
!
!*****************************************************************
**********

    PROGRAM input_generator

    IMPLICIT NONE

    ! Variables:
    CHARACTER (300) :: charFileInput, charFileOutput =
'mat_crystals'                          ! Name of DYNA3D®file input,
output
    INTEGER :: iError
! I/O status for opening the file
    INTEGER :: i, ii, n, j, k
    REAL, DIMENSION (6) :: rnd
! 6 random numbers for two vectors
    INTEGER, DIMENSION (6) :: rnd_int
    INTEGER, DIMENSION (:), ALLOCATABLE :: seed
    INTEGER :: clock,z
! time in seconds


    INTEGER :: card1_1, card1_2, card1_4, card1_5, card1_7,
card1_10, card1_11, card1_12    ! Material properties card1
    REAL :: card1_3, card1_6, card1_8, card1_9
! Material properties card1
    CHARACTER (73) :: head1
! Head of the material file
    CHARACTER (1) :: head2
    CHARACTER (100) :: card2
! Name of the material

    REAL :: card31, card32, card33, card34, card35, card36, card37,
card38                  ! Mat prop card3
    REAL :: card41, card42, card43, card44, card45, card46, card47,
card48                  ! Mat prop card4
    REAL :: card51, card52, card53, card54, card55, card56, card57,
card58                  ! Mat prop card5
    REAL :: card61, card62, card63, card64, card65, card66, card67,
card68                  ! Mat prop card6
    REAL :: card74, card75, card76, card77, card78
! Mat prop card7
    REAL :: card84, card85, card86, card87, card88
! Mat prop card8
    REAL :: card71, card72, card73, card81, card82, card83
! 6 coordinates for defining lattice orientation

   !real, dimension (:), allocatable :: x
   !integer, dimension(2) :: seed, seed_old
   !integer :: L,i2,n_min,n_max,ran_int,sizer,clock
```

```
    ! Body of Console1

    ! Declaration of characters seed
    head1 = '*--------------------------- MATERIAL CARDS ----------
-----------------*'
    head2 = '*'

    !Declare name of the input file
    WRITE (*,*) 'Insert a name of DYNA3D® input file'
    READ (*,*) charFileInput
    WRITE (*,1000) charFileInput
    1000 Format (' ', 'Name of your input file is: ', A)

    ! Opening a DYNA3D® file and error checking
    OPEN (UNIT=10, FILE=charFileInput, STATUS='OLD', ACTION='READ',
IOSTAT=ierror)

    openif: If ( iError > 0) THEN
            WRITE (*,1010) charFileInput
            1010 FORMAT (' ','ERROR: File:' ,A, 'does not exist!')
    END IF openif

    ! Opening an output file for writing material properties down
    OPEN (UNIT=20, FILE=charFileOutput, STATUS='REPLACE',
ACTION='WRITE', IOSTAT=ierror)

    !! Read the material properties CARD 1 from line 89
    READ (10,1020) card1_1, card1_2, card1_3, card1_4, card1_5,
card1_6, card1_7, card1_8, card1_9, card1_10, card1_11, card1_12
    1020 FORMAT (88/, 2I5, E10.0, I5,2(I5,E10.0), E10.0, 3I5)
    !WRITE (*,*) 'card1 test', card1_1

    ! Read CARD2
    READ (10, 1040) card2
    1040 FORMAT (A100)
    !WRITE (*,*) 'card2 test', card2

    ! Read CARD3
    READ (10, 1060) card31, card32, card33, card34, card35, card36,
card37, card38
    1060 FORMAT (8ES10.4)
    !WRITE (*,*) 'card3 test', card31

    ! Read CARD4
    READ (10, 1080) card41, card42, card43, card44, card45, card46,
card47, card48
    1080 FORMAT (8ES10.4)

    ! Read CARD5
    READ (10, 1100) card51, card52, card53, card54, card55, card56,
card57, card58
    1100 FORMAT (8ES10.4)
    !WRITE (*,*) 'card3 test', card31
```

```
    ! Read CARD6
    READ (10, 1120) card61, card62, card63, card64, card65, card66,
card67, card68
    1120 FORMAT (8ES10.4)

    ! Read CARD7
    READ (10, 1140) card71, card72, card73, card74, card75, card76,
card77, card78
    1140 FORMAT (8ES10.4)
    !WRITE (*,*) 'card3 test', card31

    ! Read CARD8
    READ (10, 1160) card81, card82, card83, card84, card85, card86,
card87, card88
    1160 FORMAT (8ES10.4)

    ! Generating random seed used later for random vectors
    CALL RANDOM_SEED (SIZE = n)             ! setting up the size
of the seed
    ALLOCATE (seed(n))

    CALL SYSTEM_CLOCK (COUNT = clock)       ! getting 'random'
number from the current time
    !WRITE (*,*) 'clock', clock

    seed=clock + 37* (/ (ii-1, ii=1, n) /)
    CALL RANDOM_SEED (PUT = seed)
    !WRITE (*,*) 'seed', seed

    DEALLOCATE (seed)

    ! Loop, write down n materials with random orientation
    DO i = 0, 4095
        CALL RANDOM_NUMBER (rnd)

        card71 = rnd(1)*2-1
        card72 = rnd(2)*2-1
        card73 = rnd(3)*2-1
        card81 = rnd(4)*2-1
        card82 = rnd(5)*2-1
        card83 = rnd(6)*2-1

        ! Write  the material properties CARD1 to the output file
        card1_1 = 1+i
        WRITE (20,1030) card1_1, card1_2, card1_3, card1_4,
card1_5, card1_6, card1_7, card1_8, card1_9, card1_10, card1_11,
card1_12
        1030 FORMAT (2I5, ES10.4, I5,2(I5,ES10.4), ES10.4, 3I5)

        ! Write card2 to the output file
        WRITE (20,1050) card2
        1050 FORMAT (A)

        ! Write card3 to the output file
```

```
        WRITE (20,1070) card31, card32, card33, card34, card35,
card36, card37, card38
        1070 FORMAT (3ES10.3, 5ES10.3)

        ! Write card4 to the output file
        WRITE (20,1090) card41, card42, card43, card44, card45,
card46, card47, card48
        1090 FORMAT (3E10.3, 5ES10.3)

        ! Write card5 to the output file
        WRITE (20,1110) card51, card52, card53, card54, card55,
card56, card57, card58
        1110 FORMAT (3E10.3, 5ES10.3)

        ! Write card6 to the output file
        WRITE (20,1130) card61, card62, card63, card64, card65,
card66, card67, card68
        1130 FORMAT (8ES10.3)

        ! Write card7 to the output file
        WRITE (20,1150) card71, card72, card73, card74, card75,
card76, card77, card78
        1150 FORMAT (8ES10.3)

        ! Write card8 to the output file
        WRITE (20,1150) card81, card82, card83, card84, card85,
card86, card87, card88

        !WRITE (20,*) head2

    END DO
    WRITE (*,*) 'Material cards where succesfully writen in the
file', charfileoutput

    ! Close input file
    CLOSE ( UNIT=10 )

    ! Close output file
    CLOSE ( UNIT=20 )

    end program input_generator
```

A.4 Extraction of Material Data Information

This script written in VBA uses data from a forrct file generated by DYNA3D®. The script loads data from forrct file and then generates stress strain curves.

```
Option Explicit

Sub Open_File()

    Dim FolderOut As String
    Dim FileName As String, ArchiveName As String
```

```
    Dim wbMaster As Workbook, wbTemp As Workbook
    Dim wsFORRCT As Worksheet
    Dim fileToOpen As String
    Dim strNombre As String, msg As String, strPriklad As String
    Dim rgAdress As Range


    Set wbMaster = ThisWorkbook
    Set wsFORRCT = wbMaster.Sheets("FORRCT")
    fileToOpen = Application.GetOpenFilename("Text Files (*), *", ,
"Open FORRCT")
    If fileToOpen = "Falso" Then
        Sheets("Main").Select
        Exit Sub
    End If

        Workbooks.OpenText FileName:=fileToOpen, Origin _
        :=xlMSDOS, StartRow:=1, DataType:=xlFixedWidth,
FieldInfo:=Array(Array(0 _
        , 1), Array(10, 1), Array(25, 1), Array(40, 1), Array(53,
1)), TrailingMinusNumbers:= _
        True
        Set wbTemp = ActiveWorkbook

        Cells.Copy
        wsFORRCT.Cells.PasteSpecial
        Application.DisplayAlerts = False
        wbTemp.Close False
        Application.DisplayAlerts = True

End Sub

Sub SumOfForrces()

Dim wbMaster As Workbook
Dim wsFORRCT As Worksheet, wsRESULTS As Worksheet
Dim rgData As Range, rgNode As Range, rgObsah As Range
Dim cl As Range
Dim strNode As String, strForce2 As String
Dim rgForceX As Range, rgForceY As Range, rgForceZ As Range, rgTime
As Range
Dim rgDataX As Range, rgDataY As Range, rgDataZ As Range,
rgDataTime As Range
Dim lParametr As Long, strTime As String, lTime As Long


Set wbMaster = ThisWorkbook
Set wsFORRCT = wbMaster.Sheets("FORRCT")
Set wsRESULTS = wbMaster.Sheets("RESULTS")

With wsFORRCT
    Set rgData = .Range("A1", .Cells(.Rows.Count, "A").End(3))
End With

For Each cl In rgData
    strNode = cl.Value
```

```
    If strNode = "node" Then
        Set rgNode = cl
        Set rgNode = rgNode.Offset(2)

        With wsFORRCT
            Set rgObsah = .Range(rgNode, rgNode.End(xlDown))
        End With

'Setting regions for each forces for each time
        Set rgDataX = rgObsah.Offset(, 1)
        Set rgDataY = rgObsah.Offset(, 2)
        Set rgDataZ = rgObsah.Offset(, 3)
        Set rgDataTime = rgNode.Offset(-4, 4)

'Summ of forces for each time for each direction
        With wsRESULTS
            Set rgForceX = .Cells(.Rows.Count, "B").End(3)
            Set rgForceX = rgForceX.Offset(1)
            rgForceX.Value = "=Sum(FORRCT!" & rgDataX.AddressLocal
& ")"

            Set rgForceY = .Cells(.Rows.Count, "C").End(3)
            Set rgForceY = rgForceY.Offset(1)
            rgForceY.Value = "=Sum(FORRCT!" & rgDataY.AddressLocal
& ")"

            Set rgForceZ = .Cells(.Rows.Count, "D").End(3)
            Set rgForceZ = rgForceZ.Offset(1)
            rgForceZ.Value = "=Sum(FORRCT!" & rgDataZ.AddressLocal
& ")"

            Set rgTime = .Cells(.Rows.Count, "A").End(3)
            Set rgTime = rgTime.Offset(1)
'            strTime = rgDataTime
'            lParametr = "11"
'            strTime = Right(strTime, lParametr)
'            rgTime.NumberFormat = "@"
             rgTime = rgDataTime
        End With
    End If
Next
End Sub

Sub FillingXYZ()

Dim wbMaster As Workbook
Dim wsFORRCT As Worksheet, wsRESULTS As Worksheet, wsMain As
Worksheet
Dim rgData As Range, rgNode As Range, rgObsah As Range
Dim cl As Range, cl2 As Range, cl3 As Range, cl4 As Range, cl5 As
Range
Dim strNode As String, strForce2 As String
Dim rgForceX As Range, rgForceY As Range, rgForceZ As Range, rgTime
As Range
Dim rgDataX As Range, rgDataY As Range, rgDataZ As Range,
rgDataTime As Range
```

```
Dim lParametr As Long, strTime As String, lTime As Long
Dim Counter As Long, Steps As Long
Dim wsX As Worksheet, wsY As Worksheet, wsZ As Worksheet
Dim X As String, Y As String, Z As String, SpeedX As String, SpeedY
As String, SpeedZ As String
Dim strStrain As String, strStress As String

Set wbMaster = ThisWorkbook
Set wsMain = wbMaster.Sheets("Main")
Set wsFORRCT = wbMaster.Sheets("FORRCT")
Set wsRESULTS = wbMaster.Sheets("RESULTS")
Set wsX = wbMaster.Sheets("X")
Set wsY = wbMaster.Sheets("Y")
Set wsZ = wbMaster.Sheets("Z")
Counter = "0"
Steps = wsMain.Range("A25")
X = wsMain.Range("B4")
X = Replace(X, ",", ".")
Y = wsMain.Range("B5")
Y = Replace(Y, ",", ".")
Z = wsMain.Range("B6")
Z = Replace(Z, ",", ".")
Set rgForceX = wsRESULTS.Range("B3")
Set rgForceY = wsRESULTS.Range("C3")
Set rgForceZ = wsRESULTS.Range("D3")
Set rgTime = wsRESULTS.Range("A3")
SpeedX = wsMain.Range("B9")
SpeedY = wsMain.Range("B10")
SpeedZ = wsMain.Range("B11")

Do While Counter < Steps
    Set cl = wsX.Range("A3").Offset(Counter) 'Displacement For X
        cl.Value = rgTime.Offset(Counter).Value * SpeedX
'    cl.Value = "=Main!A14*Main!B9*" & Counter
    Set cl2 = wsX.Range("A3").Offset(Counter, 1) 'Strain For X
    strStrain = "=" & cl.Address & "/" & X
    cl2.Value = strStrain
    Set cl3 = wsX.Range("A3").Offset(Counter, 2) 'Stress For X
    strStress = "=RESULTS!" & rgForceX.Offset(Counter).Address &
"/" & "(" & Y & "*" & Z & ")"
    cl3.Value = strStress
    Set cl4 = wsX.Range("A3").Offset(Counter, 4) 'Strain true For X
    cl4.FormulaR1C1 = "=LN(1+RC[-3])"
    Set cl5 = wsX.Range("A3").Offset(Counter, 5) 'Stress true For X
    cl5.FormulaR1C1 = "=RC[-3]*(1+RC[-4])"

    Set cl = wsY.Range("A3").Offset(Counter) 'Displacement For Y
    cl.Value = rgTime.Offset(Counter).Value * SpeedY
'    cl.Value = "=Main!A14*Main!B10*" & Counter
    Set cl2 = wsY.Range("A3").Offset(Counter, 1)
    strStrain = "=" & cl.Address & "/" & Y
    cl2.Value = strStrain
    Set cl3 = wsY.Range("A3").Offset(Counter, 2) 'Stress For Y
    strStress = "=RESULTS!" & rgForceY.Offset(Counter).Address &
"/" & "(" & X & "*" & Z & ")"
```

```
    cl3.Value = strStress
    Set cl4 = wsY.Range("A3").Offset(Counter, 4) 'Strain true For X
    cl4.FormulaR1C1 = "=LN(1+RC[-3])"
    Set cl5 = wsY.Range("A3").Offset(Counter, 5) 'Stress true For X
    cl5.FormulaR1C1 = "=RC[-3]*(1+RC[-4])"

    Set cl = wsZ.Range("A3").Offset(Counter) 'Displacement For Z
    cl.Value = rgTime.Offset(Counter).Value * SpeedZ
'    cl.Value = "=Main!A14*Main!B11*" & Counter
    Set cl2 = wsZ.Range("A3").Offset(Counter, 1)
    strStrain = "=" & cl.Address & "/" & Z
    cl2.Value = strStrain
    Set cl3 = wsZ.Range("A3").Offset(Counter, 2) 'Stress For Z
    strStress = "=RESULTS!" & rgForceZ.Offset(Counter).Address &
"/" & "(" & X & "*" & Y & ")"
    cl3.Value = strStress
    Set cl4 = wsZ.Range("A3").Offset(Counter, 4) 'Strain true For X
    cl4.FormulaR1C1 = "=LN(1+RC[-3])"
    Set cl5 = wsZ.Range("A3").Offset(Counter, 5) 'Stress true For X
    cl5.FormulaR1C1 = "=RC[-3]*(1+RC[-4])"

    Counter = Counter + 1
Loop
End Sub

Sub GrafikaX()

Dim wbMaster As Workbook
Dim wsFORRCT As Worksheet, wsRESULTS As Worksheet, wsMain As
Worksheet
Dim rgData As Range, rgNode As Range, rgObsah As Range
Dim cl As Range, cl2 As Range, cl3 As Range, cl4 As Range, cl5 As
Range
Dim strNode As String, strForce2 As String
Dim rgForceX As Range, rgForceY As Range, rgForceZ As Range, rgTime
As Range
Dim rgDataX As Range, rgDataY As Range, rgDataZ As Range,
rgDataTime As Range
Dim lParametr As Long, strTime As String, lTime As Long
Dim Counter As Long, Steps As Long
Dim wsX As Worksheet, wsY As Worksheet, wsZ As Worksheet
Dim X As String, Y As String, Z As String
Dim strStrain As String, strStress As String

Set wbMaster = ThisWorkbook
Set wsMain = wbMaster.Sheets("Main")
Set wsFORRCT = wbMaster.Sheets("FORRCT")
Set wsRESULTS = wbMaster.Sheets("RESULTS")
Set wsX = wbMaster.Sheets("X")
Set wsY = wbMaster.Sheets("Y")
Set wsZ = wbMaster.Sheets("Z")

With wsX
    Set rgDataX = .Range("E3", .Cells(.Rows.Count, "E").End(3))
    Set rgDataY = .Range("F3", .Cells(.Rows.Count, "F").End(3))
End With
```

```
Sheets("GraphX").Select

    ActiveChart.ChartArea.Select
    ActiveChart.SeriesCollection.NewSeries
    ActiveChart.SeriesCollection(1).Values = rgDataY
    ActiveChart.SeriesCollection(1).XValues = rgDataX

End Sub

Sub GrafikaY()

Dim wbMaster As Workbook
Dim wsFORRCT As Worksheet, wsRESULTS As Worksheet, wsMain As
Worksheet
Dim rgData As Range, rgNode As Range, rgObsah As Range
Dim cl As Range, cl2 As Range, cl3 As Range, cl4 As Range, cl5 As
Range
Dim strNode As String, strForce2 As String
Dim rgForceX As Range, rgForceY As Range, rgForceZ As Range, rgTime
As Range
Dim rgDataX As Range, rgDataY As Range, rgDataZ As Range,
rgDataTime As Range
Dim lParametr As Long, strTime As String, lTime As Long
Dim Counter As Long, Steps As Long
Dim wsX As Worksheet, wsY As Worksheet, wsZ As Worksheet
Dim X As String, Y As String, Z As String
Dim strStrain As String, strStress As String

Set wbMaster = ThisWorkbook
Set wsMain = wbMaster.Sheets("Main")
Set wsFORRCT = wbMaster.Sheets("FORRCT")
Set wsRESULTS = wbMaster.Sheets("RESULTS")
Set wsX = wbMaster.Sheets("X")
Set wsY = wbMaster.Sheets("Y")
Set wsZ = wbMaster.Sheets("Z")

With wsY
    Set rgDataX = .Range("E3", .Cells(.Rows.Count, "E").End(3))
    Set rgDataY = .Range("F3", .Cells(.Rows.Count, "F").End(3))
End With

    Sheets("GraphY").Select

    ActiveChart.ChartArea.Select
    ActiveChart.SeriesCollection.NewSeries
    ActiveChart.SeriesCollection(1).Values = rgDataY
    ActiveChart.SeriesCollection(1).XValues = rgDataX

End Sub

Sub GrafikaZ()

Dim wbMaster As Workbook
Dim wsFORRCT As Worksheet, wsRESULTS As Worksheet, wsMain As
Worksheet
```

```
Dim rgData As Range, rgNode As Range, rgObsah As Range
Dim cl As Range, cl2 As Range, cl3 As Range, cl4 As Range, cl5 As
Range
Dim strNode As String, strForce2 As String
Dim rgForceX As Range, rgForceY As Range, rgForceZ As Range, rgTime
As Range
Dim rgDataX As Range, rgDataY As Range, rgDataZ As Range,
rgDataTime As Range
Dim lParametr As Long, strTime As String, lTime As Long
Dim Counter As Long, Steps As Long
Dim wsX As Worksheet, wsY As Worksheet, wsZ As Worksheet
Dim X As String, Y As String, Z As String
Dim strStrain As String, strStress As String

Set wbMaster = ThisWorkbook
Set wsMain = wbMaster.Sheets("Main")
Set wsFORRCT = wbMaster.Sheets("FORRCT")
Set wsRESULTS = wbMaster.Sheets("RESULTS")
Set wsX = wbMaster.Sheets("X")
Set wsY = wbMaster.Sheets("Y")
Set wsZ = wbMaster.Sheets("Z")

With wsZ
    Set rgDataX = .Range("E3", .Cells(.Rows.Count, "E").End(3))
    Set rgDataY = .Range("F3", .Cells(.Rows.Count, "F").End(3))
End With

    Sheets("GraphZ").Select

    ActiveChart.ChartArea.Select
    ActiveChart.SeriesCollection.NewSeries
    ActiveChart.SeriesCollection(1).Values = rgDataY
    ActiveChart.SeriesCollection(1).XValues = rgDataX

End Sub

Sub ChangeSign()

Dim wbMaster As Workbook
Dim wsFORRCT As Worksheet, wsRESULTS As Worksheet, wsMain As
Worksheet
Dim rgData As Range, rgNode As Range, rgObsah As Range
Dim cl As Range, cl2 As Range, cl3 As Range, cl4 As Range, cl5 As
Range
Dim strNode As String, strForce2 As String
Dim rgForceX As Range, rgForceY As Range, rgForceZ As Range, rgTime
As Range
Dim rgDataX As Range, rgDataY As Range, rgDataZ As Range,
rgDataTime As Range
Dim lParametr As Long, strTime As String, lTime As Long
Dim Counter As Long, Steps As Long
Dim wsX As Worksheet, wsY As Worksheet, wsZ As Worksheet
Dim X As String, Y As String, Z As String
Dim strStrain As String, strStress As String

Set wbMaster = ThisWorkbook
```

```
Set wsMain = wbMaster.Sheets("Main")
Set wsFORRCT = wbMaster.Sheets("FORRCT")
Set wsRESULTS = wbMaster.Sheets("RESULTS")
Set wsX = wbMaster.Sheets("X")
Set wsY = wbMaster.Sheets("Y")
Set wsZ = wbMaster.Sheets("Z")

With wsX
    Set rgData = .Range("C3", .Cells(.Rows.Count, "C").End(3))
End With

rgData.Value = rgData.Value

For Each cl In rgData
    If cl.Value < 0 Then
        cl.Value = cl.Value * -1
    End If
Next

With wsY
    Set rgData = .Range("C3", .Cells(.Rows.Count, "C").End(3))
End With

rgData.Value = rgData.Value

For Each cl In rgData
    If cl.Value < 0 Then
        cl.Value = cl.Value * -1
    End If
Next

With wsZ
    Set rgData = .Range("C3", .Cells(.Rows.Count, "C").End(3))
End With

rgData.Value = rgData.Value

For Each cl In rgData
    If cl.Value < 0 Then
        cl.Value = cl.Value * -1
    End If
Next


End Sub
```

A.5 Tracing an Evolution of Crystallographic Orientation

In our CP model the information about a crystal orientation is given in the orientation matrix $\mathbf{T}$ (3×3) in terms of <1 0 0> directions. This matrix is updated in every time increment, see Equation (4-10). Each column in this matrix represents an orthonormal base of a crystal $\boldsymbol{e}_i^c$. This matrix $\mathbf{T}$ and its evolution

during deformation is passed to the d3plot file, which can be open by post-processing software Ls-PrePost [43]. The information of the crystal orientation (expressed as 9 components of the matrix **T**) can be found under the history of an element as variables “history var#1 – history var#9”.

Then each variable history var#1 – history var#9 has to be plotted within LS-PrePost and saved as MSoft CSV (Single X-Axis) within the desired time so 9 files (1.csv to 9.csv) are obtained. These files are then copy to the same file where is this script written in the Matlab code.

The main script is:

```
%This soft loads csv data (crystal orientation) and plots pole
figure

%Read x coordinate part of vector a
file_name = '1.csv';
% This comand csvread reads csv file, it skips first line and first
%column:
[A] = csvread(file_name, 1, 1);

%Read y coordinate part of vector a
file_name = '2.csv';
[B] = csvread(file_name, 1, 1);

%Read z coordinate part of vector a
file_name = '3.csv';
[C] = csvread(file_name, 1, 1);

%Read x coordinate part of vector b
file_name = '4.csv';
[D] = csvread(file_name, 1, 1);

%Read y coordinate part of vector b
file_name = '5.csv';
[E] = csvread(file_name, 1, 1);

%Read z coordinate part of vector b
file_name = '6.csv';
[F] = csvread(file_name, 1, 1);

%Read x coordinate part of vector c
file_name = '7.csv';
[G] = csvread(file_name, 1, 1);

%Read y coordinate part of vector c
file_name = '8.csv';
[H] = csvread(file_name, 1, 1);

%Read z coordinate part of vector c
file_name = '9.csv';
```

```
[I] = csvread(file_name, 1, 1);

%It is needed compile three coordinates to a vector for all
crystals
V(:,1) = [A(1,:) D(1,:) G(1,:)];
V(:,2) = [B(1,:) E(1,:) H(1,:)];
V(:,3) = [C(1,:) F(1,:) I(1,:)];


%Make 3d vectors, X (i=1:X,) which is below has to be changed
X=3xnumber of
%elements
for i=1:1536,
    vector(i) = vector3d(V(i,1),V(i,2),V(i,3));
end

%Plot crystal orientation in iqual-area projection
close all; figure('position',[50 50 500 500])
%
plot(vector,'Marker','l','MarkerSize',10,'MarkerFaceColor','Black',
'MarkerEdgeColor','Black','grid','antipodal')
plot(vector,'Marker','o','MarkerSize',2,'MarkerFaceColor','Black','
MarkerEdgeColor','Black','grid','antipodal')
```

After running this script desired pole figure is obtained.

Appendix B Material Input File for DYNA3D®®

Material Type 94 (Crystal plasticity)

Material model added by Cranfield University. This material is implemented for hexahedral elements only.

Columns		Quantity	Format
1-10	Card 3	Elastic modulus in longitudinal direction, E_a	E10.0
11-20		Elastic modulus in transverse direction, E_b	E10.0
21-30		Elastic modulus in normal direction, E_c	E10.0
31-40		Rate sensitivity exponent for slip system 1, *n.*	E10.0
41-50		Reference strain rate for slip system 1, $\dot{a}$.	E10.0
51-60		Hardening option	E10.0
		EQ.1.0: Hypersecant hardening law (Umat Documentation)	
		else: Hardening law used in Kalidindi 1992 (Crystallographic Texture evolution in bulk deformation processing of FCC Metals) motivated by the work of Brown et al. (An internal variable constitutive model for hot-working of metals 1989)	
61-70		Slip hardening parameter, a	E10.0
1-10	Card 4	Poisson's ratio, ν_{ba}	E10.0
11-20		Poisson's ratio, ν_{ca}	E10.0
21-30		Poisson's ratio, ν_{cb}	E10.0
Columns		Quantity	Format

31-40		Rate sensitivity exponent for slip system 2, *n.*	E10.0
41-50		Reference strain rate for slip system 2, $\dot{a}$.	E10.0
1-10	Card 5	Shear modulus, G_{ab}	E10.0
11-20		Shear modulus, G_{bc}	E10.0
21-30		Shear modulus, G_{ca}	E10.0
31-40		Rate sensitivity exponent for slip system 3, *n.*	E10.0
41-50		Reference strain rate for slip system 3, $\dot{a}$.	E10.0
1-10	Card 6	Material axes definition option, AOPT	E10.0

EQ.0.0: locally orthotropic with material axes determined by element nodes n_1, n_2, n_4 and as shown in Figure 2. Cards 7 and 8 are blank with this option.

EQ.1.0: locally orthotropic with material axes determined by a point in space *P* and the global location of the element center, as shown in Figure 2. Card 8 below is blank.

EQ.2.0: globally orthotropic with material axes determined by vectors defined on Cards 7 and 8. (See Figure 3).

EQ.3.0: Applicable to shell element only – will result in an error termination if used with this model

EQ.4.0: locally orthotropic with cylindrical material axes determined by point *P*, located on the axis of revolution, and the vector ***d***, which parallels axis of revolution. (See Figure 3)

Columns	Quantity	Format

11-20		Unused at this time.	E10.0
		Reserved for: Material axes change flag for brick elements	
21-30		Crystal structure flag	E10.0
	EQ.1.0:	FCC (1 slip system)	
	EQ.2.0:	BCC (3 slip systems)	
31-40		Initial hardening modulus for slip system 1, h_0	E10.0
41-50		Stage I stress for slip system 1, τ_s	E10.0
51-60		Initial yield stress for slip system 1, τ_c	E10.0
61-70		Latent hardening parameter q for slip system 1	E10.0
71-80		Latent hardening parameter q_1 for slip system 1	E10.0
1-10	Card 7	x_p, define only if AOPT = 1.0 or 4.0	E10.0
11-20		y_p, define only if AOPT = 1.0 or 4.0	E10.0
21-30		z_p, define only if AOPT = 1.0 or 4.0	E10.0
1-10	Card 7	a_x, define only if AOPT = 2.0	E10.0
11-20		a_y, define only if AOPT = 2.0	E10.0
21-30		a_z, define only if AOPT = 2.0	E10.0
31-40		Initial hardening modulus for slip system 2, h_0	E10.0
41-50		Stage I stress for slip system 2, τ_s	E10.0
51-60		Initial yield stress for slip system 2, τ_0	E10.0

Columns	Quantity	Format

61-70		Latent hardening parameter q for slip system 2	E10.0
71-80		Latent hardening parameter q_1 for slip system 2	E10.0
1-10	Card 8	d_x, define only if AOPT = 2.0 or 4.0	E10.0
11-20		d_y, define only if AOPT = 2.0 or 4.0	E10.0
21-30		d_z, define only if AOPT = 2.0 or 4.0	E10.0
31-40		Initial hardening modulus for slip system 3, h_0	E10.0
41-50		Stage I stress for slip system 3, τ_s	E10.0
51-60		Initial yield stress for slip system 3, τ_0	E10.0
61-70		Latent hardening parameter q for slip system 3.	E10.0
71-80		Latent hardening parameter q_1 for slip system 3.	E10.0

An FCC material contains one set of slip systems, the {111} planes with the <110> directions. If an FCC material is defined then the parameters for slip systems 2 and 3 on cards 4,5,7 and 8 are ignored. Additionally the q_1 on card 6 will be ignored.

A BCC material contains three sets of slip systems:

Slip system	Normal to slip plane	Slip direction
1	{110}	<111>
2	{112}	<111>
3	{123}	<111>

All parameters must be defined.

Example of Input File DYNA3D® - MAT94

The following is an input file for a single crystal compression used in Section 5.2.

```
*
* This file was created using TrueGrid by XYZ Scientific
Applications, Inc.
* For further information, call (925) 373-0628 or write to:
*
*      XYZ Scientific Applications, Inc.
*      1324 Concannon Blvd.
*      Livermore, Ca. 94550
*
*
*------------------- ANALYSIS INPUT DATA FOR DYNA3D® -------------
-----*
* TrueGrid version  2.3.4   dated 01/05/11
*    generated on Mar 29 2012 at 22:29:56
*
*-------------------------- CONTROL CARD #2 ----------------------
----*
*
* number of materials[1] nodal points[2] solid hexahedron
elements[3] beam
* elements[4] 4-node shell elements[5] 8-node solid shell
elements[6]
* interface segments[7] interface interval[8] min. shell time
step[9]
    1         8         1         0         0         0         0
0.000E+00  0.0
*
*-------------------------- CONTROL CARD #3 ----------------------
----*
*
* number of time history blocks for nodes[1] hexahedron elements[2]
beam
* elements[3] shell elements[4] thick shell elements[5] and report
interval[6]
* reaction forces print flag[7] discrete element forces print
flag[8]
* element deletion/SAND database flag[9]
    0    0    0    0    0    0    1    0    1
*
*-------------------------- CONTROL CARD #4 ----------------------
----*
*
* number of sliding boundary planes[1]
* sliding boundary planes w/ failure[2] points in density vs depth
* curve[3] brode function flag[4] number of rigid body merge
cards[5]
* nodal coordinate format[6] force cross sections[7]
* cross section forces interval[8]
         0    0    0    0    0e20.0    0 0.000E+00
```

```
*
*-------------------------- CONTROL CARD #5 ----------------------
----*
*
* number of load curves[1] concentrated nodal loads[2] element
sides having
* pressure loads applied[3] velocity/acceleration boundary
condition cards[4]
* rigid walls (stonewalls)[5] nodal constraint cards[6] initial
condition
* parameter[7] sliding interfaces[8] base acceleration in x[9]
y[10] and
* z-direction[11] angular velocity about x[12] y[13] and z-axis[14]
number of
* solid hexahedron elements for momentum deposit[15] detonation
points[16]
    1    0    0    4    0    0    0    0    0    0    0    0    0
0    0    0
*
*-------------------------- CONTROL CARD #6 ----------------------
----*
*
* termination time[1] time history dump interval[2] complete dump
interval[3]
* time steps between restart dumps[4] time steps between running
restart
* dumps[5] initial time step[6] sliding interface penalty factor[7]
thermal
* effects option[8] default viscosity flag[9] computed time step
factor[10]
 4.000E-02 0.000E+00 4.000E-04    0    0 0.000E+00 0.000E+00    0
0 0.400E+00
*
*-------------------------- CONTROL CARD #7 ----------------------
----*
*
* number of joint definitions[1] rigid bodies with extra nodes[2]
shell-
* solid interfaces[3] tie-breaking shell slidelines[4] tied node
sets with
* failure[5] limiting time step load curve number[6] springs-
dampers-masses
* flag[7] rigid bodies with inertial properties[8] dump shell
strain flag[9]
* number of material groups for deformable-rigid switching[10]
number of
* mass proportional damping sets[11] Hughes-Liu shell update[12]
shell
* thickness change[13] shell formulation[14] number of
nonreflecting boundary
* segments[15]
    0    0    0    0    0    0    0    0    0    0    0    0    0
0    0
*
*-------------------------- CONTROL CARD #8 ----------------------
----*
```

```
*
* number of point constraint nodes[1] coordinate systems for
constraint
* nodes[2] minimum step factor[3] number of beam integration
rules[4]
* maximum integration points for beams[5] number of shell
integration rules[6]
* maximum integration points for shells[7] relaxation iterations
between
* checks[8] relaxation tolerance[9] dynamic relaxation factor[10]
dynamic
* relaxation time step factor[11] 4-node shell time step option[12]
    0    0 0.000E+00    0    0    0    0  250 1.000E-03 9.950E-01
0.000E+00    0
*
*-------------------------- CONTROL CARD #9 ----------------------
----*
*
* plane stress plasticity[1] printout flag[2] number of 1D
slidelines[3]
* relaxation database[4] Rayleigh coefficient[5]
* materials w/Rayleigh damping[6] materials for initial rotation[7]
* materials w/ body force loads[8]
    0    0    0    0 0.000E+00    0    0    0
*
*-------------------------- MATERIAL CARDS ----------------------
----*
*
    1   948.9300E-09    0    00.0000E+00    00.0000E+000.0000E+00
0    0    0
Copper properties from Kalidindi_92 and Li_08
 6.700E+04 6.700E+04 6.700E+04 8.333E+01 1.000E-03 0.000E+00
2.500E+00 0.000E+00
 4.200E-01 4.200E-01 4.200E-01 0.000E+00 0.000E+00 0.000E+00
0.000E+00 0.000E+00
 75000.000 75000.000 75000.000 0.000E+00 0.000E+00 0.000E+00
0.000E+00 0.000E+00
 2.000E+00 0.000E+00 1.000E+00 2.500E+02 1.900E+02 1.600E+01
1.400E+00 1.400E+00
 1.000E+00 0.000E+00 0.000E+00 0.000E+00 0.000E+00 0.000E+00
0.000E+00 0.000E+00
 0.000E+00 1.000E+00 1.000E+00 0.000E+00 0.000E+00 0.000E+00
0.000E+00 0.000E+00
*
*-------------------------- NODE DEFINITIONS ----------------------
----*
*
       1    3 0.0000000000000E+00 0.0000000000000E+00
0.0000000000000E+00    0
       2    0 0.0000000000000E+00 0.0000000000000E+00
1.0000000000000E+00    0
       3    3 0.0000000000000E+00 1.0000000000000E+00
0.0000000000000E+00    0
       4    0 0.0000000000000E+00 1.0000000000000E+00
1.0000000000000E+00    0
```

```
       5    3 1.0000000000000E+00 0.0000000000000E+00
0.0000000000000E+00    0
       6    0 1.0000000000000E+00 0.0000000000000E+00
1.0000000000000E+00    0
       7    3 1.0000000000000E+00 1.0000000000000E+00
0.0000000000000E+00    0
       8    0 1.0000000000000E+00 1.0000000000000E+00
1.0000000000000E+00    0
*
*------------------- ELEMENT CARDS FOR SOLID ELEMENTS --------------
----*
*
       1    1       1       5       7       3       2       6
8       4
*
*------------------------------ LOAD CURVES -------------------------
----*
*
    1    2    0
 0.000E+00 1.000E+00
 1.000E+00 1.000E+00
*
*-------------- PRESCRIBED VELOCITIES AND ACCELERATIONS -----------
----*
*
       2    1    3-1.000E+01 0.000E+00 0.000E+00-1.000E+00    0
       4    1    3-1.000E+01 0.000E+00 0.000E+00-1.000E+00    0
       6    1    3-1.000E+01 0.000E+00 0.000E+00-1.000E+00    0

       8    1    3-1.000E+01 0.000E+00 0.000E+00-1.000E+00    0
```